Distribution Category:
Coal-Based Materials
and Components (UC-114)

ARGONNE NATIONAL LABORATORY
9700 South Cass Avenue, Argonne, Illinois 60439

ANL/FE--90/1

ANL/FE-90/1

DE91 002960

LABORATORY STUDIES ON CORROSION OF MATERIALS FOR FLUIDIZED BED COMBUSTION APPLICATIONS

by

K. Natesan

Materials and Components Technology Division

October 1990

Work sponsored by

U.S. DEPARTMENT OF ENERGY
Office of Fossil Energy
Advanced Research and Technology Development Materials Program

CONTENTS

FIGURES

TABLES

LABORATORY STUDIES ON CORROSION OF MATERIALS FOR FLUIDIZED BED COMBUSTION APPLICATIONS

by

K. Natesan

ABSTRACT

Metallic materials selected for the construction of in-bed heat exchangers and tube supports in fluidized bed combustion (FBC) systems must withstand the corrosive conditions prevalent in these systems. Oxidation/sulfidation interactions that lead to accelerated metal wastage of in-bed materials can occur owing to the presence of sorbent deposits on the metal surfaces and/or low oxygen partial pressures in the exposure environment. An extensive corrosion test program was conducted at Argonne National Laboratory to evaluate the corrosion performance of metallic structural materials in environments that simulate both steady-state and off-normal exposure conditions anticipated in FBC systems. This report discusses the possible roles of key parameters, such as sorbent and gas chemistries, metal temperature, gas cycling conditions, and alloy pretreatment, in the corrosion process. Data on scale thickness and intergranular penetration depth are presented for several alloys as a function of the chemistry of the exposure environment, deposit chemistry, and exposure time. Test results were obtained to compare the corrosion behavior of materials in the presence of reagent grade sorbent compounds and spent-bed materials from bubbling- and circulating-fluid-bed systems. Finally, the laboratory test results were compared with metal wastage information developed over the years in several fluidized bed test facilities.

INTRODUCTION

Combustion of coal in a fluidized bed is widely considered a viable process for producing electric power and generating industrial-process steam. In power-generating applications, tubes carry a working fluid (either steam or air) that eventually drives a turbine. In steam cycles, the temperature of the fireside surfaces of superheater tubes is 550-700°C, whereas in air cycles, the temperatures of the tubes can be as high as the bed temperature, i.e., in the range of 850-900°C.

Two types of fluidized bed combustion (FBC) systems, namely bubbling and circulating-fluid beds (BFB and CFB), are popular today. Heat exchanger tubes in the BFB system are immersed in the bed and in the convective sections of the system, whereas in a CFB, the heat exchanger tubes are generally situated outside the bed. As a result, the tubes in a CFB are generally exposed to an environment in which coal combustion does not occur (i.e., a more stable oxidizing atmosphere is prevalent), and the tubes are exposed to much finer particles. System pressure is another important variable in current systems. Combustion of coal has been achieved in both atmospheric and pressurized FBC (AFBC and PFBC) systems; the method of coal feeding and the sorbent materials in the two systems are different, but the prevalent combustion environment is similar. Figure 1 shows schematic diagrams of typical BFB and CFB systems.

Research sponsored by the U.S. Department of Energy, Fossil Energy AR&TD Materials Program, DOE/FE AA 15 10 10 0, Work Breakdown Structure Element ANL-3.

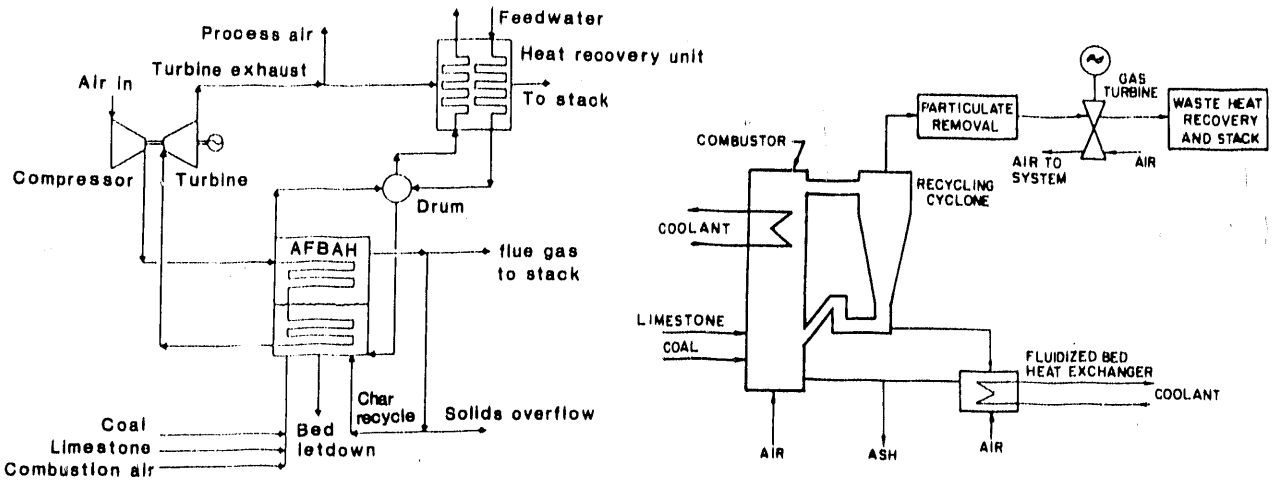

Bubbling-fluid-bed System

Circulating-fluid-bed System

Fig. 1. Schematic Diagrams of Bubbling- and Circulating-fluid-bed Systems

The operating temperature of the fluid bed directly affects sulfidation of calcined limestone (CaO) or dolomite (CaO, MgO), NO_x formation from fuel-bound nitrogen, combustion of the coal feed and char recycle, and heat transfer to the in-bed surface. On the basis of these factors, a bed temperature of 900°C has been selected for FBC operation. The design temperature of the in-bed tube materials can range from 500 to 870°C, depending on the concept and objective of the system. The alloys selected for heat exchange should exhibit adequate erosion/corrosion resistance and sufficient mechanical properties at the service temperature.

Corrosion and erosion of FBC materials are of practical concern because several AFBC and PFBC bubbling units have experienced substantial metal wastage of their in-bed and above-bed components. The affected components have been tube bundles, supports, or feed system units in regular service, or special material probes inserted into the fluidized bed to determine the erosive/corrosive potential of the unit. In some instances, the damage appears to have been dominated by erosion; in other instances, evidence of corrosion or a combined erosion-corrosion type of attack has been detected.

Several factors, acting singly or in concert with each other, have been identified as possible causes of metal damage. These are (a) feedstock characteristics such as size, size distribution, hardness, and chemical composition; (b) mechanical-design features such as air distribution and tube bundle geometry, and design and location of the solids feeder; and (c) operating conditions, such as fluidizing velocity, temperature, and gas and solids composition. Owing to these factors, the environment inside an FBC system is complex and not fully understood as a function of time and position. The FBC environment is dynamic and constantly changing, with local regions alternating between oxidizing, reducing, and possibly sulfidizing conditions even though the fluidized bed is operating in an overall oxidizing state. Deposits composed of sulfur sorbent may form on tube surfaces and establish oxidizing/sulfidizing conditions locally, underneath a deposit in the vicinity of the deposit/scale interface, and may thereby accentuate corrosion. In such an environment,

many so-called high-temperature alloys exhibit inadequate performance owing to the loss of protective adherent oxide scales and subsequent reaction of the base alloy with the gaseous environment, leading to internal oxidation and sulfidation.

Numerous research programs have been conducted over the past 15 years to evaluate the performance of materials in FBC environments. Details of the combustion characteristics, coal feedstock and sulfur-sorbent chemistry, and operating parameters such as temperature, fluidization velocity, excess-air level, and Ca/S ratio are presented in earlier publications.[1,2] Figure 2 is a representation of how various bubbling-bed systems have been operated in terms of two key variables, namely, fluidization velocity and Ca/S ratio.

BACKGROUND

Early developers of the FBC process expected that the problems associated with corrosion and erosion of heat exchanger surfaces, as encountered in conventional coal combustion systems, would be minimized by the introduction of FBC. It was reasoned that the low combustion temperature in FBC systems would result in considerably less evolution of corrosive species, such as alkali salts, and that the buildup and subsequent sintering of deposits on heat exchangers would be less than in conventional systems, thus deterring fireside corrosion. In practice, traditional fireside corrosion, featuring attack by molten salt species has not been reported in FBC systems; however, a form of oxidation/sulfidation has been observed. One of the major material concerns in FBC systems is the oxidation/sulfidation behavior of the alloys in the in-bed heat exchanger tubes and uncooled structural supports. During 1980–83, several investigators have evaluated the corrosion/erosion performance of engineering materials with either small-scale fluidized beds[1-8] or laboratory setups with simulated combustion gas chemistry.[9,10] These investigators established that nickel-base alloys, when exposed to FBC environments, can undergo sulfidation attack that

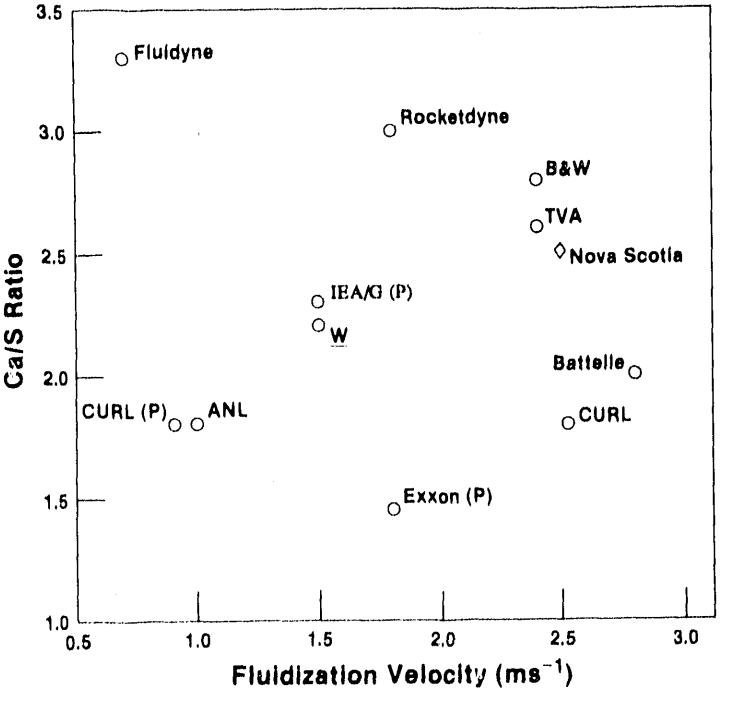

Fig. 2. Fluidization Velocity and Ca/S Ratio Combinations in Various Bubbling FBC Systems Used for Testing of Materials. (P) signifies a pressurized unit; all other units are atmospheric.

leads to catastrophic failures. Further, the corrosion/erosion data showed wide variation in the extent of degradation in specimens exposed in various locations within the same bed, as well as in specimens exposed in various beds with nominally similar environments.

Efforts have been made to measure oxygen partial pressure (p_{O2}) in the FBC environment *in situ*, with solid electrolyte cells. Experiments conducted in an 0.3-m^2 FBC system at the Coal Research Establishment (CRE)[1] showed significant variations in cell response with both axial and radial positions in the bed. Because the cell response is assumed to be directly related to p_{O2} in the gas phase, as determined by equilibrium between different species, one can conclude that the oxygen concentration in the bed is not uniform but can actually vary over a wide range during operation of the system. Bolarski et al.[12] have made actual in-bed measurements of fluctuating p_{O2} and time-averaged combustion gas chemistry for a 0.6-m-diameter high-temperature fluidized bed that operated on Illinois No. 6 coal. The p_{O2} values calculated from the cell response are shown in Fig. 3 as a function of time and location in the bed. The results show that in the middle of the bed, Figs. 3(a) and (b), the p_{O2} remained at $\approx 3 \times 10^{-2}$ atm for extended periods of time, interrupted by short excursions to very low oxygen pressures (i.e., p_{O2} of $\approx 3 \times 10^{-3}$ atm). The results obtained in the bottom of the bed, Fig. 3(d), indicate a time-averaged p_{O2} of $\approx 10^{-14}$ atm, with fluctuations to higher p_{O2} values. The results obtained for a location ≈225 mm from the centerline of the bed at the bottom plane, Fig. 3(c), indicate that time-averaged p_{O2} values ranged between 10^{-2} and 10^{-14} atm for extended time periods. Furthermore, the response time for the oscillations in cell voltage is much less than 1 s.

Minchener et al.[13] made a detailed analysis of the sensor outputs obtained at the CRE under various combustion conditions and concluded that high and low levels of p_{O2} in the environment correspond to bubble and emulsion phases, respectively. Ljungstrom[14] measured the in-bed p_{O2} in a 9.9-m^2 experimental AFBC system at Chalmers University of Technology (Goteborg, Sweden) in tests in which the fuel was Swedish peat, German brown coal, and two sizes of a U.S. bituminous coal. He concluded that the higher the devolatilization rate, i.e., the higher the concentration of gaseous fuel in the dense phase of the bed, the faster the bubbles lose their oxygen. He postulated the penetration of combustible gas from the dense phase into air bubbles and subsequent burning of the gas inside the bubbles. As a result, he suggested that the study of bubble behavior with oxygen probes may not be useful when a fuel with a high volatilization rate is used.

An in-situ oxygen probe has been used to evaluate the effects of underbed and overbed feed systems in the Tennessee Valley Authority (TVA) 20-MW AFBC boiler.[15] The measurements showed that, for both feed methods, the conditions at the top of the bed were more strongly reducing than were those in the lower portions of the bed. Increased metal wastage observed at the top of the bed for both coupon and pin specimens of Incoloy 800 was rationalized on the basis of these oxygen probe results. Researchers at Rocketdyne[16] also attempted to correlate the corrosion wastage of materials with the fraction of time the alloys are exposed to an environment in which the p_{O2} was less than 10^{-3} atm, but the results were not conclusive.

In contrast to the successful electrochemical-probe detection of p_{O2} in the bed of an FBC system, the sulfur partial pressure (p_{S2}) can be determined only by the calculation of gas-phase equilibria among the various molecular species present in the combustion environment. Figure 4 shows the calculated partial pressures of several molecular species in flue gas as a function of air/fuel ratio for the flue gas resulting from Illinois No. 6 coal

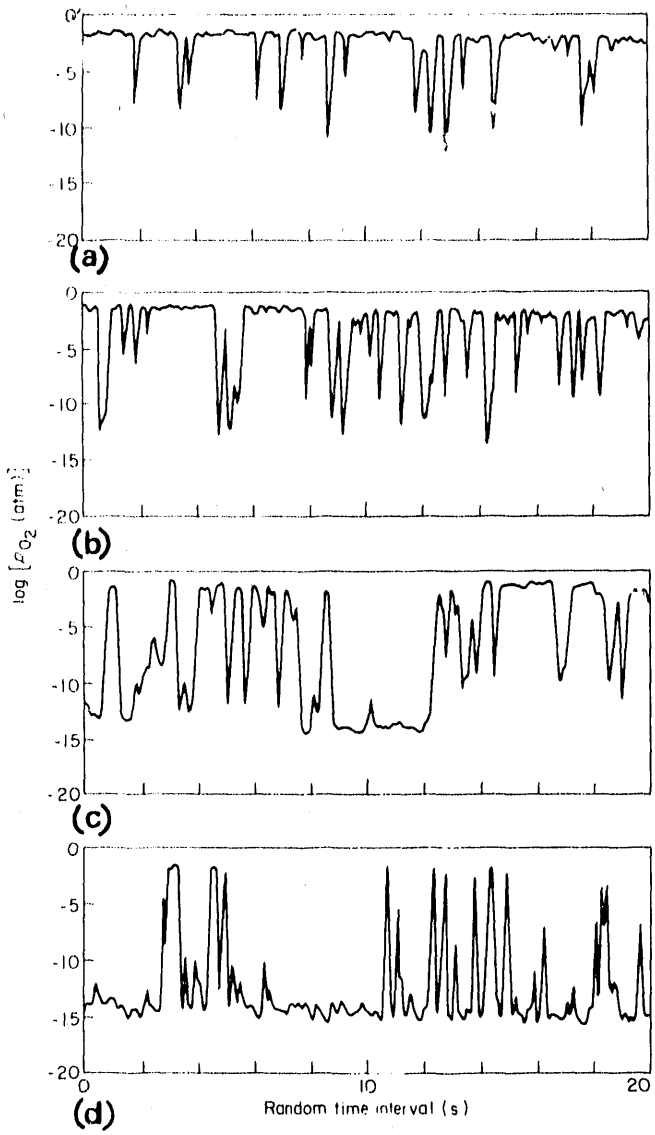

Fig. 3.
Time Dependence of Oxygen Partial Pressures Calculated from Responses of an Electrochemical Cell Placed at Various Locations in a Fluidized Bed (data from Ref. 12). (a) mid-bed centerline; (b) (repeat at later time); (c) bottom of bed + 9" (≈225 mm) from centerline; (d) bottom of bed centerline.

burning at 900°C.[17] It is evident from this figure that at excess-air conditions (air/fuel ratio >1) the p_{O2} is in the range of 10^{-2} to 10^{-3} atm and the p_{S2} is in the range of 10^{-22} to10^{-25} atm. As the air/fuel stoichiometric ratio decreases to 1 and below, the p_{O2} can decrease by 10 to 12 orders of magnitude, and the p_{S2} can increase correspondingly.

The calculated p_{S2} in the gas phase will be determined largely by the thermodynamic equilibrium between CaO and $CaSO_4$, both of which are present in significant quantities during bed operation. Figure 5 shows the CaO-CaS-$CaSO_4$ phase stability fields calculated for temperatures of 704, 840, and 900°C. Superimposed on this plot is the p_{O2}-p_{S2} curve (dashed curve) calculated with thermodynamic equilibria between various gas species in the combustion environment at 900°C. It is evident that, at a given p_{O2} in the environment, the p_{S2} established in the gas phase will be orders of magnitude higher in the absence of sulfur sorbent. Because sulfated lime ($CaSO_4$) and calcined limestone (CaO) are always present in the in-bed environment, the p_{O2} and p_{S2} in the bed will follow along the CaO-$CaSO_4$ equilibrium line. On this basis, the lowest value of p_{O2} that can be attained is $\approx 2 \times 10^{-12}$ atm at

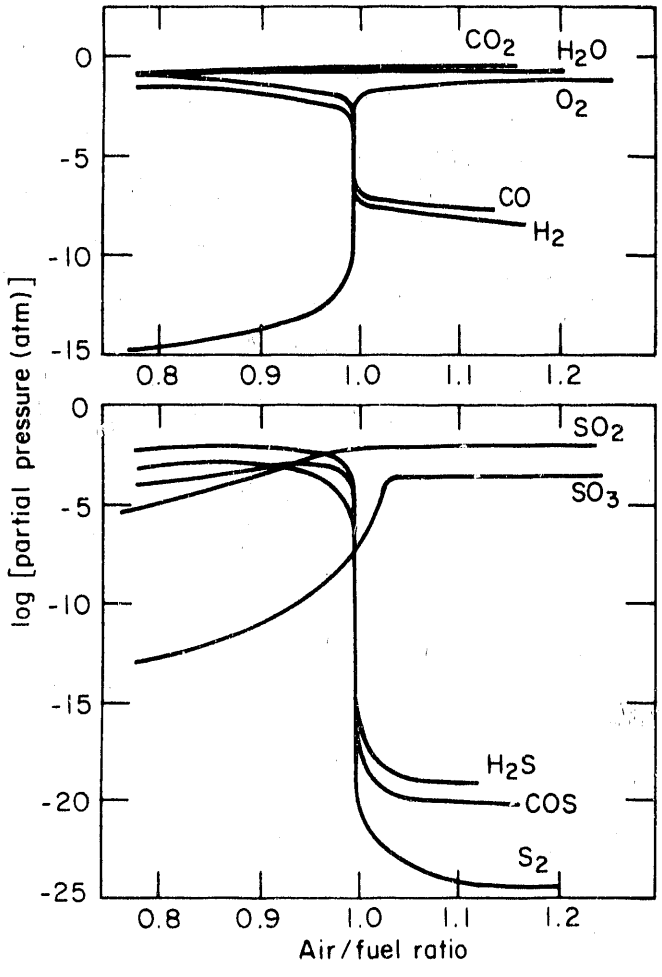

Fig. 4.
Calculated Values for Partial Pressures of Various Gas Species in the Combustion Environment as a Function of Substoichiometric (<1.0) or Hyperstoichiometric (>1.0) Air/Fuel Ratio. Data based on Illinois No. 6 coal at 900°C (from Ref. 17).

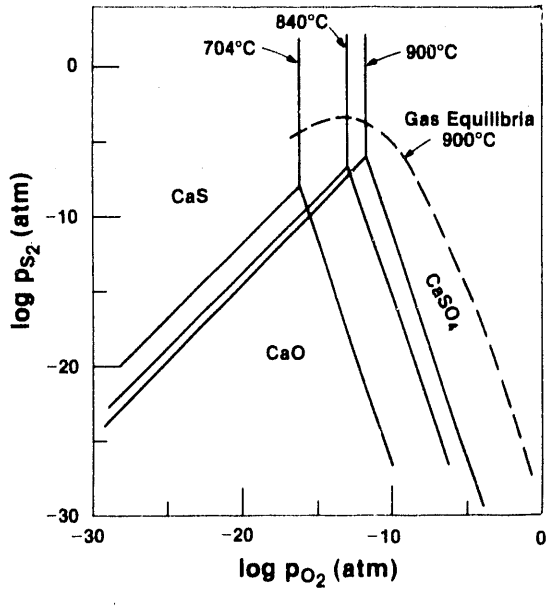

Fig. 5.
CaO-CaS-$CaSO_4$ Phase Stability Fields Calculated for Several Temperatures. Dashed curve represents thermodynamic gas-phase equilibria in combustion atmosphere.

900°C and the corresponding p_{S2} is $\approx 0^{-6}$ atm. Inasmuch as p_{O2} as low as 10^{-14} atm has been measured in FBC systems, thermodynamic analysis leads to the inference of either the presence of CaS in equilibrium with CaO in the vicinity of the probe, or combustion of coal particles on the probe surface, leading to higher CO and lower oxygen content there.

It is also evident that the materials performance in FBC systems should not be correlated with only the p_{O2} in the exposure environment, because the in-bed heat transfer surfaces generally exhibit a layer of sulfated lime deposit after exposure. The combination of a low-p_{O2} environment and the presence of deposits on the tube surface has been suggested, in a qualitative way, as a major cause for sulfidation corrosion of in-bed materials; but the relative influences of low p_{O2} in the gas phase and the deposit on the metal surface are not known. The purpose of the present work is to establish the relative effects of variations in gas chemistry in an exposure environment and the presence of deposits on the corrosion degradation of candidate in-bed FBC materials. As a first step in understanding the role of deposits in the development/breakdown of surface scales, reagent-grade $CaSO_4$ and CaO were used in the present investigation. As a result, the ash components, such as Al_2O_3, SiO_2, etc., and alkali compounds, such as Na_2SO_4, which may be present in deposits from large FBC systems, will be absent in the laboratory test program. Results from ongoing research activities are used to evaluate the effect of actual deposits from FBC facilities such as TVA, IEA/Grimethorpe (IAE/G), and Nova Scotia Power on the corrosion processes.

The purposes of this report are to (a) present corrosion test data for candidate heat exchanger materials developed at Argonne National Laboratory (ANL); (b) review the impact of key variables such as metal and gas temperature, gas and deposit chemistry, and gas composition cycling on corrosion; (c) review the mechanisms of corrosion in FBC environments; (d) assess the role of pretreatment of materials in mitigating corrosion; and (e) correlate laboratory corrosion test data with metal wastage data obtained in large-scale FBC systems.

EXPERIMENTAL PROCEDURE

CORROSION PROBE

In the series of corrosion experiments described below, internally air-cooled ring specimens were used to simulate the heat exchanger tubes exposed in an environment arising from the combustion of coal. A schematic of the experimental setup used in the present studies is shown in Fig. 6. The experimental apparatus consisted of a corrosion probe, to which the ring specimens of different alloys were attached. The probe was approximately 0.4 m in length, with a specially designed head that incorporated a cooling-air path and thermocouples. A photograph of a fully assembled corrosion probe is shown in Fig. 7. The temperature in the gas environment was measured with a Chromel/Alumel couple inserted in the thermowell. In addition, two Chromel/Alumel couples were spot welded on the inside surfaces of the specimens so as to be on the top and bottom samples of the specimen assembly. The entire specimen probe was inserted in a reaction chamber fabricated from aluminized Type 310 stainless steel. The specimens and gases were heated by resistance-wound heating elements situated outside the reaction chamber. A control thermocouple at the outer surface of the reaction chamber was used to adjust the controller set points to achieve the desired temperatures. In general, the metal temperature of the gas side (which defines the exposure temperature for the alloys) was controlled to within ±5°C of the desired value by adjusting the flow rate of the cooling air. In the present experiments, the

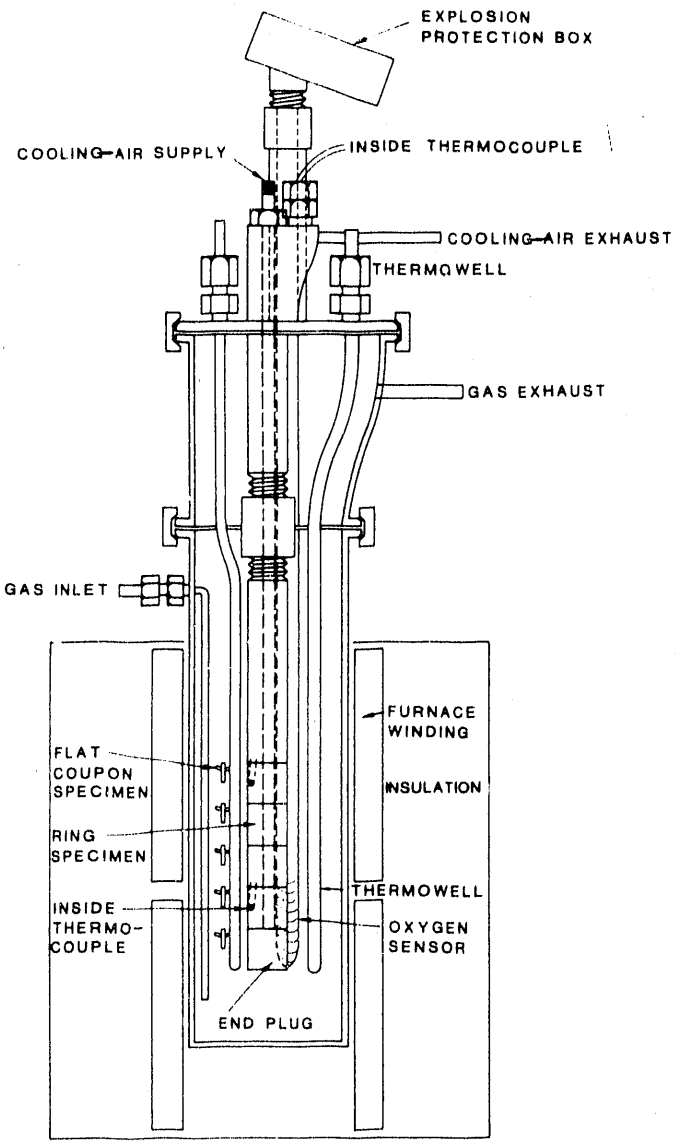

Fig. 6.
Schematic of Experimental Setup Used in Present Study

metal temperature was maintained at 593, 704, or 840°C while the gas temperature was controlled at 840°C.

MATERIALS AND SAMPLE PREPARATION

Candidate metallic alloys chosen for the tests were carbon steel, Fe-2 1/4Cr-1Mo and Fe-9Cr-1Mo ferritic steels, Types 304 and 310 stainless steel, and Incoloy 800. The chemical compositions of the alloys are listed in Table 1. The alloys were procured in pipe form and specimens were fabricated in the form of rings (≈16 mm inside diameter and 16 mm long) and coupons (≈15 x 15 x 1-2 mm). A construction drawing of the ring specimens, indicating detailed dimensions, is shown in Fig. 8.

CHEMISTRY OF EXPOSURE ENVIRONMENT

Because the primary purpose of the present corrosion tests was to examine the relative influences of sulfur sorbent deposit chemistry and the exposure environment on corrosion

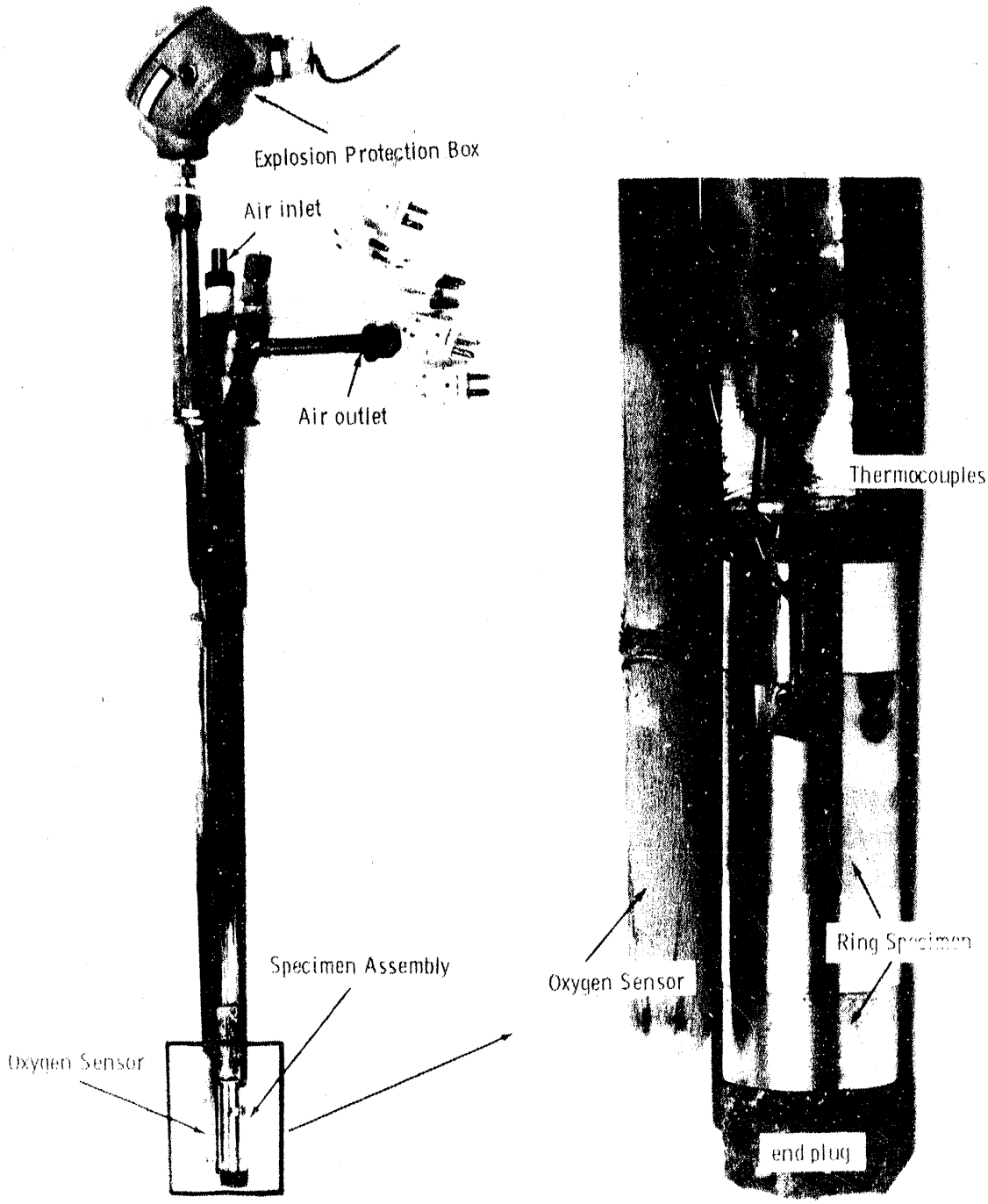

Fig. 7. Photograph of Fully Assembled Corrosion Probe

of metallic alloys, two gas mixtures with widely differing p_{O2} and p_{S2} were used in the experiments. Flow rates of pure gases, such as O_2, N_2, CO_2, and SO_2, and mixed gases, such as O_2-N_2 and SO_2-N_2, were adjusted through a gas flow system to achieve the desired p_{O2} and p_{S2} in the reaction mixture. The gases were passed over a honeycomb platinum catalyst to ensure SO_2-SO_3 equilibrium in the reaction mixture. In addition, three corrosion runs were conducted with $CaSO_4$-coated specimens at metal temperatures of 593, 704, and 840°C in an argon environment. The calculated partial pressures of various gas

Table 1. Chemical Composition of Alloys Used in Present Corrosion Experiments (wt.%)

Material	C	Cr	Ni	Mn	Si	Fe	Other
Carbon steel	0.18	-	-	0.3	0.2	Bal.[a]	-
Fe-2 1/4Cr-1Mo	0.11	2.3	-	0.8	0.3	Bal.	0.98Mo
Fe-9Cr-1Mo	0.10	9.0	-	b	0.4	Bal.	0.99Mo
Type 304 SS	0.06	19.2	10.0	1.1	0.35	Bal.	-
Type 310 SS	0.16	25.1	20.0	1.2	0.4	Bal.	-
Incoloy 800	0.05	21.0	32.5	0.75	0.35	Bal.	0.4Ti, 0.4Al

[a]Bal. = balance.
[b]Not analyzed.

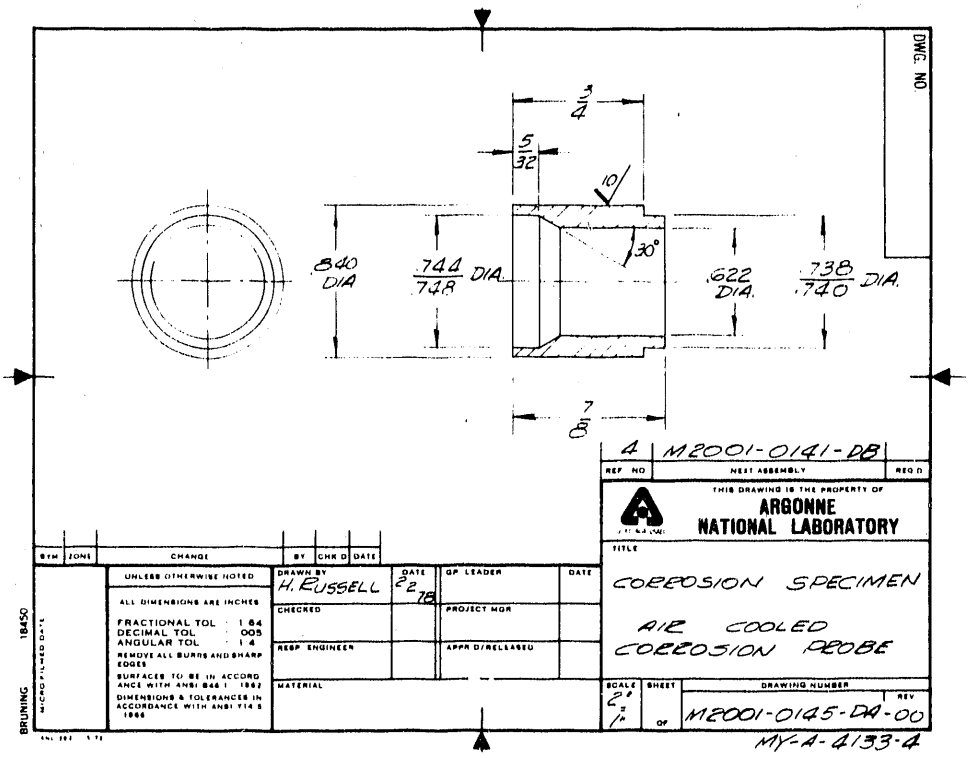

Fig. 8. Fabrication Drawing of a Corrosion Test Specimen

species used in the experimental runs are listed in Table 2 for both high- and low-p_{O_2} environments and for the three metal temperatures. The high-p_{O_2}/low-p_{S_2} (columns 2, 3, and 4) and low-p_{O_2}/high-p_{S_2} (columns 5, 6, and 7) conditions will be referred to as 'high p_{O_2}' and 'low p_{O_2}' environments, respectively, in further discussions in this report.

EXPERIMENTAL RUNS AND SPECIMEN EXAMINATIONS

A listing of various experiments, along with the corresponding gas chemistry conditions and deposit types, is given in Table 3. The corrosion runs were designed[18,19] to

Table 2. Partial Pressures of Components of Simulated FBC Environments Used in Present Laboratory Tests (atm)

Component	High-p_{O_2}/Low-p_{S_2} Environment[a]			Low-p_{O_2}/High-p_{S_2} Environment[a]		
	840°C	704°C	593°C	840°C	704°C	593°C
p_{O_2}	7.0×10^{-3}	6.9×10^{-3}	6.6×10^{-3}	7.5×10^{-9}	1.8×10^{-11}	6.0×10^{-15}
p_{S_2}	2.6×10^{-28}	$<10^{-30}$	$<10^{-30}$	8.9×10^{-12}	3.0×10^{-11}	2.8×10^{-9}
p_{SO_2}	1.7×10^{-3}	1.5×10^{-3}	9.2×10^{-4}	3.3×10^{-1}	3.3×10^{-1}	3.3×10^{-1}
p_{SO_3}	7.7×10^{-5}	2.9×10^{-4}	8.4×10^{-4}	1.6×10^{-5}	3.3×10^{-6}	2.8×10^{-7}

[a]Referred to in the text as high-p_{O_2} and low-p_{O_2} environments.

examine four different aspects of the environmental/material interactions: the effect of exposure temperature, the effects of sorbent deposits alone, the simultaneous effects of sorbent and gas environment, and the effects of gas chemistry cycling. In addition, 500- and 2000-h experiments were conducted under selected exposure conditions to evaluate the corrosion rates. Bare metal alloys were exposed in the high-p_{O_2} atmosphere (Runs 116, 115, and 211) and in the low-p_{O_2} atmosphere (Runs 101 and 109). In runs 130, 131, and 213, $CaSO_4$-coated specimens were exposed to a flowing argon atmosphere for 500 h to evaluate deposit/substrate interactions. In addition, several runs were conducted at metal temperatures of 593, 704, and 840°C with $CaSO_4$- or CaO-coated specimens that were exposed to either high- or low-p_{O_2} atmospheres. In Run 155, the specimens initially coated with $CaSO_4$ were exposed alternately (for 100-h periods, or 'cycle times') to high-p_{O_2} and low-p_{O_2} gas mixtures for a total time of 2000 h at a metal temperature of 593°C. A similar experiment (Run 168) with a cycle time of 10 h was performed with $CaSO_4$- and CaO-coated specimens. In Runs 170 and 171, the 10-h cycle was split between high-p_{O_2} to low-p_{O_2} mixtures in ratios of 9:1 and 1:9, respectively, with a total exposure time of 2000 h. In all the above-mentioned runs, the virgin specimens (with sorbent coatings) were exposed first to the high-p_{O_2} gas mixture. Specimens in Run 172 were exposed to conditions similar to those in Run 171 except that in the former run the virgin specimens were exposed first to the low-p_{O_2} atmosphere.

Thermogravimetric analyses (under isothermal conditions at 840°C) were conducted with coupon specimens of Type 310 stainless steel and Incoloy 800 to examine the combined effect of sorbent/gas chemistry on the corrosion by six deposit mixtures, namely, CaO + CaS, CaS + $CaSO_4$, CaO + $CaSO_4$, CaO + CaS + $CaSO_4$. Spent-bed materials from the TVA 20-MW AFBC and the IEA/G PFBC, argon gas, and three mixed gases, namely, 1 vol.% SO_2 in N_2, air + N_2 + SO_2, and 1 vol.% CO-CO_2, were also used in the study.

Specimens were subjected to three different initial treatments: one set of specimens, in the as-received condition, was surface-ground with 400-grit silicon carbide paper and cleaned with water and ethyl alcohol; another set was pretreated by oxidation at 840°C in a low-p_{O_2} atmosphere (1% CO-CO_2 gas mixture) for ≈80 h; the third set was pretreated by carburization at 840°C in a 0.1, 1.0, and 5 vol.m%. CH_4-H_2 gas mixture for time periods in the range of 64-140 h.

Table 3. Experimental Details of Several Corrosion Runs at a Gas Temperature of ≈840°C, Conducted in Support of FBC In-bed Application

Metal Temperature (°C)	Run No.	Gas Chemistry	Deposit Type	Exposure Time (h)
593	116	High p_{O2}	None	500
	101	Low p_{O2}	None	500
	131	Argon	$CaSO_4$	500
	124	High p_{O2}	$CaSO_4$	500
	143	High p_{O2}	CaO	500
	154	High p_{O2}	$CaSO_4$	2000
	157	Low p_{O2}	CaO	500
	158	Low p_{O2}	$CaSO_4$	2000
	169	Low p_{O2}	CaO	2000
	155	High p_{O2}/low p_{O2} (100-h cycle time)	$CaSO_4$	2000
	168	High p_{O2}/low p_{O2} (10-h cycle time)	CaO, $CaSO_4$	2000
	170	Cycling 9:1 O:R[a]	CaO, $CaSO_4$	2000
	171	Cycling 1:9 O:R	CaO, $CaSO_4$	2000
	172	Cycling 1:9 R:O	CaO, $CaSO_4$	2000
704	115	High p_{O2}	None	500
	109	Low p_{O2}	None	500
	130	Argon	$CaSO_4$	500
	125	High p_{O2}	$CaSO_4$	500
	142	Low p_{O2}	CaO	500
	149	High p_{O2}	$CaSO_4$	2000
840	211	High p_{O2}	None	500
	213	Argon	$CaSO_4$	500
	143	High p_{O2}	CaO	500
	163	High p_{O2}	$CaSO_4$	2000

[a]O and R indicate high- and low-p_{O2} gases, respectively.

DEPOSIT COMPOSITION AND APPLICATION PROCEDURE

In the present tests, the outer surfaces of the ring specimens and one surface of the flat coupons were coated with reagent-grade $CaSO_4$, CaS, CaO or a mixture of these compounds. The deposit material was made into a water-based paste and applied onto the alloy specimens. The thickness of the deposit layer was in the range of 0.25–0.50 mm. The deposit-coated specimens were dried overnight at room temperature, visually examined to ensure adherence of the deposit to the substrate, loaded into the reaction chamber, and heated to the desired temperature in the test environment.

Spent-bed materials were obtained from four (coal-burning) test facilities, namely, TVA 20-MW, IEA/G, Nova Scotia Power, and Combustion Engineering (CE)/Lurgi. Materials from the first three sources were from BFBS, whereas the CE/Lurgi material was from a CFB. In addition, the IEA/G facility is a pressurized unit, whereas the others are atmospheric combustors. Spent-bed materials from the TVA facility were obtained for two different time periods, when either Reed or Fredonia limestones were used as a sulfur sorbent.

CHARACTERISTICS OF SPENT-BED MATERIALS

The bed materials were sieved through several U.S. Standard sieves of successively smaller apertures, each sieve being shaken for ≈10 min to allow smaller particles to fall through to the next sieve. Each portion was weighed and recorded as the weight percent of the total amount of material. Figure 9 shows the weight percent of the material collected in the sieves for four different spent-bed materials.

Figure 10 shows the particle size distribution of the four spent-bed materials. The distribution indicates that ≈40 wt.% of the material is ≈1690 μm in diameter and is essentially the same for the materials from the three sources The Fredonia limestone is much softer than the Reed limestone, a difference that is reflected in a much larger amount of finer-size particles in the run with the Fredonia limestone. To determine chemical differences (if any) between different mesh-size fractions, we analyzed samples (from the various sources) in mesh-size ranges of -8 to +18 and -40 to +60 (average particle sizes of ≈1690 and 335 μm, respectively), as well as a sample of ash from a CFB system. Results of the analyses are listed in Table 4. Several inferences can be made from these results: (a) the K_2SO_4 content of the TVA-bed material is approximately the same when either the Fredonia or Reed limestone was used, but is much greater than that of the material from the other sources, indicating that the K_2SO_4 content is probably related to coal and not sulfur sorbent; (b) the ash from the CFB has a low alkali sulfate content compared to that of ash from bubbling beds; (c) the $CaSO_4$ content of the CFB ash was also extremely low compared to that of bubbling beds; (d) a wide variation in SiO_2 and Al_2O_3 content was observed in the materials from the various bubbling beds; (e) the calculated values for the free silica (probably quartz) in the materials range between 0.5 and 38.0 wt.%, if one assumes that all the alumina in the spent-bed material is present as dehydrated kaolinite (with a composition of $Al_2O_3.2SiO_2$). The highest free-silica value was obtained for the IEA/G material, which had an average particle size of ≈1690 μm; and (f) the calculated value for the amount of free silica in the CFB ash was ≈27.6 wt.%.

The finer fractions of the spent-bed materials were used as a water-based paste and applied to the alloy specimens, as discussed earlier. Figure 11 shows a photograph of the corrosion probes and specimens coated with deposit materials.

SPECIMEN EXAMINATION

Upon completion of the exposures, both macroscopic and microscopic examinations of various specimens were conducted. Cross sections of the ring specimens were examined with a scanning electron microscope equipped with an energy-dispersive X-ray analyzer (EDAX) and an electron microprobe to identify the morphological features of corrosion product phases in the scale layers, and to establish the thickness of scales and depths of intergranular penetration, if any, of the substrate material. In addition, optical metallography was used to determine the unaffected wall thickness of various exposed specimens.

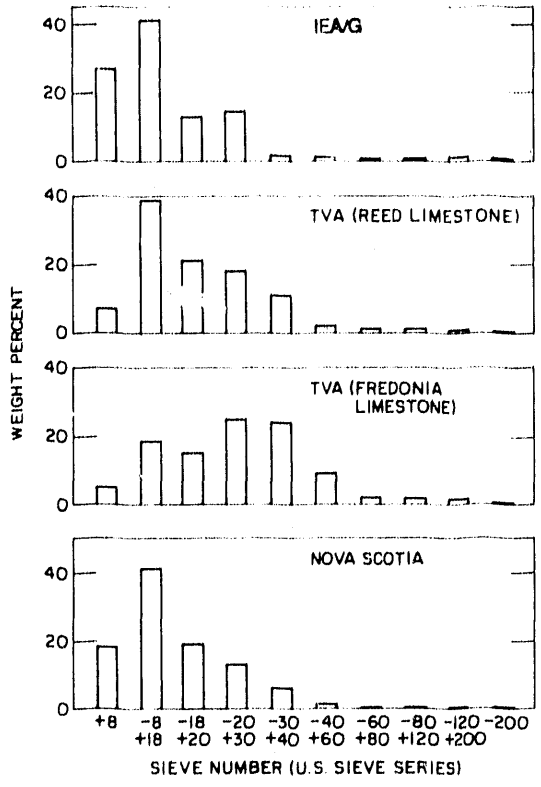

Fig. 9. Weight Distribution of Spent-bed Materials Obtained from Various FBC Systems

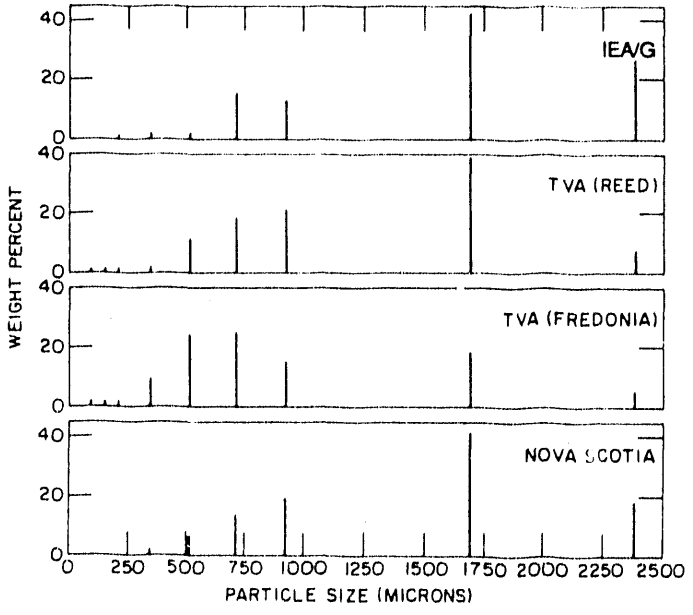

Fig. 10. Particle-size Distribution for Spent-bed Materials Obtained from Various FBC Systems

Table 4. Composition of Spent-bed Material of Two Mesh Sizes from Various FBC Systems (wt.%)

Component	Nova Scotia		TVA (Fredonia limestone)		TVA (Reed limestone)		IEA/G		CFB Ash
	-8+18	-40+60	-8+18	-40+60	-8+18	-40+60	-8+18	-40+60	
SiO_2	29.5	28.4	6.1	2.4	11.3	5.5	42.6	14.3	51.4
Al_2O_3	14.4	10.5	1.9	1.6	1.5	1.1	3.9	1.7	20.2
Fe_2O_3	3.2	4.8	233.5	2.61	1.3	1.4	4.6	2.5	9.1
$CaSO_4$	35.5	39.0	51.5	56.0	52.2	62.4	34.4	58.6	6.5[a]
K_2SO_4	11.5	12.1	31.2	33.3	26.3	22.4	9.1	15.4	5.4
Na_2O	0.08	0.07	0.06	0.06	0.09	0.09	0.08	0.08	1.1
MgO	0.9	1.0	1.5	0.8	1.7	0.9	1.0	0.7	1.1
TiO_2	-	-	-	-	-	-	-	-	0.8
LOI[b]	5.0	4.1	5.1	3.2	5.5	6.2	4.2	6.7	3.1

[a]Mixture of CaO and $CaSO_4$.
[b]Loss on ignition.

The results were compared with initial wall thicknesses of unexposed material to calculate surface recession in the specimens. Detailed analyses of sorbent deposit layers were also conducted, to address the chemical changes induced in the deposit by the gas phase and by transport of base metal elements from the substrate to the deposit.

RESULTS AND DISCUSSION

Figure 12 shows typical macroscopic photographs of $CaSO_4$- and CaO-coated specimens after exposure in Runs 158 and 169. Postexposure visual examination of the carbon steel and Fe-2 1/4Cr-1Mo and Fe-9Cr-1Mo ferritic steel specimens from several runs showed pink corrosion product layers at the gas/deposit interface, indicating substantial outward migration of iron from the substrate and subsequent oxidation to Fe_2O_3. The deposits on high-chromium austenitic alloys remained white, the original color of the sorbent slurry, indicating the absence of preferential migration of iron through the deposit. In general, the sorbent deposit (either $CaSO_4$ or CaO) was fairly adherent to the specimens even after a 2000-h exposure to either of the simulated combustion atmospheres.

The oxygen-sulfur thermochemical diagrams shown in Fig. 13 for Fe, Cr, and Ni at several temperatures indicate the thermodynamic stability of various oxide and sulfide phases. Superimposed on these diagrams are the CaO-CaS-$CaSO_4$ phase fields at the

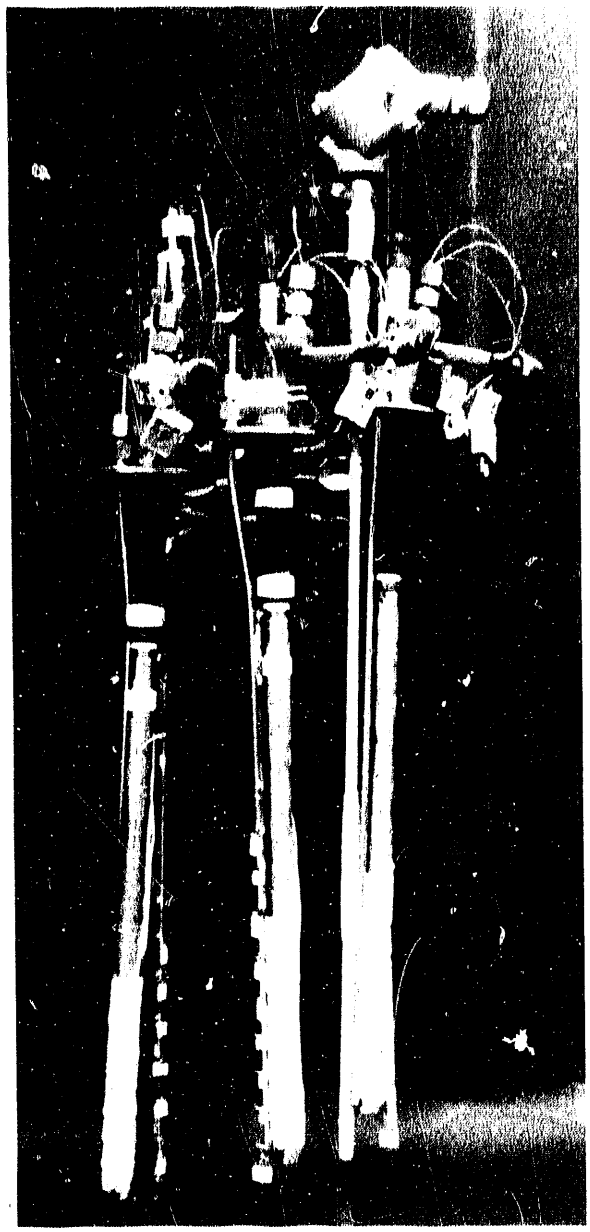

Fig. 11.
Photograph of Corrosion Probes and Specimens Coated with Various Deposits

corresponding metal temperatures. From these diagrams and the p_{O2} and p_{S2} used in the present investigation (see Table 2), it is evident that $CaSO_4$ should be the thermodynamically stable deposit phase in all the runs. The extent of interaction between the deposit and the substrate or the deposit and the scale depends on three factors: (a) the porosity of the deposit layer and the transport of gaseous molecules containing sulfur, (b) the dissociation of $CaSO_4$ to establish a sulfur pressure at the underside of the deposit, and (c) the rate of reaction between the underlying alloy elements and the reactants (such as oxygen and sulfur) to form oxide/sulfide scales and penetrate into the substrate.

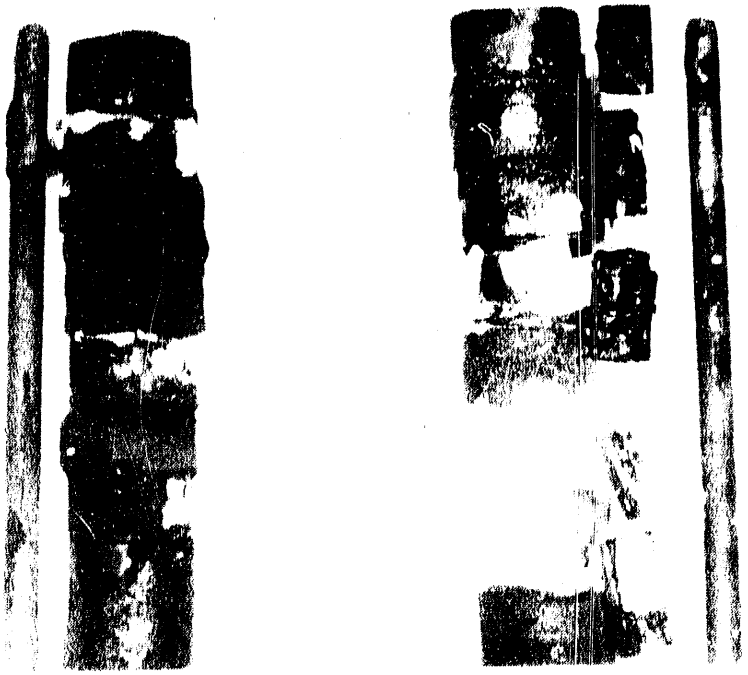

Fig. 12.
Macrographs of Various Alloy Specimens Coated with Sulfur Sorbents after 2000-h Exposures to Low-p_{O_2} Environment. Metal temperature 593°C, gas temperature 840°C. (a) Run 158, $CaSO_4$-coated. (b) Run 169, CaO-coated.

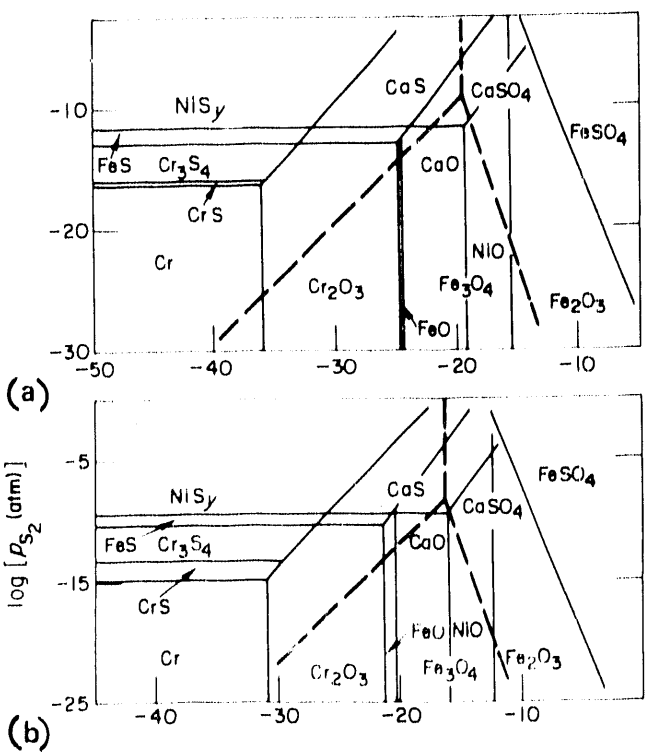

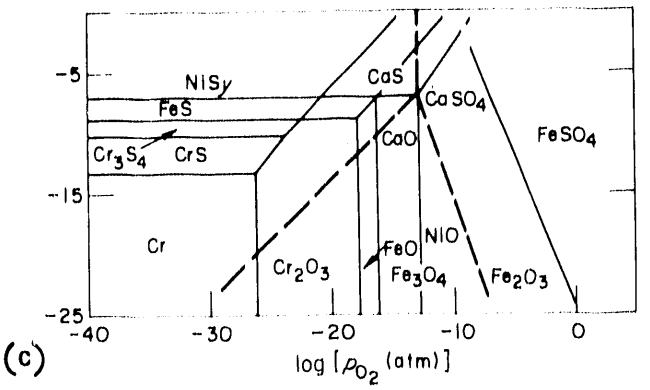

Fig. 13.
Oxygen-sulfur Thermochemical Diagrams at (a) 593, (b) 704, and (c) 840°C, Depicting Regions of Stability of Various Oxide and Sulfide Phases. The phase fields for CaO-CaS-$CaSO_4$ system (dashed lines) are also shown.

EFFECT OF GAS CHEMISTRY ALONE

In Runs 116, 115, and 211, bare specimens of several alloys were exposed to a high-p_{O_2} environment for a period of 500 h. Detailed examination of exposed specimens showed that the external scales on carbon steel and low-chromium ferritic steels consisted of iron oxide, and the internal layers were either iron sulfide or a mixture of iron sulfide and chromium sulfide. The predominant gas-solid reaction in these cases seems to be

$$2Fe + 3/2SO_2 = Fe_2O_3 + 3/4S_2 \quad (1)$$

which leads to a porous iron oxide scale and a significant sulfur pressure (much greater than that for Fe-FeS equilibrium) in the reaction zone. The released sulfur reacts to form iron sulfide, which also acts as a fast diffusion path for additional penetration of sulfur. In alloys with a higher chromium content (e.g., Fe-9Cr-1Mo steel), internal layer of chromium oxide and/or chromium sulfide was observed. High-chromium alloys, such as Type 310 stainless steel and Incoloy 800, developed thin chromium-rich oxide scales at 593 and 704°C, but the scale thickness and depth of sulfur penetration increased significantly at the exposure temperature of 840°C. Figure 14 shows the scale thickness and intergranular penetration data developed for several alloys exposed in the above runs.

In Runs 101 and 109, base specimens of several alloys were exposed to a low-p_{O_2} environment for a period of 500 h at metal temperatures of 593 and 704°C, respectively. The combination of lower oxygen and higher sulfur pressure present in the low-p_{O_2} environment did not alter the mode of interaction in the alloys compared with that exposed in the high-p_{O_2} atmosphere. However, the scale thicknesses and depths of sulfur penetration increased substantially for the carbon steel and Fe-2 1/4Cr-1Mo steel specimens, especially at the exposure temperature of 704°C. High-chromium alloys such as Type 310 stainless steel and Incoloy 800 developed thin chromium-rich oxide scales similar to those obtained in a high-p_{O_2} environment. Figure 15 shows the scale thickness and intergranular penetration data for bare alloys exposed to a low-p_{O_2} atmosphere. A comparison of the data presented in Figs. 14 and 15 indicates that the scale growth rates in carbon steel and Fe-2 1/4Cr-1Mo steel are similar at 593°C in both environments, but the rates are 12-18 times larger in a low-p_{O_2} atmosphere than in a high-p_{O_2} atmosphere when tested at 704°C. The scaling rates for high chromium alloys, tested at 704°C, are comparable in both high- and low-p_{O_2} environments.

The effect of combustion stoichiometry on the depth of corrosive penetration had been evaluated for Incoloy 800 and Types 310 and 347 stainless steel that were tested for 250 h at several bed temperatures.[20] The results, shown in Fig. 16, indicate that although an increase in metal exposure temperature leads to only a small increase in scale thickness, the depth of internal penetration in the substrate material can increase significantly. Even though the gas environment alone can affect the corrosion behavior of materials, the components in FBC systems are often covered by a deposit of bed material. Therefore, an understanding of the corrosion behavior of materials in the presence of a combination of deposit and gas atmosphere is essential.

EFFECT OF SORBENT ALONE

In Runs 130, 131, and 213, $CaSO_4$-coated specimens of several alloys were exposed to a flowing argon environment for a period of 500 h. Figure 17 shows the micrograph

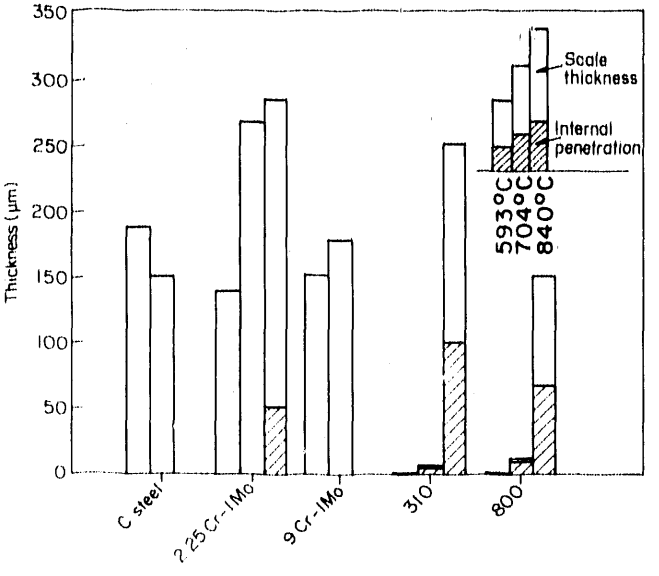

Fig. 14.
Scale Thickness and Intergranular Penetration Data for Bare Alloys after 500-h Exposures to High-p_{O_2} Environment at Three Temperatures

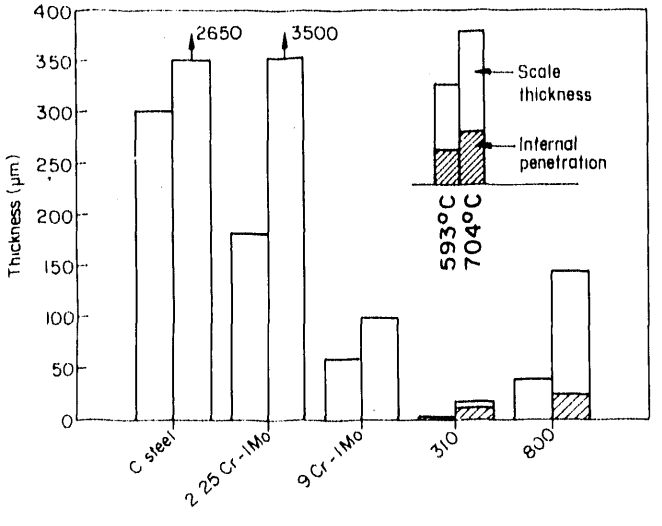

Fig. 15.
Scale Thickness and Intergranular Penetration Data for Bare Alloys after 500-h Exposures to Low-p_{O_2} Environment at Two Temperatures

obtained by scanning electron microscopy (SEM) and elemental mapping of O, S, Ca, Cr, and Fe for an Fe-2 1/4Cr-1Mo steel (typical of ferritic steels) specimen after exposure in Run 130. A detailed analysis of the carbon steel and Fe-2 1/4Cr-1Mo specimens after exposure showed the following: (a) a significant outward transport of iron occurred from the substrate material into the $CaSO_4$ deposit, and no such migration of chromium occurred; (b) the reaction product at the deposit/alloy substrate interface consisted of two distinct layers, an outer layer of predominantly iron oxide and an inner layer of iron sulfide in the carbon steel, and chromium-rich oxides in the Fe-2 1/4Cr-1Mo steel; (c) chromium-rich sulfides precipated at the grain boundary region of the Fe-2 1/4Cr-1Mo steel specimens. In contrast with the results on ferritic steels, there was virtually no migration of iron from the alloy substrate into the deposit in the high-chromium alloys such as Incoloy 800 (see Fig. 18) and Type 310 stainless steel. The oxide scale that developed at

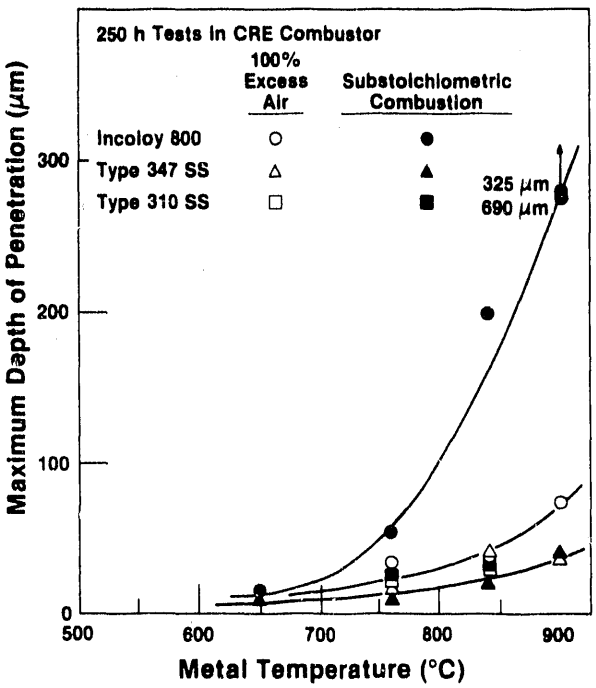

Fig. 16.
Effect of Combustion Stoichiometry on Corrosion of In-bed Alloys

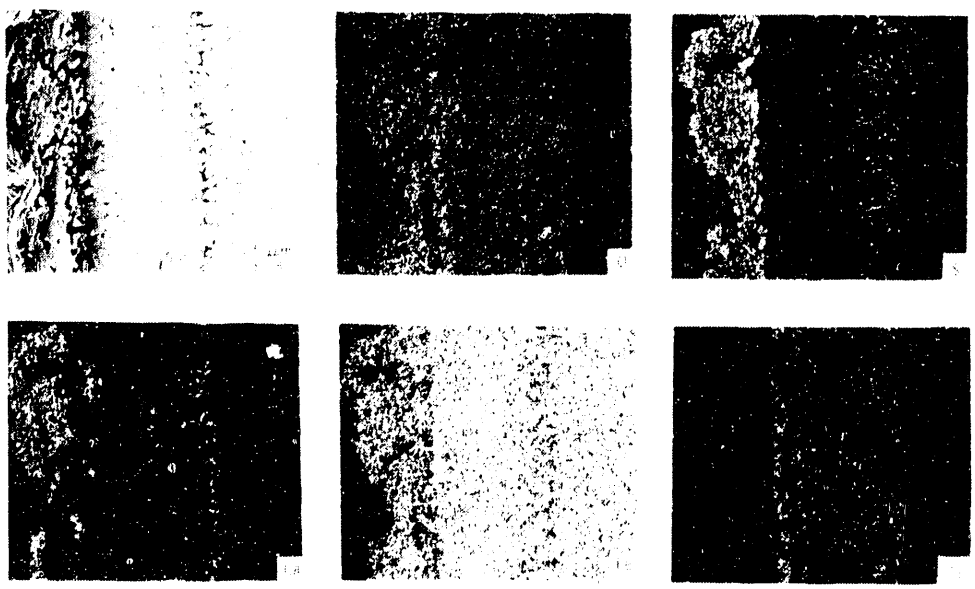

Fig. 17. SEM Photograph and EDAX Elemental Mapping for $CaSO_4$-coated Fe-2 1/4Cr-1Mo Steel Specimen after Exposure at 704°C in Run 130

the deposit/substrate interface was predominantly chromium-rich oxide. Internal penetration of sulfur in these alloys was observed only at metal temperatures of 704 and 840°C.

The results from the above experiment with deposits show that sulfidation of the alloys does not require the presence of sulfur in the gas phase. The $CaSO_4$ dissociation reaction proceeds as follows:

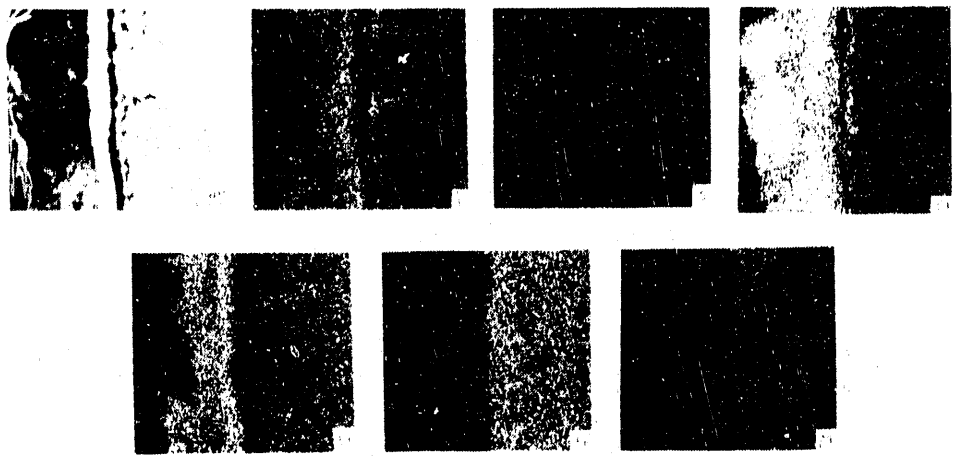

Fig. 18. SEM Photograph and EDAX Elemental Mapping for $CaSO_4$-coated Incoloy 800 Specimen after Exposure at 704°C in Run 130

Table 5. Oxygen and Sulfur Partial Pressures for Various Metal/Metal Oxide and Metal/Metal Sulfide Equilibria and for the Dissociation of $CaSO_4$ (atm)

	p_{O_2}			p_{S_2}		
Equilibria	593°C	704°C	840°C	593°C	704°C	840°C
$CaSO_4$-CaO	1.4×10^{-11}	4.0×10^{-9}	5.5×10^{-7}	2.9×10^{-36}	2.7×10^{-31}	1.4×10^{-26}
Fe-FeO	1.6×10^{-25}	5.9×10^{-22}	1.5×10^{-18}	-	-	-
Fe-FeS	-	-	-	2.3×10^{-13}	2.7×10^{-11}	2.4×10^{-9}
Cr[a]-Cr_2O_3	2.5×10^{-36}	3.2×10^{-31}	2.5×10^{-26}	-	-	-
Cr[a]-CrS	-	-	-	6.9×10^{-16}	42.9×10^{-11}	9.6×10^{-13}
Ni-NiO	6.1×10^{-20}	1.4×10^{-16}	2.2×10^{-13}	-	-	-
Ni-NI_3S_2	-	-	-	3.4×10^{-12}	6.3×10^{-10}	9.2×10^{-8}

[a]Chromium activity is assumed to be 0.25.

$$CaSO_4 = CaO + SO_2 + 1/2O_2. \quad (2)$$

The p_{O_2} values established by dissociation of $CaSO_4$ are given in Table 5 for test temperatures of 593, 704, and 840°C. The dissociation reaction will establish p_{SO_2} values of 2.8×10^{-11}, 8×10^{-9}, and 1.1×10^{-6} atm at temperatures of 593, 704, and 840°C, respectively. If the equilibrium $SO_2 = 1/2S_2 + O_2$ exists at the deposit/substrate interface, then the value of p_{S_2} can be calculated from the p_{SO_2} and p_{O_2} values of the dissociation reaction, which are also listed in Table 5. In addition, a listing of equilibrium p_{O_2} and p_{S_2} values for various metal/metal oxide and metal/metal sulfide systems is given in Table 5. On the basis of the dissociation pressures of $CaSO_4$ and the thermodynamic stability pressures of various oxides and sulfides, two possible mechanisms can be proposed for the oxidation/sulfidation

of carbon steel and low alloy steels in the presence of $CaSO_4$. The first mechanism involves the reaction

$$4Fe + CaSO_4 = 3FeO + CaO + FeS. \quad (3)$$

Reaction (3) is a solid-state reaction and depends on the outward migration of iron from the substrate. Since significant transport of iron has been observed in the exposed specimens, the extent of attack by this mechanism will be dictated by the rate of chemical reaction rather than the transport rate of iron.

The second mechanism involves the reaction

$$3Fe + SO_2(g) = 2FeO + FeS. \quad (4)$$

The p_{SO_2} values required for this reaction to proceed to the right are 4.4×10^{-20}, 6.1×10^{-17}, and 5.9×10^{-14} atm at temperatures of 593, 704, and 840°C, respectively. These values are orders of magnitude less than those calculated earlier for the dissociation of $CaSO_4$. Indirect evidence for this mechanism was reported by Ficalora[10] during differential thermal analysis (DTA)/TGA studies involving $CaSO_4$. The results showed complete utilization of SO_2 at temperatures below 850°C. The extent of attack by this mechanism will be determined by the rate of dissociation of $CaSO_4$.

In the case of high-chromium alloys, the dominant reaction between the $CaSO_4$ deposit and the substrate is

$$Cr + CaSO_4 \rightarrow CaCr_2O_4 \text{ or } Cr_2O_3 + \text{sulfur}, \quad (5)$$

even though the SO_2 pressure (generated by dissociation of $CaSO_4$) at the interface is sufficient to form chromium sulfides. Figure 19 shows the scale thickness and intergranular penetration data for the $CaSO_4$-coated alloys exposed to an argon environment at various temperatures. It is evident that, even in the absence of sulfur in the gas phase, the high-chromium alloys exhibit significant intergranular attack, especially at the higher temperatures.

Incoloy 800 specimens were also tested at 840°C in argon environments, after coating with mixtures of reagent grade CaO, CaS, and $CaSO_4$. Figure 20 shows SEM photographs of corrosion product layers that developed on Incoloy 800 specimens during exposure to a flowing argon environment at 840°C in the presence of deposit mixtures 1 through 4 (defined below and identified as lines for 1-3 and a point for 4 in the CaO–CaS–$CaSO_4$ phase stability diagram in Fig. 20). The alloy exhibited an oxidation mode of attack in the presence of all four deposit mixtures and virtually no sulfur was detected in either the scale or the substrate alloy. The specimen coated with Mixture 1 exhibited a somewhat thicker chromium oxide scale and significant intergranular oxidation of the substrate alloy, whereas the specimens coated with other deposit mixtures developed chromium-oxide scales ≈5 μm thick. The results show that the p_{O_2} and p_{S_2} established by the reactions

$$CaO + 1/2\ S_2 = CaS + 1/2\ O_2 \quad \text{(Mixture 1)}$$

$$CaS + 2\ O_2 = CaSO_4 \quad \text{(Mixture 2)}$$

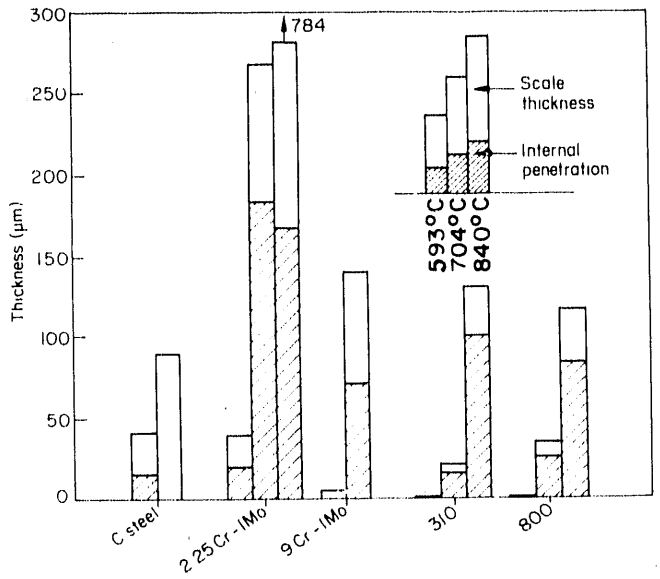

Fig. 19.
Scale Thickness and Intergranular Penetration Data for $CaSO_4$-coated Alloys after 500-h Exposures to Flowing Argon Environment at Three Temperatures

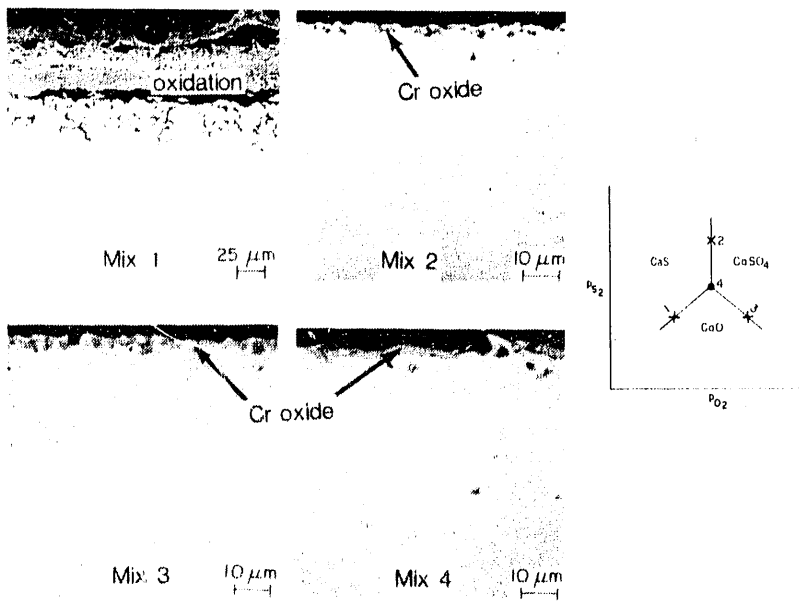

Fig. 20.
Morphologies of Oxide Layers Developed on Incoloy 800 Specimens Coated with Various Deposit Mixtures and Exposed to Argon Environment at 840°C

$$CaO + 1/2\ S_2 + 3/2\ O_2 = CaSO_4 \qquad \text{(Mixture 3)}$$

$$CaO + CaS + 1/2\ S_2 + 7/2\ O_2 = 2CaSO_4 \qquad \text{(Mixture 4)}$$

predominantly lead to oxidation of the alloy at 840°C. The scale morphologies also confirm previous results obtained with a $CaSO_4$ deposit in an argon environment.[19] However, Mixtures 1–3, in the absence of an external reactive gas phase, do not lead to fixed p_{O_2} and p_{S_2} values that correspond to the line indicated by 1 in Fig. 20, and the values can change with time during exposure of the specimens.

COMBINED SORBENT/GAS CHEMISTRY EFFECT

Several corrosion experiments were conducted with $CaSO_4$-coated specimens in high- and low-p_{O2} gas environments at a gas temperature of 840°C (see Table 3). The deposit thickness in different specimens varied between 0.25 and 0.5 mm. Figure 21 shows the morphological features of Fe-2 1/4Cr-1Mo steel and Type 310 stainless steel specimens after exposure at 593°C in high- and low-p_{O2} gas environments (Runs 154 and 158, respectively). In all cases, the deposit layer was essentially intact, even after 2000 h of exposure. The ferritic alloy developed thick iron oxide/iron sulfide scales in both these environments, indicating that the sulfur in the gas phase had very little effect on the morphology of scale layers that developed in specimens coated with $CaSO_4$ deposit. The thicknesses of scale layers in $CaSO_4$-coated alloys tested in a low-p_{O2} environment were significantly larger than those tested in a high-p_{O2} environment. For example, in Fe-2 1/4Cr-1Mo steel, the scale thicknesses were ≈378 and 750 μm, respectively, in high- and low-p_{O2} atmospheres. Further, the depth of internal penetration increased from an almost negligible amount to ≈350 μm as the environment was changed from a high- to a low-p_{O2} atmosphere.

In the case of austenitic alloys, Type 310 stainless steel definitely exhibited superior corrosion resistance (in terms of both the scale thickness and depth of internal penetration) compared with that of Incoloy 800. For example, at a metal temperature of 593°C

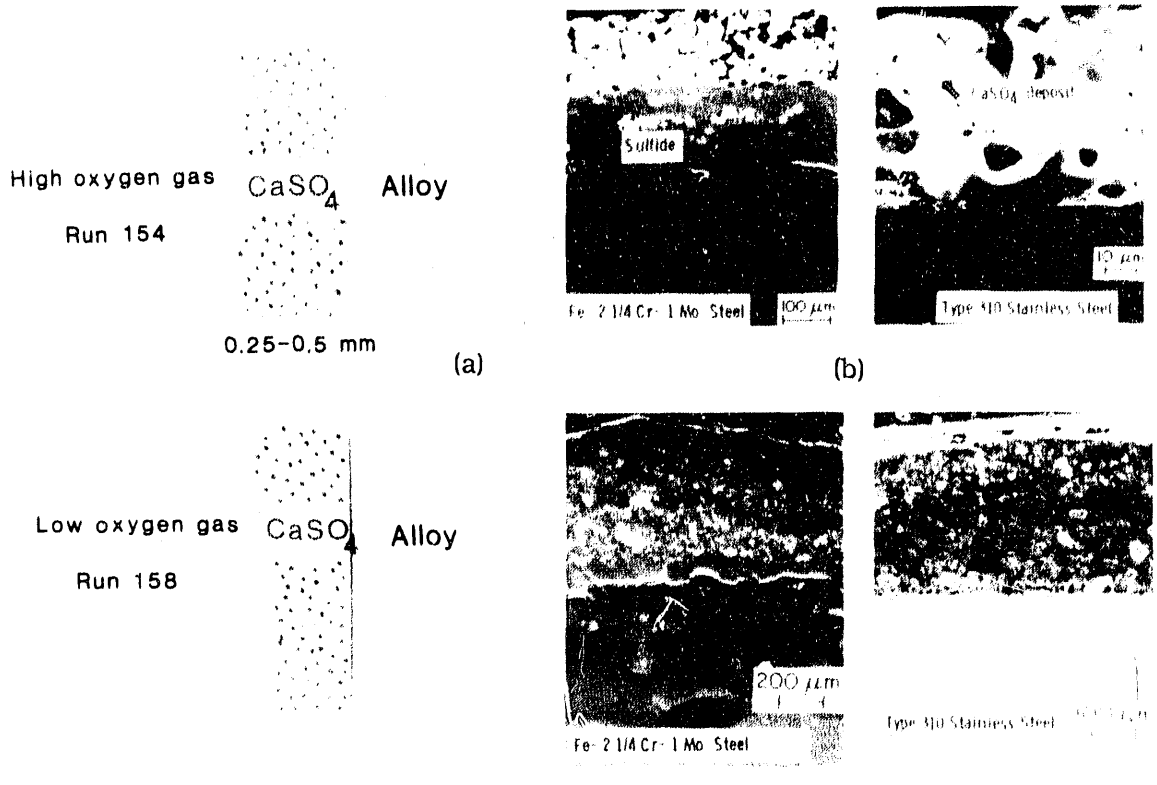

Fig. 21. (a) Sorbent/Gas Chemistry Effect (gas temperature = 840°C, metal temperature = 593°C) and (b) Morphology of $CaSO_4$-coated Alloys after 2000-h Exposures to High-p_{O2} (Run 154) and Low-p_{O2} (Run 158) Environments

and after a 2000-h exposure, the scale thicknesses in Type 310 stainless steel are 5 and 10 μm, in high- and low-p_{O2} environments respectively; the corresponding values for Incoloy 800 are 10 and 500 μm, respectively, in the two environments. Similarly, the depth of penetration in Type 310 stainless steel was negligible when exposed in either atmosphere; the internal penetration in Incoloy 800 increased from an almost negligible amount to ≈200 μm as the environment was changed from a high- to a low-p_{O2} atmosphere.

The CaO-coated specimens exposed to a high-p_{O2} environment (e.g., Run 143) exhibited either thin oxide scales or no scale at all, indicating that molecular diffusion of SO_2 from the gas phase to the deposit/scale interface and subsequent oxidation of the alloy are slow processes because the SO_2 pressure in the gas is high enough to sulfidize the calcium oxide. On the other hand, the CaO deposit on alloys exposed to a low-p_{O2} atmosphere in Run 157 was almost entirely converted to $CaSO_4$ as can be seen from the SEM photographs and elemental mapping for calcium and sulfur, in Fe-2 1/4Cr-1Mo and Type 310 stainless steel specimens (Figs. 22 and 23). The mapping of oxygen is not shown in the figures. The ferritic alloy developed an iron oxide scale and the Type 310 stainless steel developed a thin layer of (Cr, Fe) sulfide as a reaction product. Figure 24 shows the SEM photographs of CaO-coated specimens of the two alloys after a 2000-h exposure in Run 169. The ferritic alloy developed an internal layer of (Cr, Fe) sulfide, whereas the austenitic alloy still exhibited a thin chromium sulfide layer, as indicated by the elemental spectra in Fig. 24.

Figure 25 shows scale thickness and depth-of-penetration data for several $CaSO_4$- and CaO-coated specimens after exposure to the high-p_{O2} environment at different temperatures. Figure 26 shows similar data for deposit-coated specimens after exposure to the low-p_{O2} atmosphere at a metal temperature of 593°C. A comparison of the data in Figs. 25 and 26 for a metal temperature of 593°C shows that, in a high-p_{O2} environment, the deposit has very little added degrading effect on the corrosion resistance of the materials. In fact, the presence of a CaO deposit seemed to lower the corrosion wastage, especially in high-chromium alloys. On the other hand, the combination of a low-p_{O2} atmosphere and either a $CaSO_4$ or a CaO deposit on the metal surfaces produced the greatest scale thickness and intergranular penetration depth observed in the present work.

The increased scaling rate for ferritic alloys in a low-p_{O2} versus a high p_{O2} atmosphere can be explained by a much larger increase in sulfur activity that results from consumption of oxygen via oxidation of iron in the former environment. A detailed discussion of the effect of gas composition on the scaling rate of iron, based on thermodynamic stability of various oxide phases and the gas chemistry conditions, has been presented by Yang and Whittle.[21] In the present study, we found that Incoloy 800 was particularly susceptible to sulfidation attack under such conditions and that Type 310 stainless steel exhibited the least attack. However, the absence of chromium oxide on Type 310 stainless steel indicates that the sulfidation reaction is the dominant mode of interaction in a low-p_{O2}/high-p_{S2} environment, similar to observations in coal gasification environments.[22]

EFFECT OF EXPOSURE TIME

The effect of exposure time on the corrosion process was evaluated from results for $CaSO_4$-coated specimens exposed in Runs 124 and 154 at 593°C and Runs 125 and 149 at 704°C. Figure 27 shows scale thickness and depth-of-penetration data for several alloys

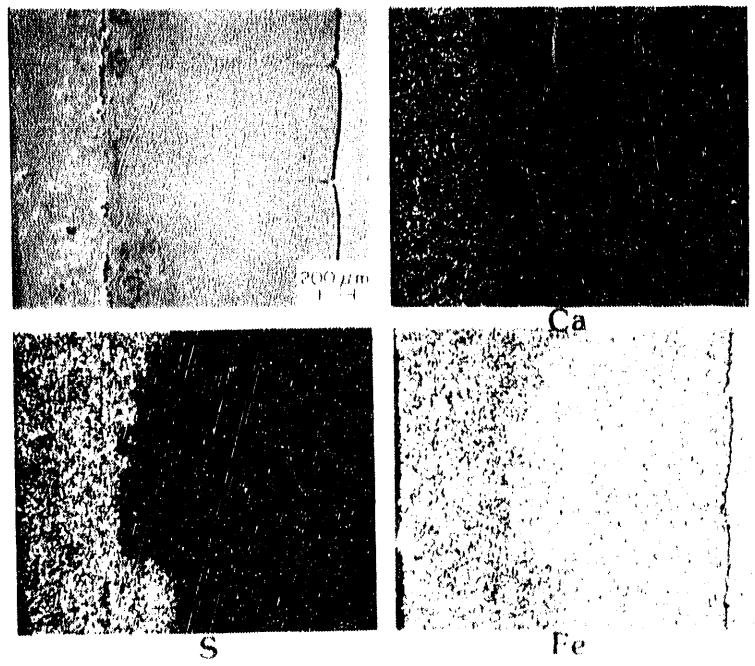

Fig. 22. SEM Photograph and EDAX Elemental Mapping for CaO-coated Fe-2 1/4Cr-1Mo Steel Specimen after 500-h Exposure at 593°C in Run 157

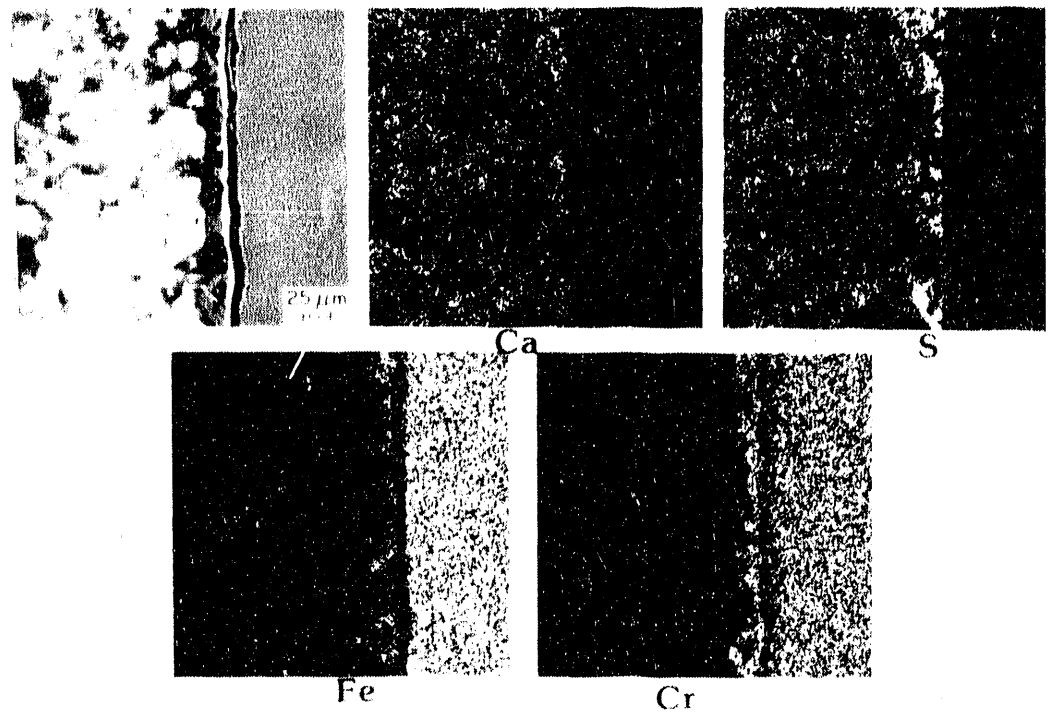

Fig. 23. SEM Photograph and EDAX Elemental Mapping for CaO-coated Type 310 Stainless Steel Specimen after 500-h Exposure at 593°C in Run 157

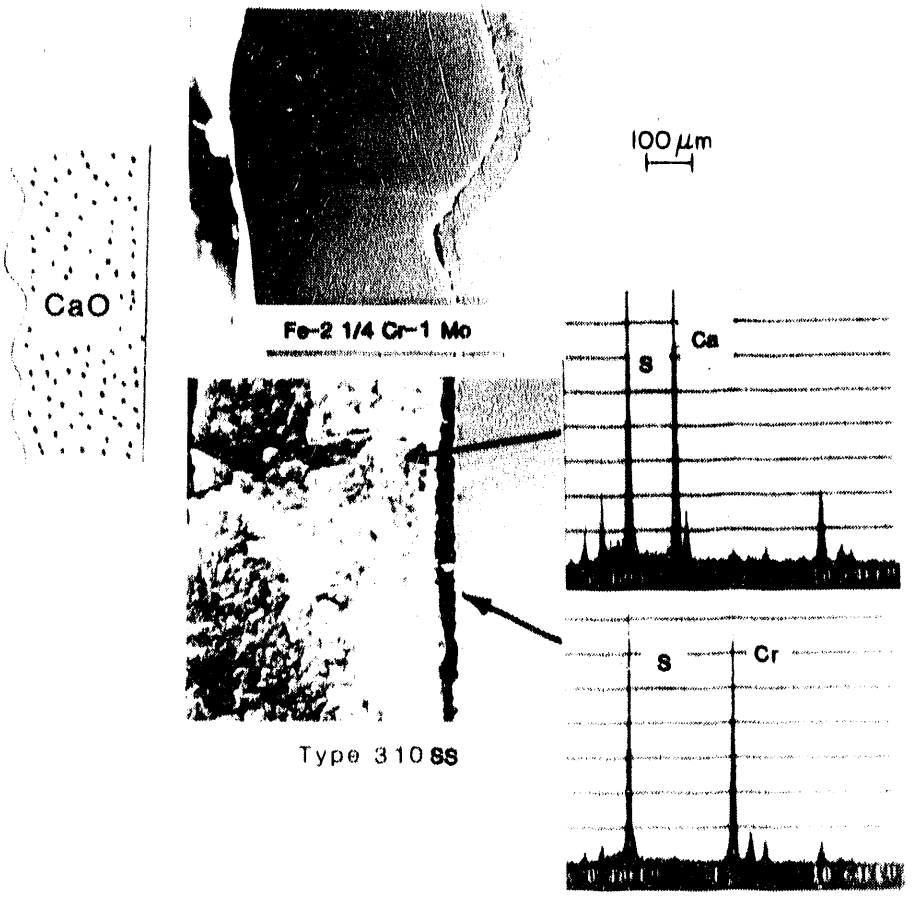

Fig. 24. Morphological Features in CaO-coated Specimens after 2000-h Exposure to Low-p_{O2} (Run 169) Environment

tested in these experiments. It is evident that increasing the exposure time from 500 to 2000 h, in general, increases the scale thickness by approximately a factor of four in carbon and Fe-2 1/4Cr-1Mo steels, which indicates that scale growth follows a linear rate law. Among the higher chromium alloys, Type 310 stainless steel exhibited superior corrosion resistance in terms of both scale thickness and internal penetration; Incoloy 800 seemed to develop much larger surface scale (especially at 704°C) and sulfides in the grain boundaries of the alloy substrate.

EFFECT OF CaO, CaS, AND $CaSO_4$ MIXTURES

Thus far, corrosion information was presented on alloys that were coated with $CaSO_4$ and/or $CaSO_4$-CaO mixtures (which comprise the bed material in a well-run FBC system); however, it is conceivable that in certain locations within the bed, such as coal feedport regions and sections of bed bypassed by combustion air due to fouling/deposit, the local gas chemistry may lead to deposits that may contain CaS and/or CaO-CaS mixtures. To examine the effect of such changes in deposit chemistry on corrosion of heat exchanger materials, thermogravimetric tests were conducted at 840°C with Incoloy 800 and Type 310 stainless

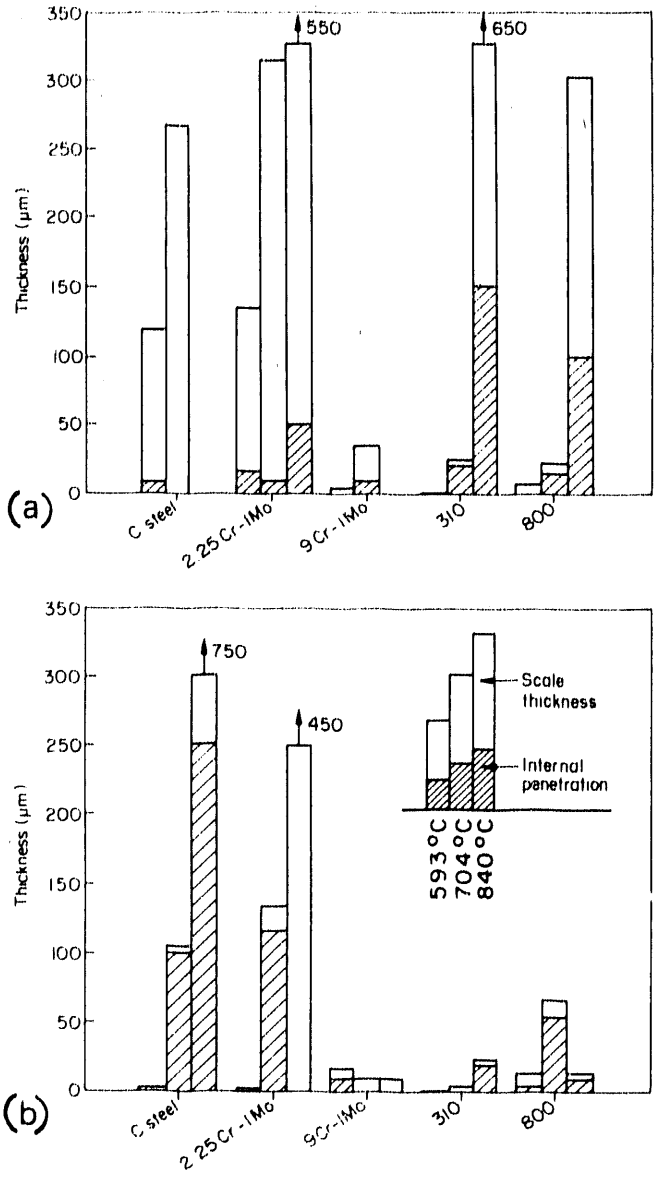

Fig. 25.
Scale Thickness and Intergranular Penetration Data for (a) $CaSO_4$-coated and (b) CaO-coated Alloys after 500-h Exposures to High-p_{O_2} Environment

steel that were coated with CaO/CaS, CaS/$CaSO_4$, CaO/$CaSO_4$, and CaO/CaS/$CaSO_4$ mixtures (identified as lines 1, 2, and 3, and as point 4, respectively, in the oxygen-sulfur stability diagram for the CaO-CaS-$CaSO_4$ system).

Figures 28 and 29 show the weight change data for Incoloy 800 and Type 310 stainless steel specimens (coated with various deposit mixtures), respectively, after exposure at 840°C to a gas mixture with p_{O_2} and p_{S_2} of 5.4×10^{-12} and 1.6×10^{-8} atm, respectively. Figure 30 shows SEM photographs of corrosion product layers that developed on Incoloy 800 specimens that were coated with deposit mixtures (defined by lines 1-3 and point 4 in the p_{O_2}-p_{S_2} diagram in Fig. 30). Specimens coated with Mixtures 1, 2, and 4 exhibited sulfidation attack in these

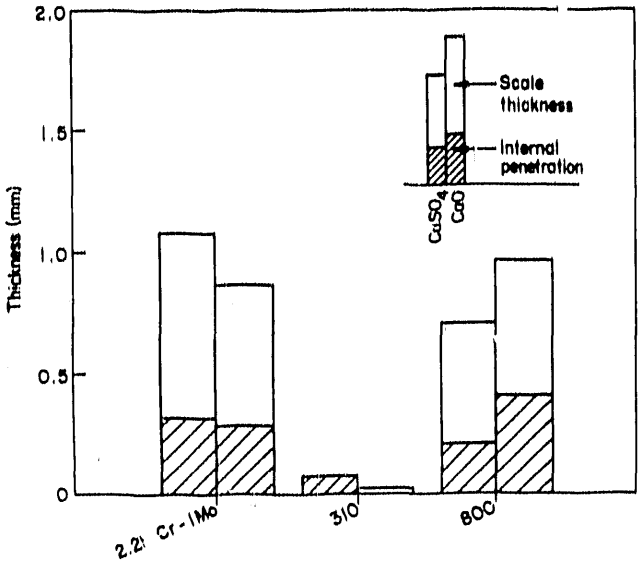

Fig. 26. Scale Thickness and Intergranular Penetration Data for $CaSO_4$- and CaO-coated Alloys after 2000-h Exposures to Low-p_{O_2} Environment at a Metal Temperature of 593°C

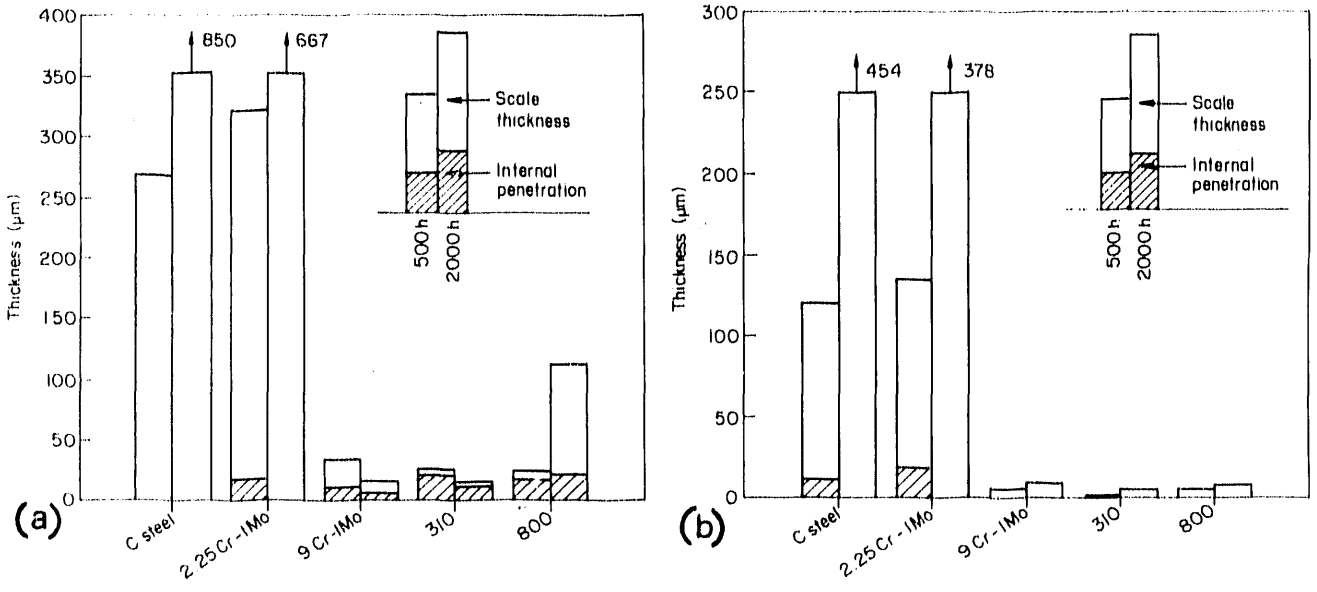

Fig. 27. Scale Thickness and Intergranular Penetration Data for $CaSO_4$-coated Alloys after 500- and 2000-h Exposures to High-p_{O_2} Environment at Metal Temperatures of (a) 704°C and (b) 593°C

experiments, whereas the specimen coated with Mixture 3 still developed a thin chromium oxide scale. The implication of these tests is that, when Mixtures 2 and 4 are in the presence of SO_2 in the gas phase, a fairly high p_{S_2} and low p_{O_2} can be established in the pores of the deposit material and in the deposit/alloy interface region. Consequently, the alloy has a tendency to undergo sulfidation attack in these two tests. In the presence of Mixture 1 and SO_2 in the gasphase, the dominant reaction in the deposit will be sulfation of

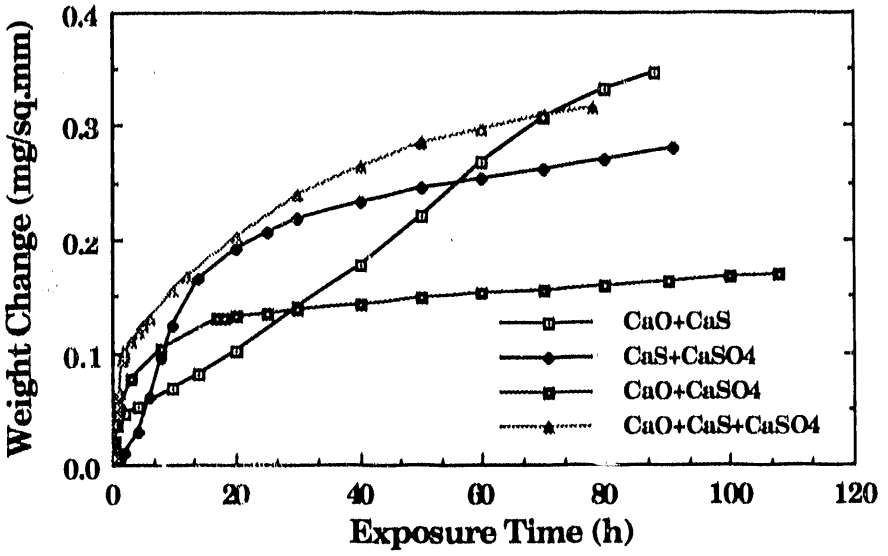

Fig. 28. Weight Change Data for Incoloy 800 Specimens Coated with Various Deposit Mixtures after Exposure at 840°C to Gas Mixture with p_{O2} = 5.4 x 10^{-12} and p_{S2} = 1.6 x 10^{-8} atm

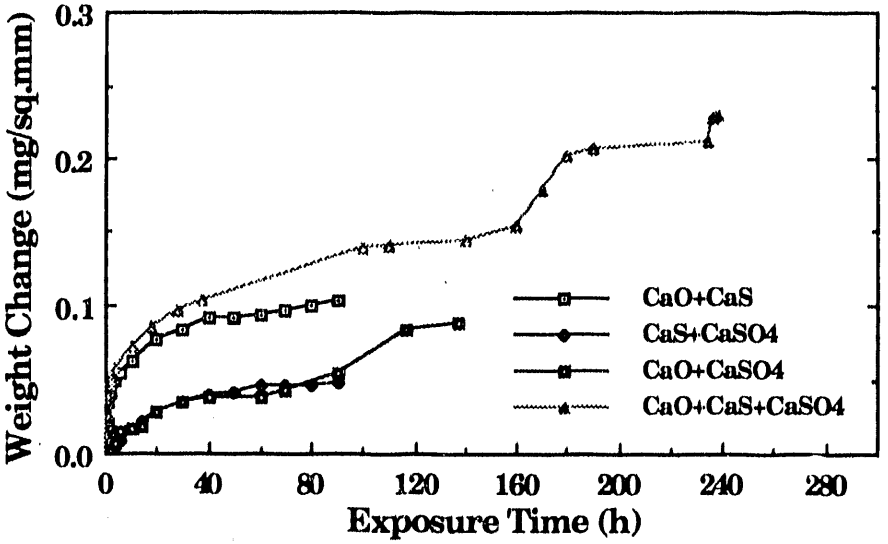

Fig. 29. Weight Change Data for Type 310 Stainless Steel Specimens Coated with Various Deposit Mixtures after Exposure at 840°C to Gas Mixture with p_{O2} = 5.4 x 10^{-12} and p_{S2} = 1.6 x 10^{-8} atm

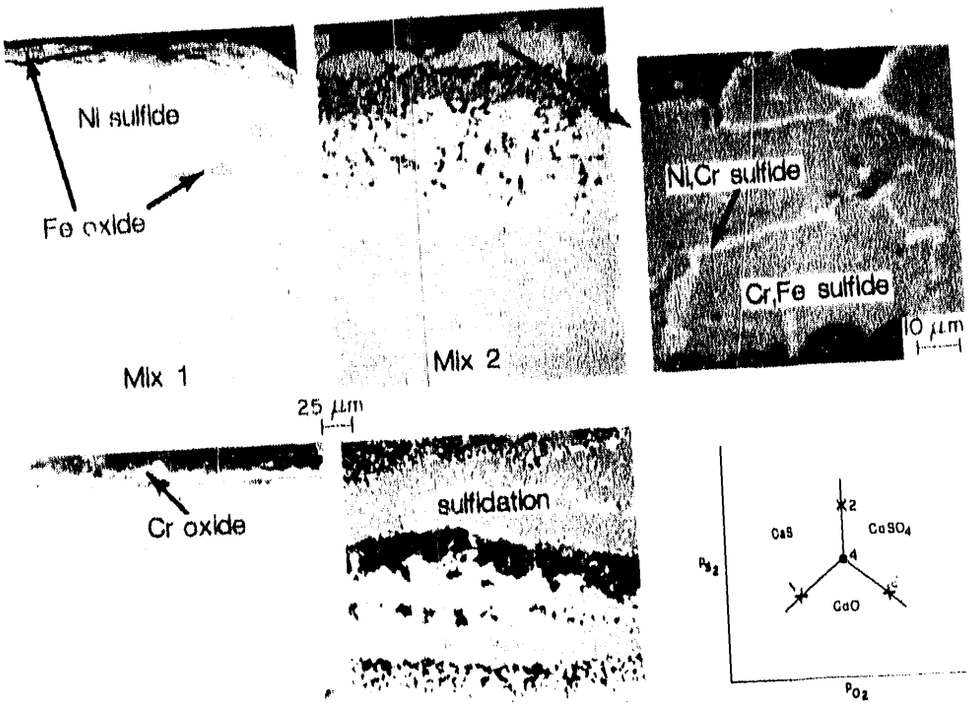

INCOLOY 800; GAS B: $p_{O_2} = 5.4 \times 10^{-12}$ atm, $p_{S_2} = 1.6 \times 10^{-8}$ atm

Fig. 30. Morphologies of Scale Layers that Developed on Incoloy 800 Specimens Coated with Various Deposit Mixtures (defined by lines 1-3 and point 4 of the CaO-CaS-$CaSO_4$ phase stability diagram) and Exposed to Gas Mixture with p_{O_2} and p_{S_2} of 5.4×10^{-12} and 1.6×10^{-8} atm, Respectively

CaO, which will result in an increase in p_{O_2} and p_{S_2} in the pores of the deposit; however, the p_{O_2} will still be at a value dictated by the CaO/CaS/$CaSO_4$ triple point. As a result, the alloy will undergo sulfidation attack, and nickel sulfide and iron oxide will be the reaction product phases. In the presence of Mixture 3 and SO_2 in the gas phase, the dominant reaction in the deposit will be sulfation of CaO to $CaSO_4$ (which can decrease the p_{S_2} in the pores of the deposit material) and the alloy will have a tendency to undergo oxidation. On the other hand, similar experiments conducted with Type 310 stainless steel showed (Fig 31) only an oxidation mode of attack in the presence of any of the four deposit mixtures. However, these specimens were exposed at an elevated temperature for only ≈100 h. In earlier 3000-h tests,[23] it was shown that the presence of a $CaSO_4$ deposit and a low-p_{O_2}/moderate-p_{S_2}/gas mixture can trigger sulfidation of the underlying base alloy, even in Type 310 stainless steel, but the extent of attack is much less than in Incoloy 800.

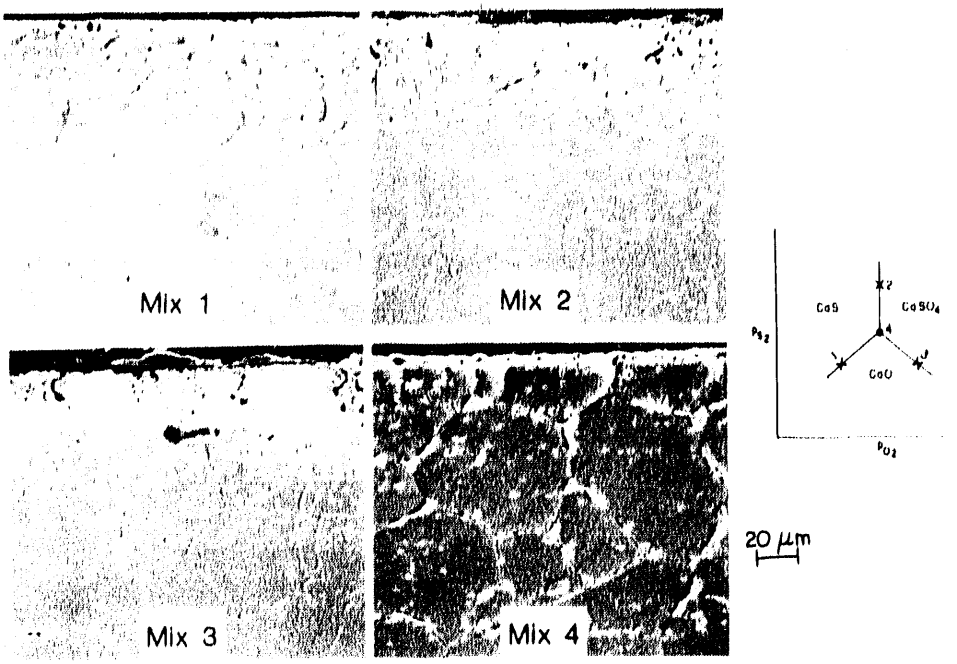

Fig. 31. Morphologies of Scale Layers that Developed on Type 310 Stainless Steel Specimens Coated with Various Deposit Mixtures and Exposed to Gas Mixture with p_{O2} and p_{S2} of 5.4 x 10^{-12} and 1.6 x 10^{-8} atm, Respectively

EFFECT OF PRETREATMENT

The role of two pretreatments (preoxidation and precarburization) of alloy specimens in the subsequent corrosion of alloys in the presence of different deposit mixtures and gas environments was examined. In the preoxidation treatment, the alloys were oxidized for ≈80 h at 840°C in a sulfur-free gas atmosphere with a p_{O2} of 3.6 x 10^{-14} atm. In the precarburization treatment, 140, 96, and 64 h, respectively.

Figure 32 shows the weight change data for preoxidized Incoloy 800 specimens coated with various deposit mixtures and exposed at 840°C to a gas mixture with p_{O2} and p_{S2} of 5.4 x 10^{-12} and 1.6 x 10^{-8} atm, respectively. Figure 33 shows SEM photographs of the morphologies of initially preoxidized Incoloy 800 specimens subsequent to TGA. Preoxidation of the specimens in a low-p_{O2} environment produced thin, chromium-rich oxide scales on the specimens. Subsequent exposure of the specimens to the deposit mixtures in the presence of a SO_2-containing gas mixture had no deleterious effect on the preformed oxide scales, indicating that sulfidation of Cr_2O_3 scale (once developed) is extremely slow. However, such thin oxide scales may not offer protection in the erosive environment of the FBC systems, especially over the tens of thousands of hours of service required of the tube banks.

In the precarburization treatment, the three gas mixtures, 0.1, 1.0, and 5.0 vol.% CH_4H_2, established carbon activities of 0.031, 0.31, and 1.0, respectively. Carburization of the alloy specimens at high-carbon activities simulates carbon pickup in the alloy because of

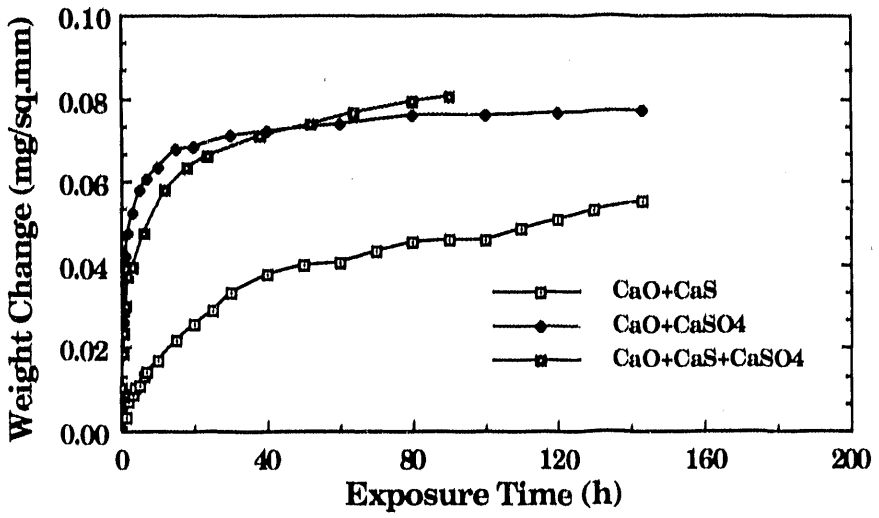

Fig. 32. Weight Change Data for Preoxidized Incoloy 800 Specimens Coated with Various Deposit Mixtures and Exposed to Gas Mixture with p_{O_2} and p_{S_2} of 5.4 x 10^{-12} and 1.6 x 10^{-8} atm, Respectively

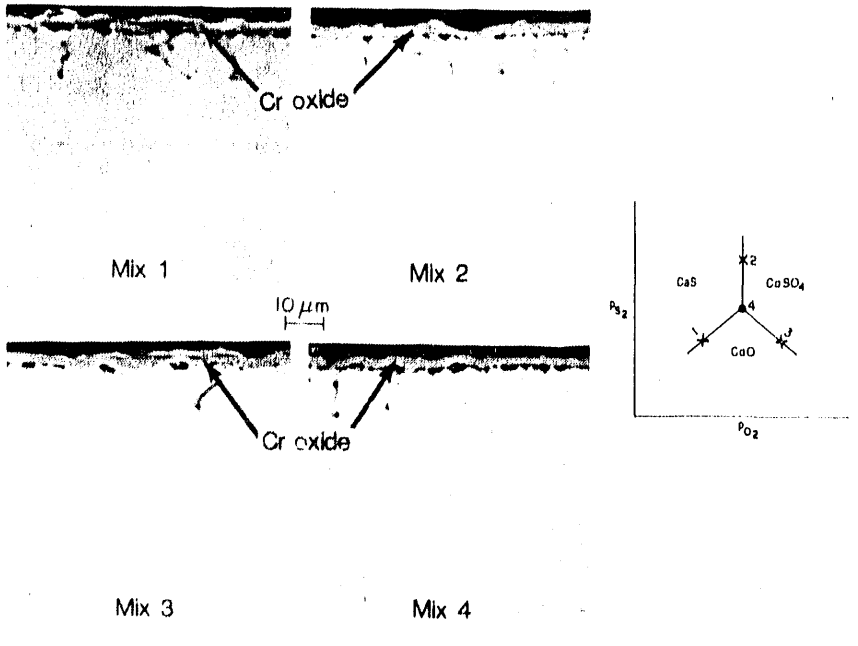

INCOLOY 800; PREOXIDIZED IN GAS C: p_{O_2} = 3.6 x 10^{-14} atm, p_{S_2} = 0

Fig. 33. Morphologies of Scale Layers that Developed on Initially Oxidized Incoloy 800 Specimens Coated with Various Deposit Mixtures and Exposed to Gas with p_{O_2} and p_{S_2} of 5.4 x 10^{-12} and 1.6 x 10^{-8} atm, Respectively

the deposition of unburnt carbon (i.e., in the vicinity of coal feedports or in areas with incomplete combustion) on the alloy components. Precarburization of the alloys at 840°C resulted in precipitation of (Cr,Fe) carbides in the alloy, the amount of precipitates increasing with increase in carbon activity. As a result, the effective chromium concentration and activity in the alloy decreased and caused the alloy to behave (from a scaling standpoint) as a medium-chromium alloy. For example, if carburization proceeds via the reaction

$$23/6\ Cr(\gamma) + C(\gamma) = 1/6\ Cr_{23}C_6 \text{ (in mixed carbide)},$$

where $Cr(\gamma)$ and $C(\gamma)$ are concentrations of chromium and carbon in the austenite phase, the free-energy change for the reaction, as a function of temperature ($\Delta F° = -16380 - 1.54\ T$) and the equilibrium constant for the reaction $K = a^{1/6}Cr_{23}C_6 / a\ C(\gamma)\ aCr(\gamma)^{23/6}$ can be used to calculate chromium activity/concentration in the austenite phase for a given level of carbide precipitation. At a carbon activity of ≈0.3, up to which $M_{23}C_6$ carbide is stable, the precipitation of carbides can lower the chromium content in the matrix phase to less than 15 wt.%. At carbon activities above 0.3, M_7C_3 and M_3C carbides will precipitate and further decrease the chromium activity in the austenite phase. Figures 34–36 show weight change data for precarburized Incoloy 800 specimens coated with various deposit mixtures and tested in an oxygen–sulfur atmosphere.

Figure 37 shows SEM photographs of initially carburized (in a 5 vol.% CH_4–H_2 gas mixture) Incoloy 800 specimens that were coated with deposit mixtures 1-4 and exposed at 840°C to a gas mixture with p_{O_2} and p_{S_2} of 5.4×10^{-12} and 1.6×10^{-8} atm, respectively. Exposure of the precarburized specimens led to the formation of nonprotective surface scale in the presence of all the deposit mixtures investigated. A comparison of photographs in Figs. 30 and 37 shows that precarburization has little effect on the morphology of the

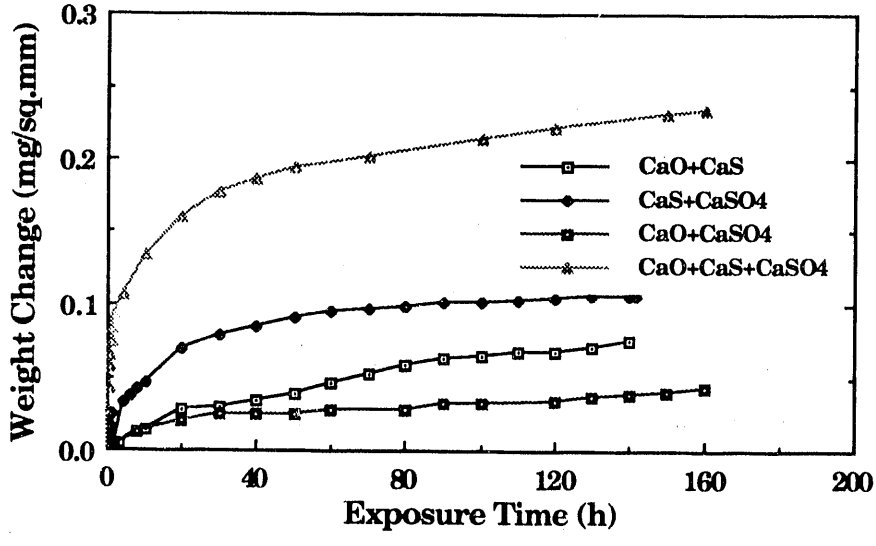

Fig. 34. Weight Change Data for Incoloy 800 Specimens that Were Precarburized in an 0.1 vol.% CH_4–H_2 Gas Mixture, Coated with Various Deposit Mixtures, and Exposed to Gas with p_{O_2} and p_{S_2} of 5.4×10^{-12} and 1.6×10^{-8} atm, Respectively

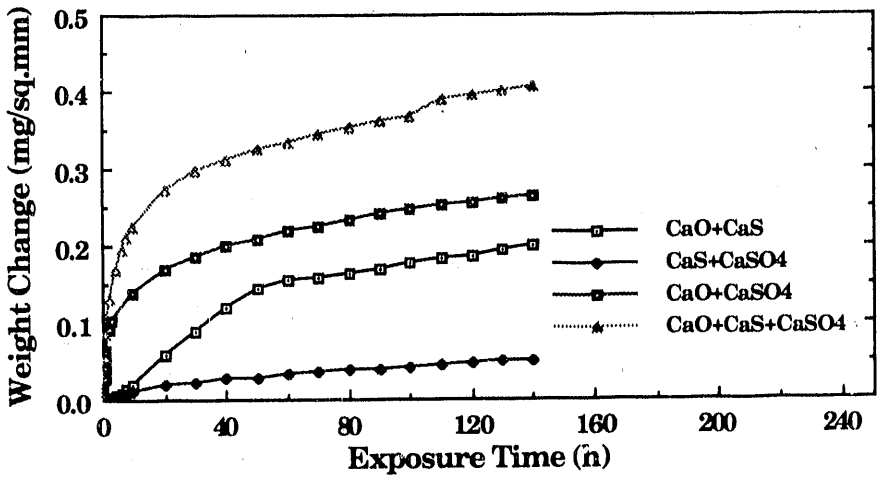

Fig. 35. Weight Change Data for Incoloy 800 Specimens that Were Precarburized in a 1.0 vol.% CH_4–H_2 Gas Mixture, Coated with Various Deposit Mixtures, and Exposed to Gas with p_{O2} and p_{S2} of 5.4 x 10^{-12} and 1.6 x 10^{-8} atm, Respectively

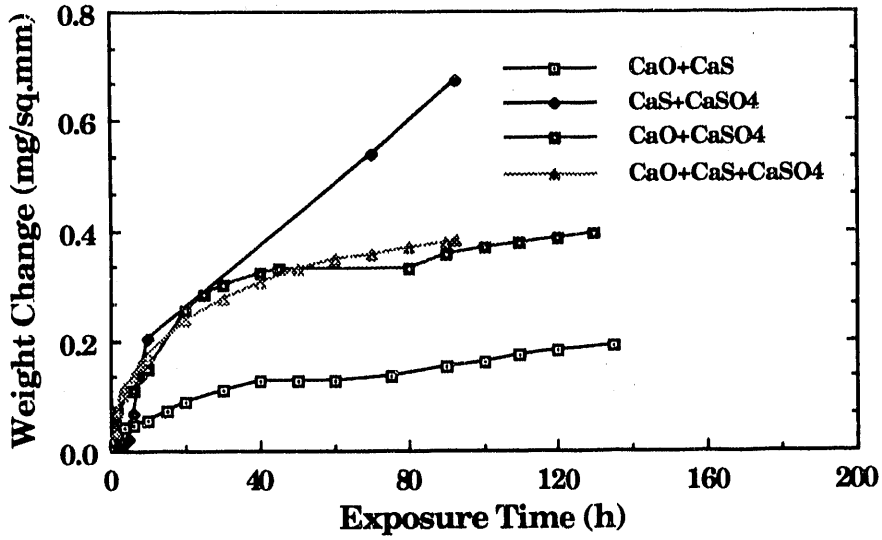

Fig. 36. Weight Change Data for Incoloy 800 Specimens that Were Precarburized in a 5.0 vol.% CH_4–H_2 Gas Mixture, Coated with Various Deposit Mixtures, and Exposed to Gas with p_{O2} and p_{S2} of 5.4 x 10^{-12} and 1.6 x 10^{-8} atm, Respectively

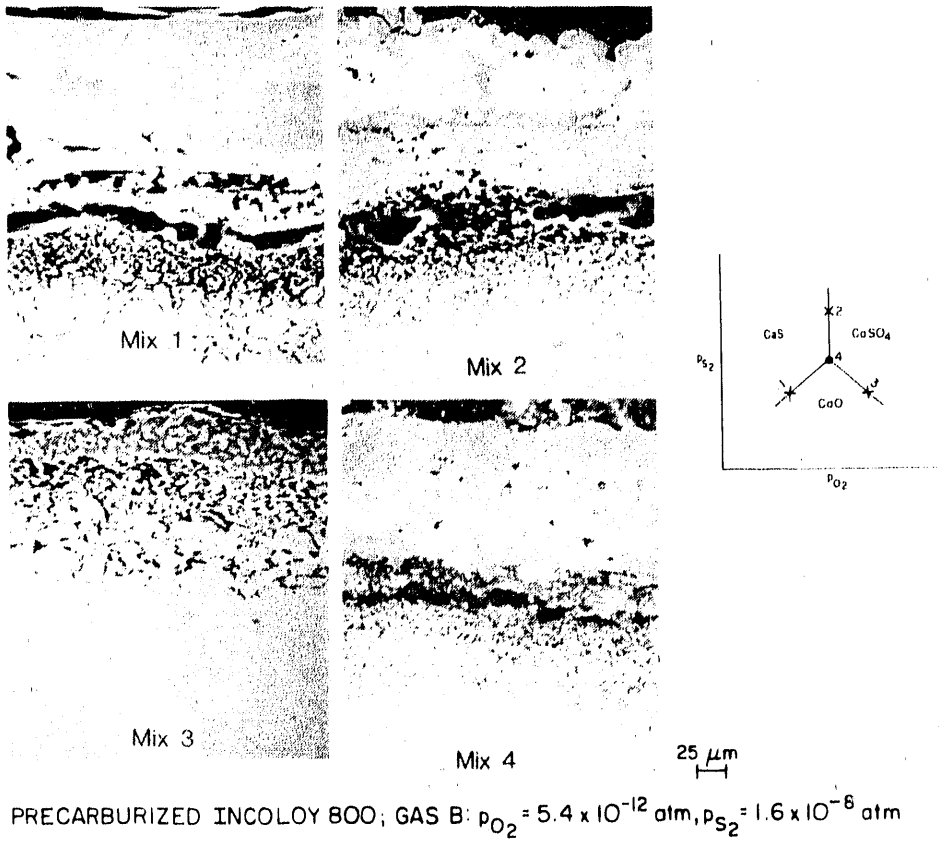

PRECARBURIZED INCOLOY 800; GAS B: $p_{O_2} = 5.4 \times 10^{-12}$ atm, $p_{S_2} = 1.6 \times 10^{-8}$ atm

Fig. 37. Morphologies of Scale Layers that Developed on Incoloy 800 Specimens that Were Initially Carburized in a 5 vol.% CH_4–H_2 Gas Mixture, Coated with Various Deposit Mixtures and Exposed to Gas with p_{O_2} and p_{S_2} of 5.4 x 10^{-12} and 1.6 x 10^{-8} atm, Respectively

scale layers and that the layers are somewhat thicker in the precarburized specimens. Sulfidation is the mode of attack in this alloy either with or without precarburization treatment. Figures 38–40 show weight change data for precarburized Type 310 stainless steel specimens coated with various deposit mixtures and tested in an oxygen–sulfur atmosphere. The SEM photographs in Fig. 41 show the scale layers that developed on precarburized Type 310 stainless steel after exposure to oxygen–sulfur environments in the presence of different deposit mixtures. The photographs show a substantial amount of carbide precipitation, but the thickness of the scale layers is much less than in Incoloy 800, confirming a superior corrosion resistance of the Type 310 stainless steel, even with carburization pretreatment. These results also indicate that carburization is not essential to subsequent sulfidation, and that the scaling behavior of the carburized alloys is determined by the effective chromium concentration in the austenite matrix.

EFFECT OF GAS CYCLING

In Run 155, specimens initially coated with $CaSO_4$ were exposed to high- and low-p_{O_2} gas mixtures for alternating 100-h periods, for a total exposure time of 2000 h. A similar

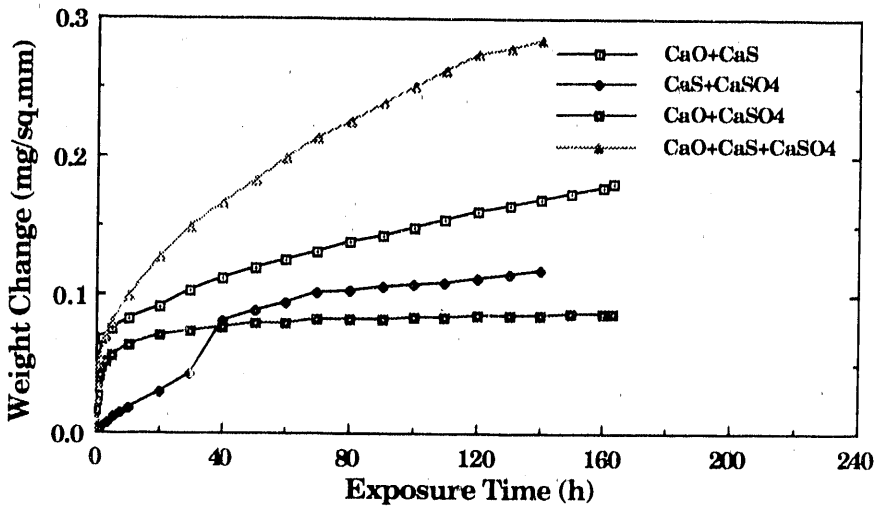

Fig. 38. Weight Change Data for Incoloy 800 Specimens that Were Precarburized in an 0.1 vol.% CH_4–H_2 Gas Mixture, Coated with Various Deposit Mixtures, and Exposed to Gas with p_{O2} and p_{S2} of 5.4 x 10^{-12} and 1.6 x 10^{-8} atm, Respectively

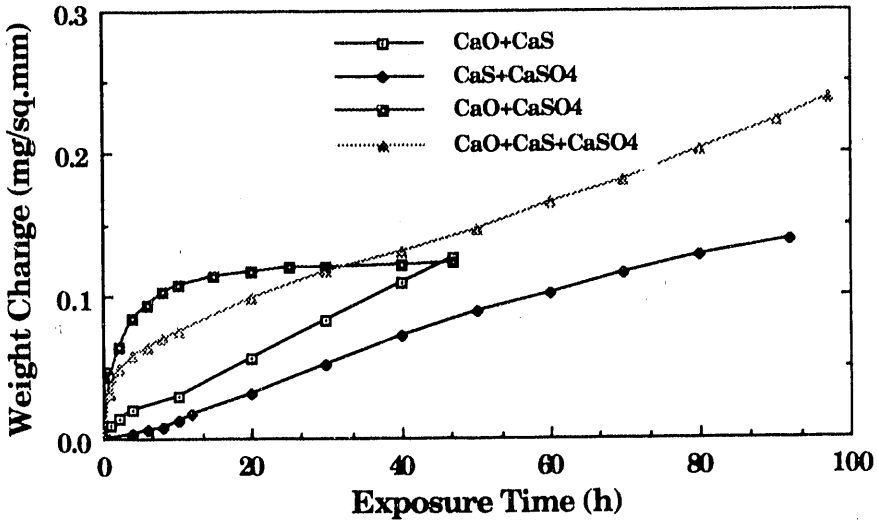

Fig. 39. Weight Change Data for Type 310 Stainless Steel Specimens that Were Precarburized in an 1.0 vol.% CH_4–H_2 Gas Mixture, Coated with Various Deposit Mixtures, and Exposed to Gas with p_{O2} and p_{S2} of 5.4 x 10^{-12} and 1.6 x 10^{-8} atm, Respectively

experiment with $CaSO_4$- and CaO-coated specimens and alternating 10-h exposure periods was conducted in Run 168. Figure 42 shows the morphological features of carbon steel, Fe-2 1/4Cr-1Mo, and Type 310 stainless steel specimens exposed in the two runs. The carbon steel and low-alloy steel specimens developed an external iron oxide layer and internal layers of iron sulfide or chromium sulfide (in the latter specimens); however, the scale features and the thicknesses of the layers were similar to those observed in runs conducted

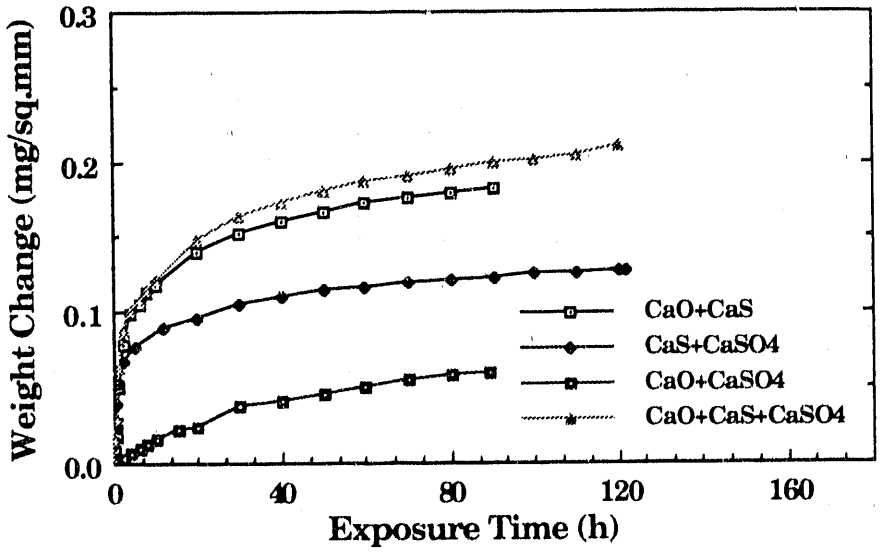

Fig. 40. Weight Change Data for Type 310 Stainless Steel Specimens that Were Precarburized in a 5.0 vol.% CH_4-H_2 Gas Mixture, Coated with Various Deposit Mixtures, and Exposed to Gas with p_{O_2} and p_{S_2} of 5.4 x 10^{-12} and 1.6 x 10^{-8} atm, Respectively

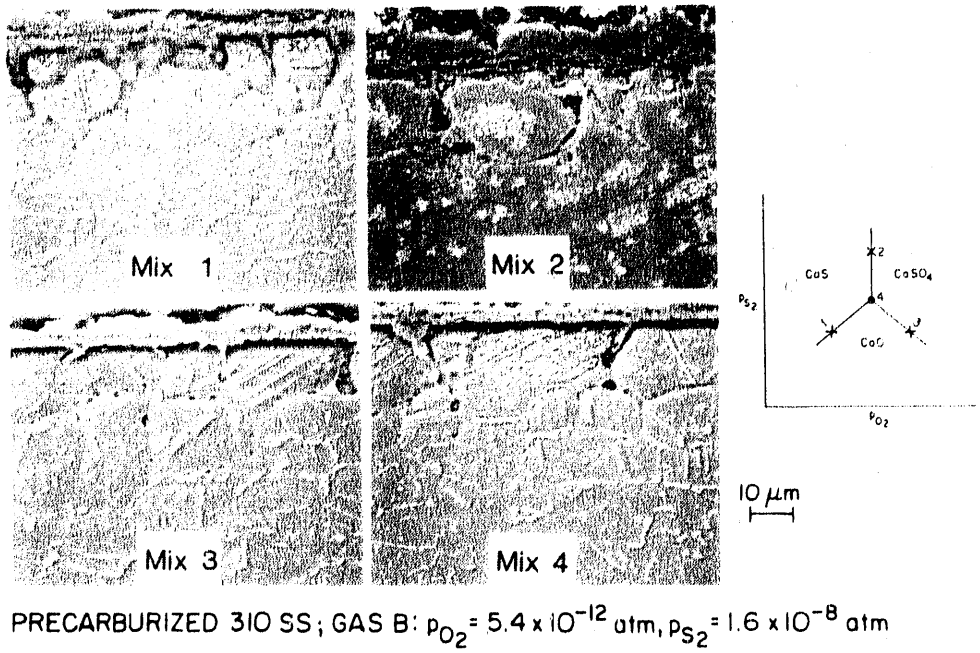

Fig. 41. Morphologies of Scale Layers that Developed on Type 310 Stainless Steel Specimens that Were Initially Carburized in a 5 vol.% CH_4-H_2 Gas Mixture, Coated with Various Deposit Mixtures, and Exposed to Gas with p_{O_2} and p_{S_2} of 5.4 x 10^{-12} and 1.6 x 10^{-8} atm, Respectively

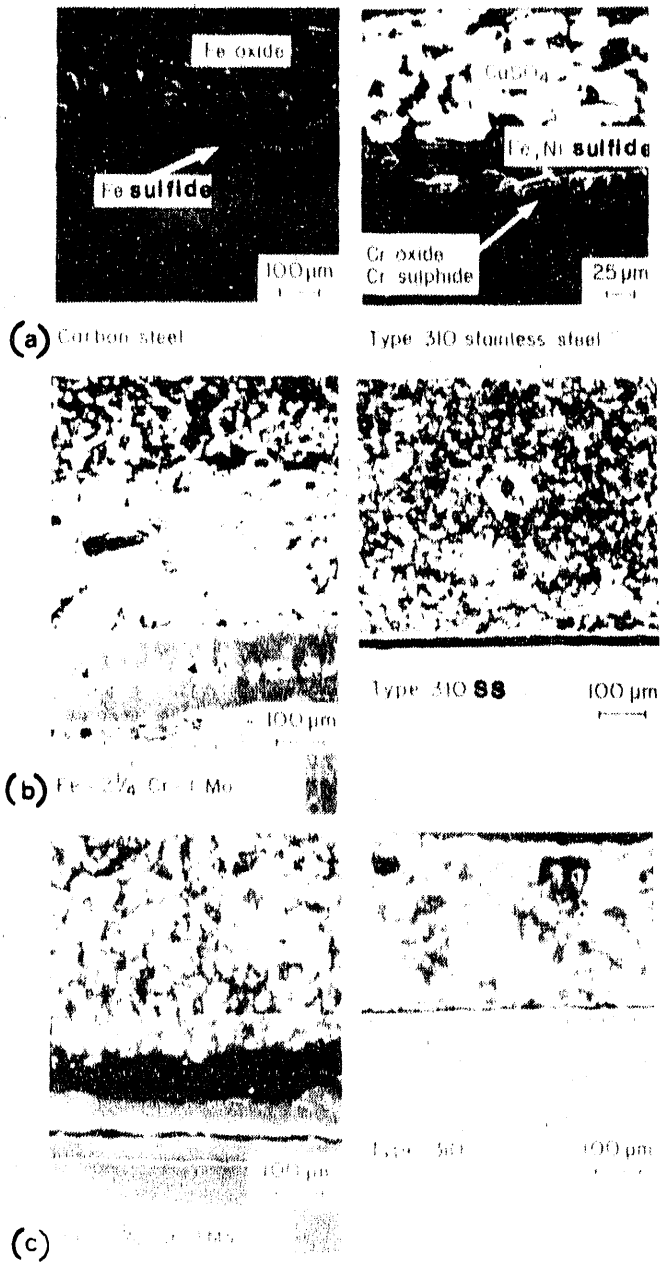

Fig. 42.
Morphological Features of CaSO4- and CaO-coated Alloys after 2000-h Exposures under Gas Cycling Conditions (gas temperature = 840°C, metal temperature = 593°C). (a) $CaSO_4$-coated, Run 155, cycle time = 100 h. (b) $CaSO_4$-coated, Run 168, cycle time = 10 h. (c) CaO-coated, Run 168, cycle time = 10 h.

without gas cycling (discussed earlier). The Type 310 stainless steel specimen in Run 155 (with 100-h gas cycling) formed a mixture of chromium oxide and chromium sulfide at the alloy side of the interface. In addition, an (Fe, Ni) sulfide phase was observed at the deposit/scale interface, and the depth of sulfur penetration into the substrate material was substantial. The Type 310 stainless steel specimens exposed in Run 168 (with 10-h gas cycling) had thin chromium oxide scales that were quite similar to those reported for specimens tested without gas cycling. These results indicate that an alternating gas environment with a cycle time of 10 h or less is not detrimental with regard to metal wastage by means of sulfidation corrosion.

EFFECTS OF GAS CYCLING WITH VARIATION IN p_{O_2} DURING A CYCLE

In the experiments discussed earlier, the high-p_{O_2}/low-p_{O_2} exposure time ratios were maintained at 1:1 whether the cycle time was 100 or 10 h. In Runs 170 and 171, the high-p_{O_2}/low-p_{O_2} exposure time ratios of 9:1 and 1:9 were used while maintaining the cycle time at 10 h. In these runs, the virgin specimens were exposed to a high-p_{O_2} environment during the first cycle. In Run 172, the high-p_{O_2}/low-p_{O_2} exposure time ratio of 1:9 was used with a cycle time of 10 h, but the virgin specimens were exposed to the low-p_{O_2} environment during the first cycle. The total exposure time in each of the three runs was 2000 h.

Figures 43 and 44 show the SEM photographs of $CaSO_4$- and CaO-coated specimens of Fe-2 1/4Cr-1Mo steel and Type 310 stainless steel after exposure in Runs 170 and 171, respectively. The morphological features and thicknesses of the scale layers in both alloys were similar to those observed in specimens exposed to fixed-p_{O_2} test conditions and gas cycling conditions with a cycle time of 10 h.

Figure 45 shows SEM photographs of $CaSO_4$-coated specimens of Fe-2 1/4Cr-1Mo and Type 310 stainless steel after a 2000-h exposure in Run 172, in which the virgin specimens were exposed to a low-p_{O_2} environment in the first cycle. As can be seen, the

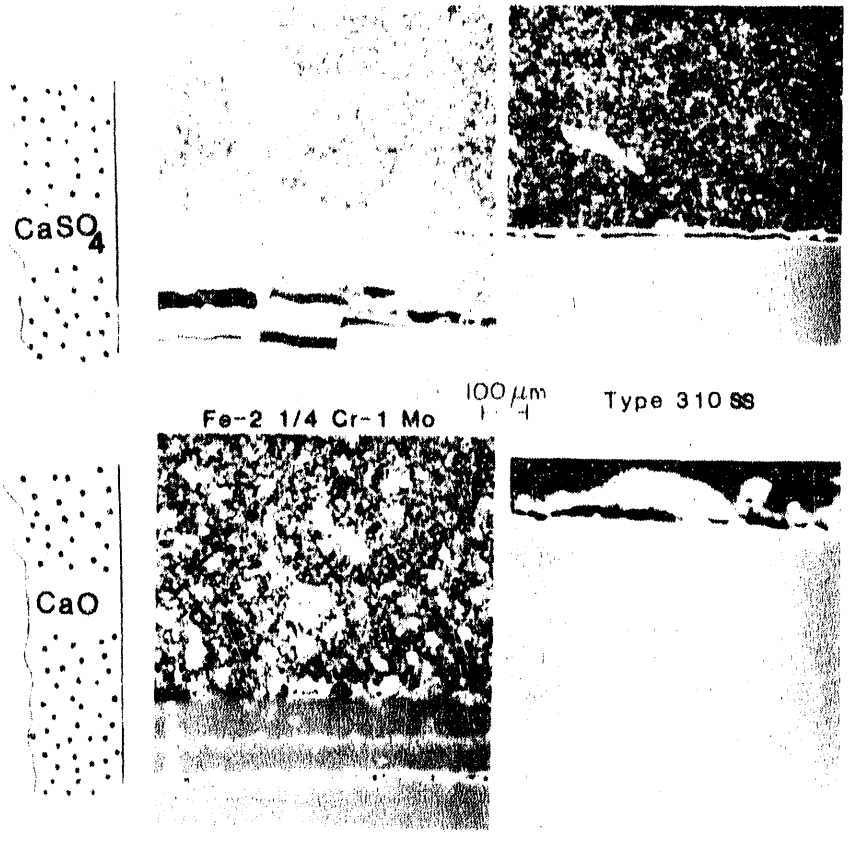

Fig. 43. Morphological Features of $CaSO_4$- and CaO-coated Alloy Specimens after 2000-h Exposure in Gas Cycling Experiment (Run 170) with High-p_{O_2}/Low-p_{O_2} Time Ratio of 9:1

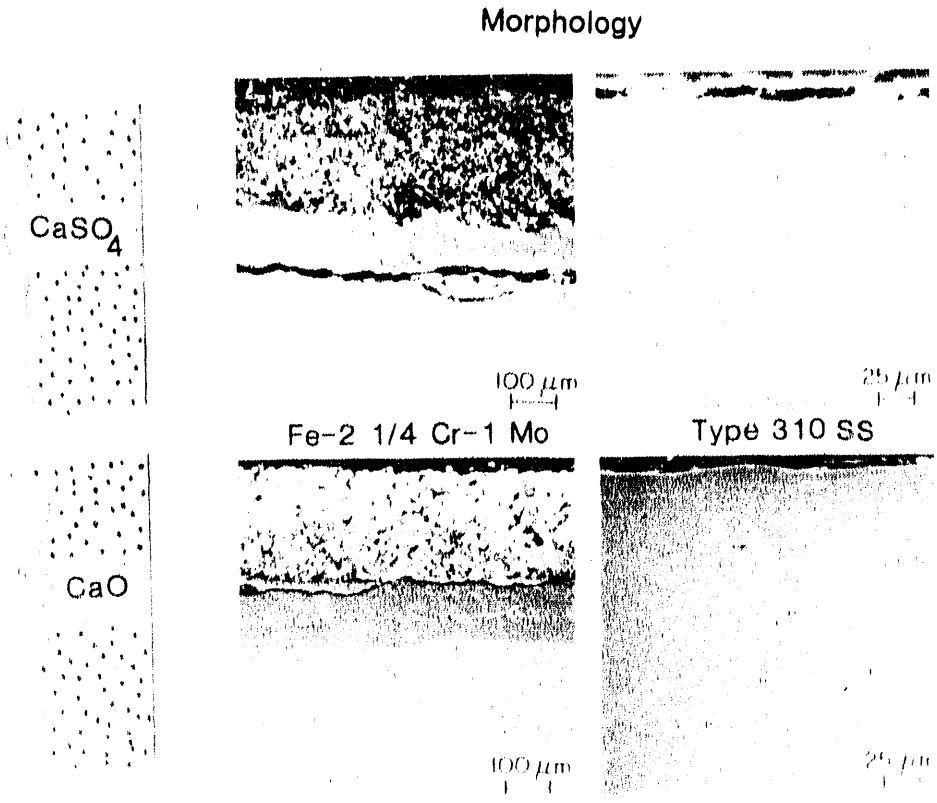

Fig. 44. Morphological Features of $CaSO_4$- and CaO-coated Alloy Specimens after 2000-h Exposure in Gas Cycling Experiment (Run 171) with High-p_{O_2}/Low-p_{O_2} Time Ratio of 1:9

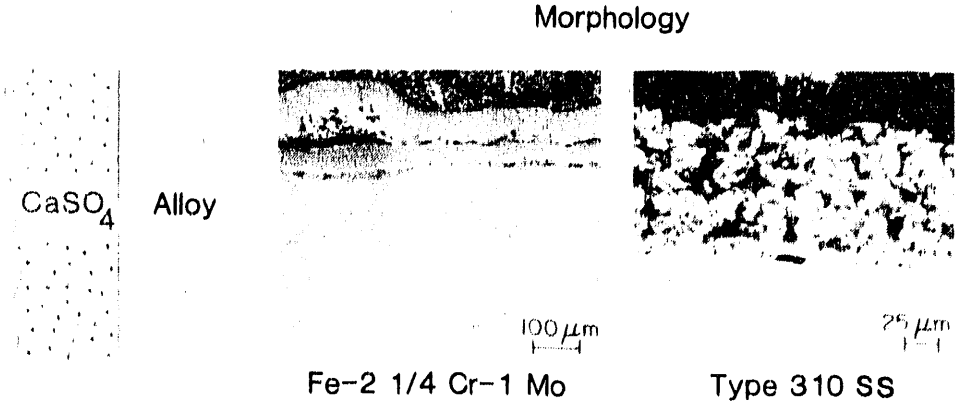

Fig. 45. Morphological Features of $CaSO_4$-coated Alloy Specimens after 2000-h Exposure in Gas Cycling Experiment (Run 172) with Low-p_{O_2}/High-p_{O_2} Time Ratio of 1:9

Fe-2 1/4Cr-1Mo steel developed a dual-layer scale consisting of external iron oxide and internal (Fe,Cr) sulfide. The Type 310 stainless steel specimen developed a very thin chromium oxide scale.

Figures 46 and 47 show the SEM photographs and elemental mapping of CaO-coated specimens of Fe-2 1/4Cr-1Mo and Type 310 stainless steel after a 2000-h exposure in Run 172. As in Run 157, the initial CaO deposit in these runs had reacted to form $CaSO_4$. The corrosion product layers consisted of external iron oxide and internal iron sulfide, and the thickness of the scale layer was 0.35 mm. In the case of a CaO-coated Type 310 stainless steel specimen exposed in Run 172, an initial exposure of the alloy to a low-p_{O_2} environment resulted in not only the conversion of CaO to $CaSO_4$, but also an enhanced oxidation/sulfidation attack of the underlying alloy. It was shown earlier (Fig. 23) that a CaO-coated Type 310 stainless steel developed a thin (Cr,Fe) sulfide layer upon exposure to a low-p_{O_2} atmosphere. The specimen in Run 172, even though exposed for only 1 h at the start of each cycle to the low-p_{O_2} atmosphere, developed a thick (Fe,Cr) oxide/sulfide scale after a 2000-h total exposure. These results indicate that the long-term corrosion behavior of an alloy (especially a high-chromium alloy) is strongly dependent on the rates of nucleation and growth of chromium oxide scale in the early stages of exposure. Any disruption (in the chromium oxide development) via formation of (Ca,Fe) oxide or sulfide nuclei leads to the development of a nonprotective, maybe porous, oxide/sulfide scale with increased corrosion wastage of the material.

IMPLICATIONS FOR CORROSION OF IN-BED TUBES AND SUPPORT STRUCTURES

The in-bed environment in FBC systems, in general, has p_{O_2} values in the range of 10^{-2} to 10^{-3} atm; however, fluctuations in p_{O_2} values to as low as 10^{-14} atm have been measured with an oxygen sensor. The time interval for fluctuations in the p_{O_2} values has been less than a second. Under these conditions, the heat exchanger materials and support structures will be exposed to an alternating high-p_{O_2}/low-p_{O_2} atmosphere with a cycle time of a second or less. The results presented in this paper indicate that an alloy are exposed to an alternating gas atmosphere with a cycle time of as long as 10 h and still exhibit acceptable corrosion performance at a metal temperature of 593°C. Initiation of the sulfidation mode of attack requires a sustained (between 10 and 100 h) exposure of the alloy to a low-p_{O_2} atmosphere. A low-p_{O_2} atmosphere may be prevalent near the coal feedports in an FBC system, and exposure of materials at these locations should be avoided. The present cycling experiments were conducted at p_{O_2} values of 7.5×10^{-9} and 7.0×10^{-3} atm at the gas temperature; the validity of the results for cyclic conditions with the much lower p_{O_2} value of 10^{-14} atm, which has been measured in FBC systems, must be verified.

The corrosion test results discussed thus far have established the influence of the chemistry of the oxygen/sulfur mixed-gas environment on the corrosion process, the effect of alloy chemistry on corrosion wastage, and the role of deposits in the wastage process. However, the long-term structural integrity of a given material is dependent on whether the material will undergo breakaway corrosion during service in the exposure environment. In general, the available information on the oxidation-sulfidation behavior of high-chromium structural alloys exposed to O_2-SO_2 gas mixtures indicates that the alloys develop predominantly oxide scales.

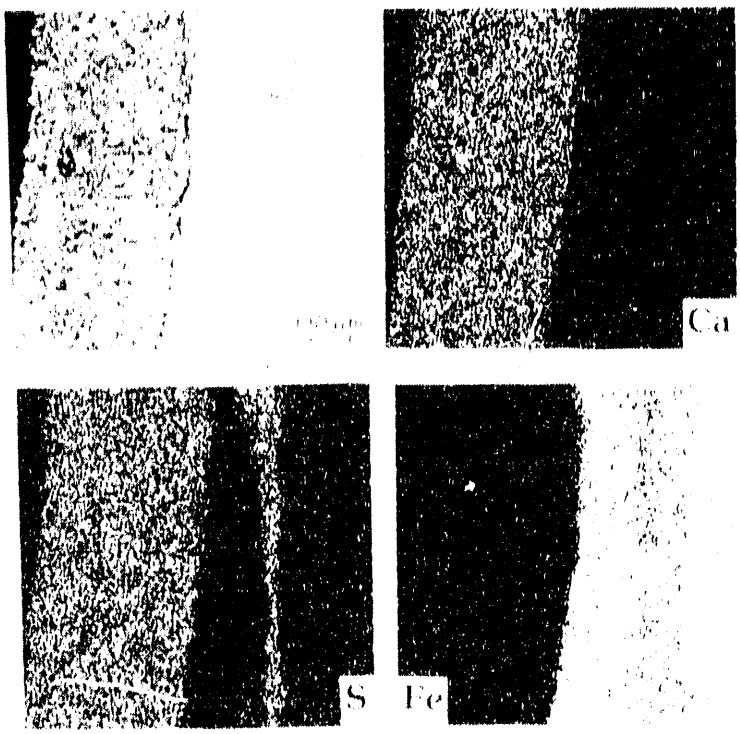

Fig. 46.
SEM Photograph and EDAX Elemental Mapping of CaO-coated Fe-2 1/4Cr-1Mo Steel Specimen after 2000-h Exposure in Gas Cycling Experiment (Run 172) with Low-p_{O2}/High-p_{O2} Time Ratio of 1:9

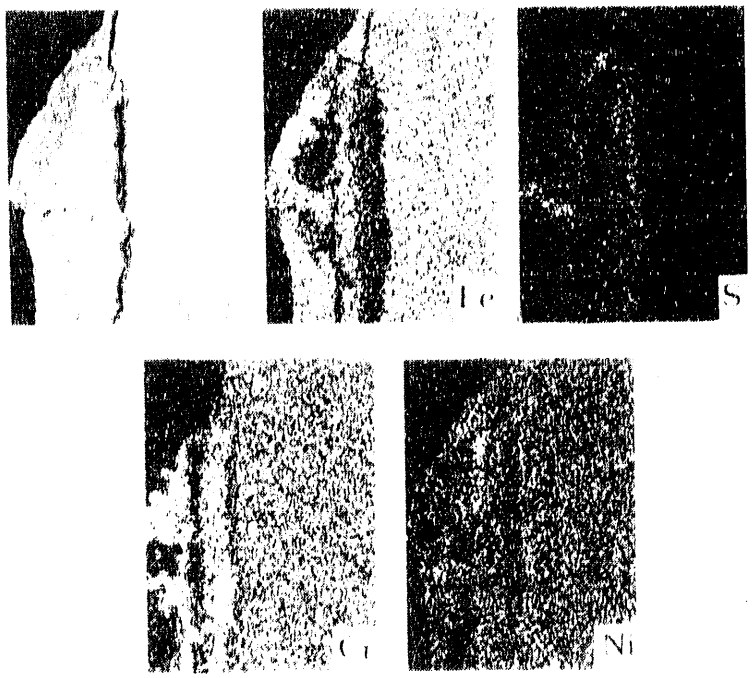

Fig. 47.
SEM Photograph and EDAX Elemental Mapping of CaO-coated Type 310 Stainless Steel Specimen after 2000-h Exposure in Gas Cycling Experiment (Run 172) with Low-p_{O2}/High-p_{O2} Time Ratio of 1:9

Figure 48 shows a schematic representation of corrosion scale development and morphological changes that occur in Cr_2O_3-forming alloys exposed to combustion atmospheres at elevated temperatures.[24] The high-chromium alloys generally develop porous oxide scales, with some sulfides in the inner portions of the scale (in the vicinity of scale/alloy substrate interface). The sulfides form by reactions between substrate elements

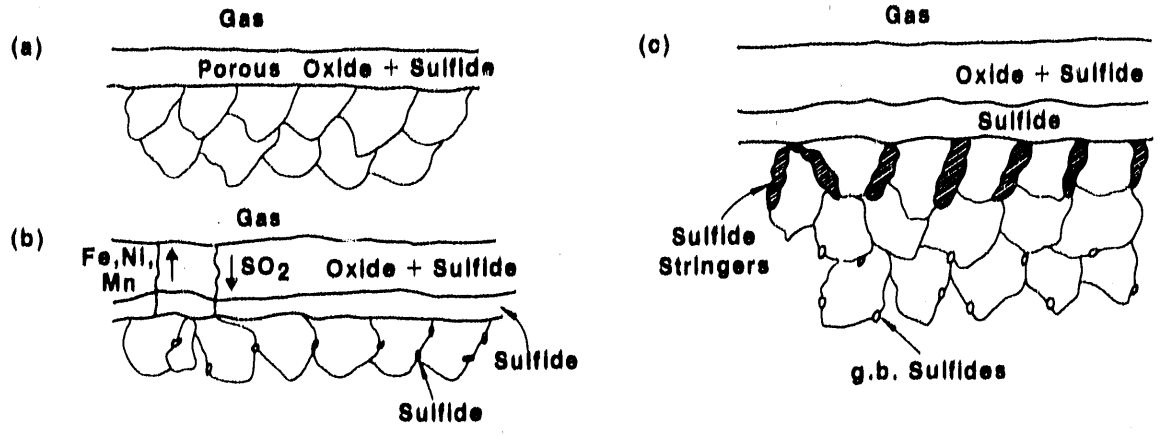

Fig. 48. Schematic Representation of Reaction Sequence for High-chromium Alloys Exposed to Combustion Environments (O_2/SO_2)

and sulfur that is released when chromium reacts with SO_2 to form an external oxide scale. The porosity present in the scale enables further molecular transport of SO_2 in the gas phase to the scale/substrate alloy interface, leading to further oxidation/sulfidation. The sulfur that is released is transported along he grain boundaries in the metal, leading to internal sulfidation of the alloy. Generally, for high-chromium alloys exposed to combustion atmospheres, the thicknesses of oxide scales are fairly small and insensitive to time of exposure. As a result, the acceptable lifetimes for these alloys, when exposed to combustion atmospheres, are influenced by the magnitude of the depth of internal penetration, which is largely determined by the alloy chemistry, temperature, SO_2 content of the gas phase, and the physical and chemical nature of the deposit.

The results from the present work also show that a combination of $CaSO_4$ or CaO as a deposit and the presence of low p_{O_2} in the gas phase leads to initiation of sulfidation of high-chromium alloys; the 2000-h test data showed that Incoloy 800 is particularly susceptible even at 593°C, whereas Type 310 stainless steel is affected at higher temperatures. The present experiments also indicate that, for acceptable corrosion performance (i.e., an oxidation mode of interaction), the alloy should develop a continuous chromium oxide scale in the early stages of exposure. Consequently, the long-term performance of materials in FBC systems at temperatures above 625°C may strongly depend on the startup conditions imposed on the in-bed materials as well as on the control of the bed chemistry to maintain fairly oxidizing conditions for structural materials during service.

EFFECT OF SPENT-BED MATERIALS

Thus far, we have presented corrosion test results obtained from alloys that were exposed in the presence of reagent-grade compounds. During the course of this work, spent-bed materials were obtained from several large FBC test facilities and these materials were used as deposits in the laboratory corrosion experiments.

EFFECT OF BUBBLING-BED DEPOSITS

As previously stated, the in-bed environment in bubbling-bed combustion systems, in general, has p_{O_2} values from 10^{-2} to 10^{-3} atm; however, fluctuations in p_{O_2} values, to as low as 10^{-14}, have been measured with an oxygen sensor. The time interval for fluctuations in

the p_{O_2} values has been less than 1 s. Under these conditions, the heat exchanger materials and support structures are exposed to an alternating high-p_{O_2}/low-p_{O_2} atmosphere with a cycle time of 1 s or less. To evaluate the effect of spent-bed materials on the corrosion of candidate materials, three gas environments (identified as A, B, and C in Fig. 49) were selected. Gas mixture A has p_{O_2} and p_{S_2} values of 7×10^{-3} and 2.6×10^{-28} atm, respectively, typifying a flue-gas environment. Gas mixture B has p_{O_2} and p_{S_2} values of 5.4×10^{-12} and 1.6×10^{-8} atm, respectively, representing a reducing environment during gas cycling. Gas C has a p_{O_2} value of 3.6×10^{-14} atm, contains no sulfur, and represents a reducing atmosphere without sulfur. It has been shown earlier[3,5] that sustained exposure (500 to 2000 h) of structural materials to gas mixture B in the presence of a $CaSO_4$ or $CaSO_4/CaO$ deposit can lead to internal sulfidation of alloys. As a result, gas mixtures A and C were used along with the spent-bed materials from various FBC systems to evaluate corrosion susceptibility of candidate materials.

The SEM photographs in Fig. 50 show scale layers that developed on Incoloy 800 and Type 310 stainless steel specimens that were coated with a reagent-grade $CaSO_4/CaO$ mixture and spent-bed materials from the TVA AFBC and IEA/G PFBC facilities. The top row of photographs, which shows the morphologies that developed when Incoloy 800 specimens with the deposits were exposed to gas mixture A (typical flue-gas atmosphere), reveals that the specimens developed thin chromium oxide scales in the presence of all three deposits. The middle row of photographs shows that, when deposit-coated Incoloy 800 was exposed to a gas mixture of low-p_{O_2} and no sulfur, the scales that developed were predominantly Fe and (Fe,Cr) oxide and (Fe,Ni) sulfide. Such scales are nonprotective. Scale layer thicknesses ranged from 0.30 to 1.2 mm; the thicker layers in the presence of spent-bed materials are indicative that the bed material is more aggressive toward Incoloy 800 than it is toward that of the reagent-grade material. Further, the source of sulfur for sulfidation of these specimens is the deposit material, because the gas phase included no sulfur-containing species. Also, in the absence of deposits (i.e., absence of a sulfur source), Incoloy 800 specimens would have developed thin chromium oxide scales when exposed to the low-p_{O_2} atmosphere used in these tests. The bottom row of photographs shows that,

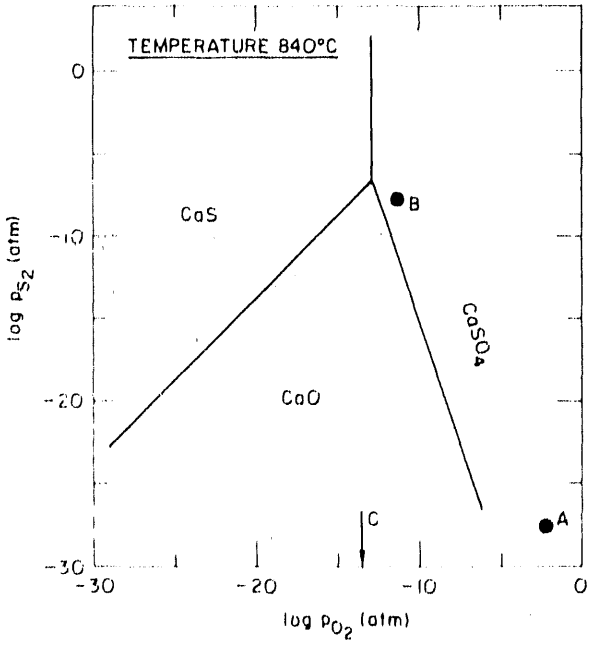

Fig. 49.
Ca-S-O Stability Diagram, Indicating Gas Environments A, B, and C Used in Experiments with Deposit Materials from Various FBC Facilities

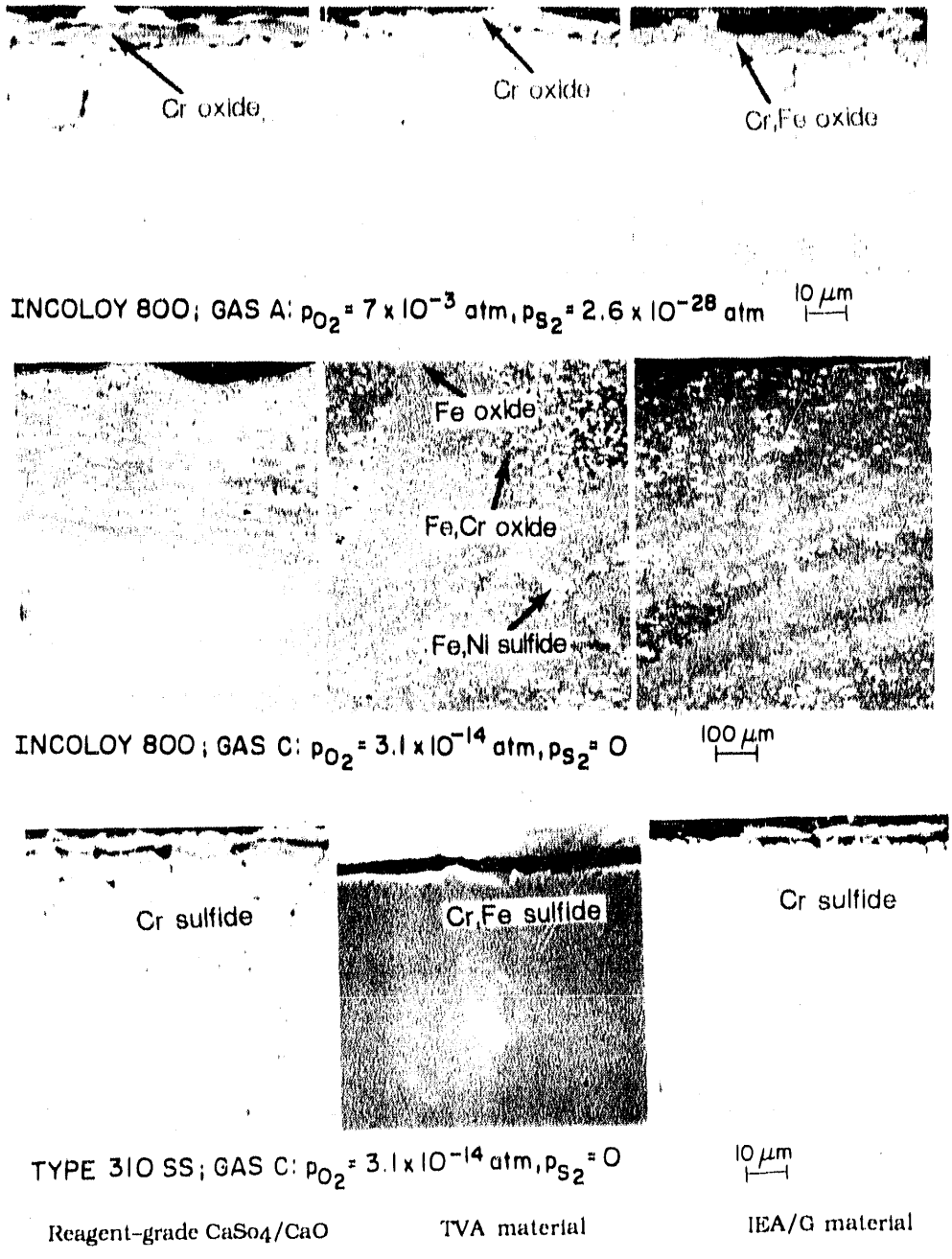

Fig. 50. Corrosion Scale Morphologies that Developed on Incoloy 800 and Type 310 Stainless Steel Specimens Coated with a Reagent-grade CaO-$CaSO_4$ Mixture or Spent-bed Materials from TVA and IEA/G and Exposed to Various Gas Mixtures

when Type 310 stainless steel specimens with the deposits were exposed to a sulfur-free low-p_{O2} atmosphere, the scales that formed were thin and composed of oxide and sulfide phases, with some intergranular precipitation of sulfides in the substrate alloy. These results conclusively indicate that the composition of the deposit material, the local gas-

phase environment, and alloy chemistry must be considered in an evaluation of oxidation-sulfidation behavior of candidate heat exchanger materials for FBC applications.

CORROSION IN BUBBLING-BED AND CIRCULATING-FLUID-BED ENVIRONMENTS

Extensive testing of materials (see Table 6 for a listing of chemical compositions) has been conducted to develop corrosion information on a variety of ASME-coded and noncoded structural alloys, coatings, and weldments in well-characterized laboratory environments that simulate both bubbling- and CFB atmospheres.[23] In these experiments, ring specimens that simulate the heat exchanger tubes were exposed to an environment arising from the combustion of coal. In addition, experimental alloys were exposed in the form of flat coupons to evaluate their corrosion resistance. The outer surfaces of the ring specimens and one surface of the flat coupons were coated with either reagent-grade $CaSO_4$ (simulating a bubbling-bed deposit) or CFB ash. The specimens were exposed for 3000 h at a metal temperature of 871°C while the gas phase was maintained at ≈900°C. The corrosion test probes were cooled to room temperature after every 500 h of exposure at the test temperature. During the cooldown period, the specimens were recoated with the deposit material to ensure that there was no lack of reactant for continuation of the corrosion process. Gas mixture B (see Fig. 49) and compressed air were used to simulate the bubbling-bed and CFB conditions, respectively.

During the course of this study, deposits from the corrosion probes were collected after every 500 h and analyzed. The specimens were recoated with fresh $CaSO_4$ deposit material after every 500 h of exposure, prior to continuation of the tests. Table 7 lists the composition of the deposits at various times for both the bubbling- and CFB simulations. In the bubbling-bed case, initially pure reagent-grade $CaSO_4$ decomposed as a function of time, and after 500 h of exposure, the deposit contained 51.2 wt.% CaO and only 7.9 wt.% $CaSO_4$. Because gas B (with lower p_{O_2} and higher p_{S_2} than a flue gas atmosphere) was used in this simulation, the dissociation of $CaSO_4$ was favored within the deposit and the sulfur released by the dissociation reaction led to sulfidation of the substrate alloy. No Cr_2O_3 phase was detected in the deposit material. As exposure time increased beyond ≈1000 h, the extent of $CaSO_4$ dissociation decreased and the process was probably controlled by the transport of sulfur and oxygen through the already-formed scale. In the CFB simulation, the initial composition of the ash changed very little with exposure time. During the initial ≈500 h, the deposit contained Cr_2O_3 and some additional Fe_2O_3, indicating oxide scaling in this simulation. These results indicate that the deposit chemistry is influenced both by the gas chemistry in the exposure environment and the scaling kinetics at the alloy/deposit interface. Consequently, the local p_{O_2} and p_{S_2} within the deposit can vary widely and change with time, at least in the early periods of exposure.

Figure 51 shows the corrosion product morphologies observed on the deposit side of Types 304 and 310 stainless steel and Incoloy 800 specimens after 3000-h exposures in the two test environments. The figure shows that Type 304 stainless steel with ≈18 wt.% Cr developed predominantly (Cr,Fe) oxide scales in the presence of either deposit. The scale thicknesses were fairly small, and the substrate exhibited significant carbide precipitation at the grain boundaries. $CaSO_4$-coated Type 310 stainless steel, even though it contained 25 wt.% Cr,

Table 6. Chemical Composition of Alloys, Claddings, and Coatings Used in BFB and CFB Simulation Tests (wt.%)

Material	C	Cr	Ni	Mn	Si	S	Mo	Cu	Al	Fe	Other
304	0.08	18.34	8.10	1.50	0.27	0.018	0.27	0.16	-	Bal.[a]	-
800	0.08	20.12	31.70	0.96	0.24	0.006	0.30	0.73	0.39	Bal.	Ti 0.31
RA 330	0.05	18.59	35.14	1.13	0.92	0.006	0.18	0.10	-	Bal.	Nb 0.12
310	0.07	25.00	18.73	1.21	0.64	0.006	0.002	0.14	-	Bal.	-
316	0.05	17.27	13.79	1.60	0.73	0.016	2.20	0.17	-	Bal.	-
188	0.08	23.4	23.3	0.7	0.4	-	0.6	-	-	1.4	Co 35.7, Al 0.22, W 14.6, La 0.05
430	0.12	17.0	-	1.0	0.03	-	-	-	-	Bal.	-
CoCrALY/800H	-	22.6	4.9	-	0.53	-	-	-	12.4	1.0	Co 59.5, Y 0.65
21-33 Nb-Mn FM[b]	0.19	22.2	33.1	1.58	0.35	-	-	-	-	Bal.	-
309 FM	0.11	23.0	14.7	0.54	0.74	-	-	-	-	Bal.	-
347	0.079	17.68	12.37	1.77	0.37	0.002	-	-	-	Bal.	Nb 0.69
IN82 FM	0.02	18.7	Bal.	3.9	0.30	-	0.68	-	-	2.74	Nb/Ta 2, Ti 0.07
308L FM	0.025	21.0	10.0	1.75	0.40	-	-	-	-	Bal.	-
253MA	0.10	20.7	10.9	0.3	1.8	-	-	-	-	Bal.	Ce 0.03
HK40	0.40	28.0	20.0	2.0	2.0	-	0.5	-	-	Bal.	-
FW-4C	0.054	19.5	20.0	4.9	2.60	-	-	-	1.4	Bal.	-
HR-3C	0.06	24.8	2.04	1.24	0.40	-	-	-	-		Nb 048, N 0.247
Mn-Nb Mod. 800H	0.069	22.09	30.32	4.48	0.13	0.003	-	-	-	Bal.	Nb 0.91, N 0.042, Ce 0.08
54E	0.016	21.79	24.98	4.99	0.10	-	1.92	-	-	Bal.	N 0.087
53C	0.016	21.5	17.14	4.90	0.12	-	-	-	-	Bal.	N. 0.251
RV 8413	0.005	18.53	0.06	0.001	0.025	0.003	-	-	5.91	Bal.	Hf 0.50
IC-50	-	-	Bal.	-	-	-	-	-	12.2	-	Hf 1.7, B 0.05
FA-41	-	-	-	-	-	-	-	-	15.0	Bal.	TiB2 1.0
IC-266	-	8.2	Bal.	-	-	-	-	-	9.3	-	Zr 1.8, B 0.02

[a]Bal. = balance.
[b]FM = filler metal only.

Table 7. Variation in Chemical Composition of Deposits in Simulated BFB and CFB Environments as a Function of Exposure Time (wt.%)

Deposit Component	Exposure Time (h)						
	0	500	1000	1500	2000	2500	3000
BFB Simulation							
$CaSO_4$	99.2	7.9	5.1	-	71.7	63.7	69.2
CaO	0	51.2	57.8	-	21.7	22.8	26.0
SiO_2	0	3.8	-	-	2.4	1.4	1.9
Al_2O_3	0	0.3	-	-	0.2	0.2	0.1
Fe_2O_3	0	0.5	-	-	2.1	1.4	2.0
LOI[a]	-	35.5	23.7	-	1.9	10.4	0.7
CFB Simulation							
$CaSO_4$	6.5	12.4	8.8	10.0	10.6	8.7	10.5
CaO	-	2.2	4.4	4.0	3.6	5.0	4.0
SiO_2	51.4	37.0	40.8	43.2	43.4	44.0	43.8
Al_2O_3	20.2	17.2	35.9	32.8	31.7	31.1	31.5
Fe_2O_3	9.1	11.9	8.4	6.8	6.9	8.0	7.1
Cr_2O_3	0	16.7	2.3	-	-	-	-
LOI[a]	3.1	0.5	0.5	0.6	0.6	0.5	0.5

[a]Loss on ignition.

developed a ragged oxide scale with substantial internal penetration of sulfur. On the other hand, CFB-ash–coated Type 310 stainless steel developed chromium oxide scale, and virtually no sulfur was detected in either the scale or the substrate alloy. In general, Type 310 stainless steel was susceptible to formation of (Fe,Cr) sigma phase during thermal exposure. An Incoloy 800 specimen coated with reagent-grade $CaSO_4$ underwent severe sulfidation, indicating susceptibility of a higher nickel (32.5 wt.%) alloy to sulfur attack. On the other hand, the same alloy coated with CFB ash developed a (Cr,Fe) oxide scale (with no trace of sulfur), indicating that negligible sulfur pressure was established by dissociation of sulfur-containing ash components in the deposit layer. RA-330 alloy coated with $CaSO_4$ developed a scale consisting of an oxide-sulfide mixture. Because the scale was nonprotective, some internal sulfidation of the substrate material was observed. Type 347 stainless steel coated with CFB ash developed a (Cr,Fe) oxide scale with virtually no trace of sulfur in either the scale or the substrate.

Figures 52–54 are SEM photographs of the morphologies of corrosion product layers developed in several coupon alloys in the presence of $CaSO_4$ and CFB ash deposits. Alloy 253MA, which contained 1.8 wt.% Si, exhibited (Cr,Fe) sulfide and (Cr,Fe) oxide scales in the presence of $CaSO_4$ and CFB ash, respectively. An increase in the silicon content to 1.8 wt.% from 0.3–0.4 wt.% in conventional austenitic steels did not improve the corrosion resistance of the alloy in the presence of the $CaSO_4$ deposit. Alloys 54E and 53C developed predominantly chromium oxide and (Cr,Mn) oxide, respectively, in the presence of either deposit examined in these tests. Alloy RV 8413 developed thin alumina scales in both tests;

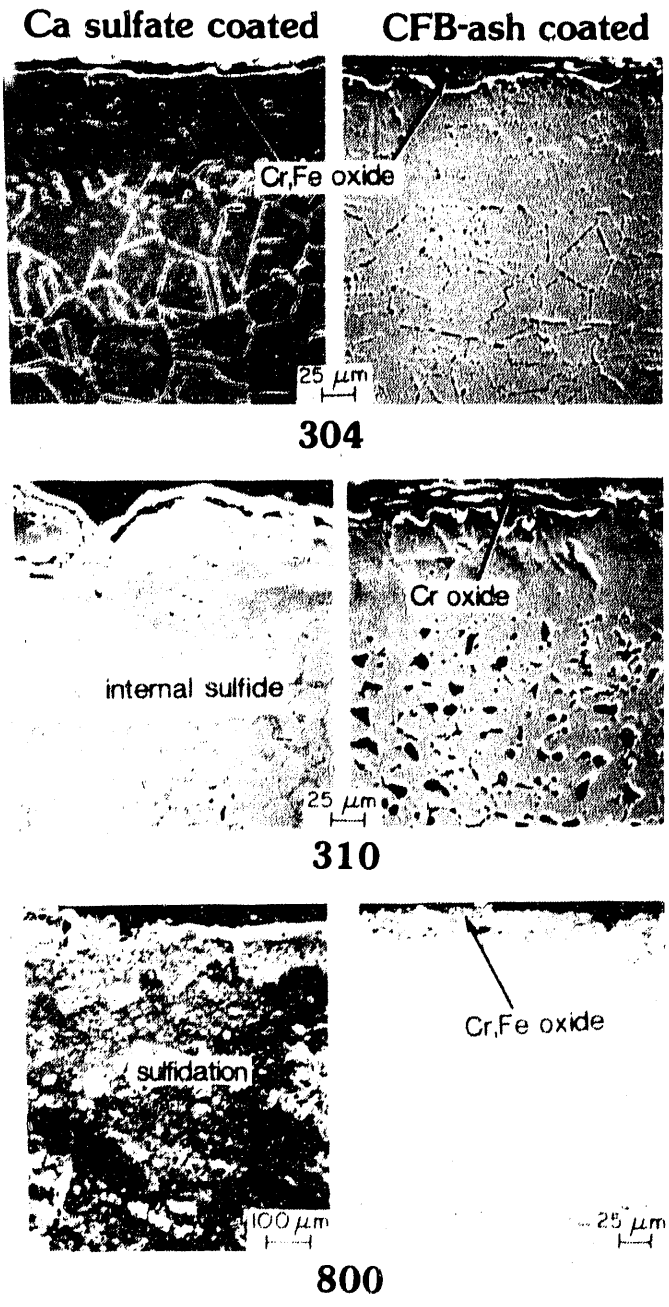

Fig. 51.
Microstructures of Types 304 and 310 Stainless Steel and Incoloy 800 with Either $CaSO_4$ or CFB-Ash Deposit after 3000-h Exposure at 871°C

however, significant precipitation of (Fe,Cr,Hf) intermetallic particles was observed in the alloy substrate. The nickel aluminide material IC-50 developed a nickel sulfide phase, the extent of sulfidation attack being more severe in the presence of $CaSO_4$ than CFB ash. Inasmuch as the Ni-Ni_3S_2 eutectic is at 645°C in prolonged exposures, the alloy will undergo catastrophic corrosion because the protective alumina scale will be destroyed by liquid sulfide. The iron-base aluminides with TiB_2 (alloy FA-41) formed aluminum-rich oxide scales in the presence of either deposit. No internal penetration of the substrate alloy was noted; however, fine (Fe,Al) intermetallic particles were obtained due to exposure at an elevated temperature. The preoxidized alloy IC-266 exhibited massive sulfidation in

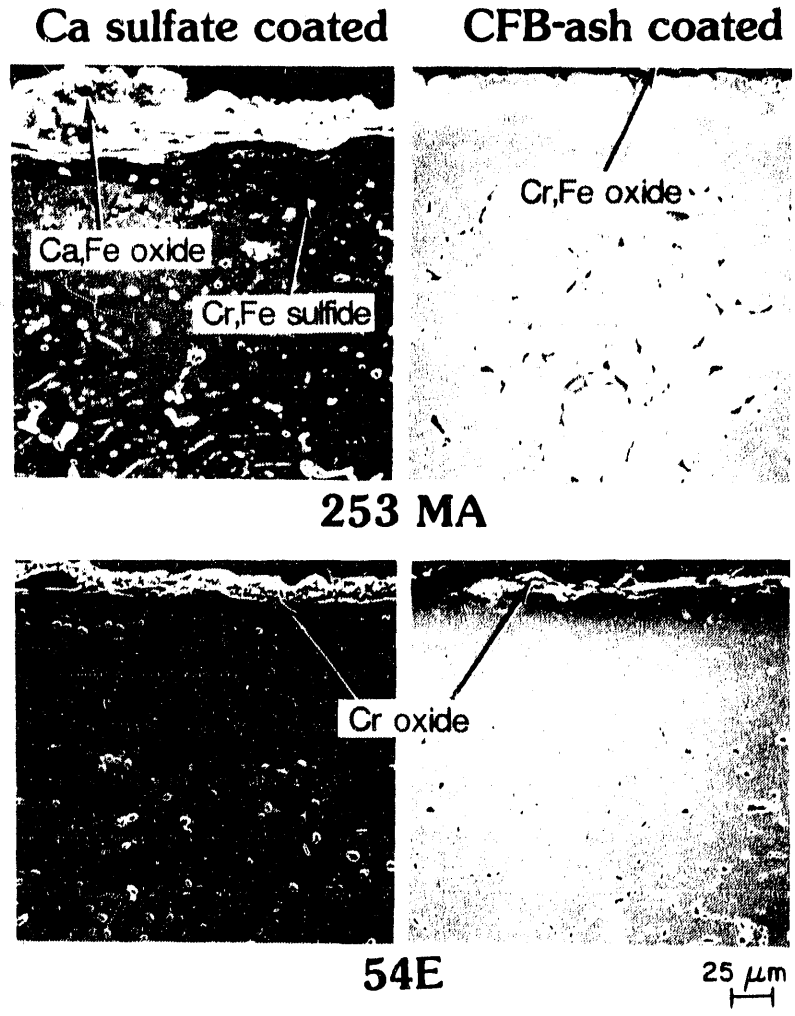

Fig. 52. Microstructures of Coupon Specimens of Alloys 253MA and 54E after 3000-h Exposure in Presence of $CaSO_4$ and CFB-Ash Deposits

the presence of $CaSO_4$ deposits, but the preoxidized layer was fairly intact when the sample was tested with CFB ash. Similar corrosion information for weldments and clad alloys after exposure to simulated FBC environments has been developed and is reported elsewhere.[23]

Table 8 is a summary of data on scale thickness, depth of penetration, and metal recession for several alloys exposed for 3000 h at temperatures between 871 and 900°C in simulated bubbling-bed and CFB environments. The contrasting corrosion behavior of several alloys in the presence of $CaSO_4$ and CFB ash deposits indicates that the p_{S_2} established by the $CaSO_4$ deposit and the low-p_{O_2} gas environment (simulating a bubbling bed) is much higher than that present in a CFB ash/air atmosphere (simulating a CFB).

IN-BED MATERIALS DATA

In the preceding sections, we showed that materials (especially high-chromium alloys exposed to an FBC environment) can undergo corrosion by oxidation-sulfidation and that life expectancy of components is strongly influenced by the internal sulfidation penetration of

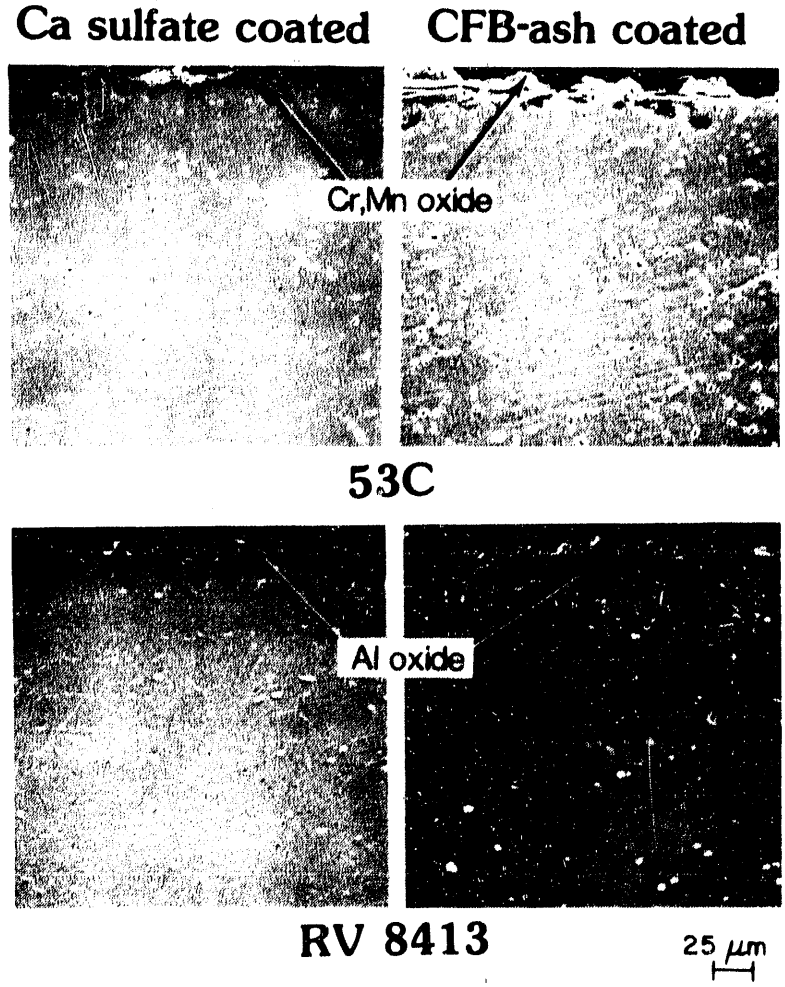

Fig. 53. Microstructures of Coupon Specimens of Alloys 53C and RV 8413 after 3000-h Exposure in Presence of $CaSO_4$ and CFB-Ash Deposits

the substrate materials. Furthermore, the bed chemistry in terms of p_{O_2} and p_{S_2} is not uniform; therefore, different tubes in a heat exchanger, although made of the same alloy, could be exposed to widely differing and varying (oxidizing to reducing) conditions in the bed. To be a viable candidate for use in FBC system, an alloy must exhibit acceptable corrosion rates, even under the most extreme in-bed reducing conditions ($p_{O_2} = 10^{-12}$ to 10^{-14} atm). In general, metallic heat exchanger tubes are coated with a dense and sometimes thick deposit, the composition of which depends on gas chemistry, exposure time, and temperature. In-bed bubbling-bed wastage data, developed over the years, in general, indicate that the erosion contribution will not be significant for components that operate between 650 and 900°C; however, the erosion processes in FBCs systems are not well understood and a few instances of unanticipated catastrophic erosion of in-bed cooling tubes have been reported. Thus, the interpretation of metal wastage data calls for caution. These difficulties not withstanding, the materials data base was reviewed earlier[25,26] to evaluate the time and temperature dependence of the wastage, scale thickness plus internal penetration, and corrosion rates for several alloys or classes of alloys tested in FBC systems.

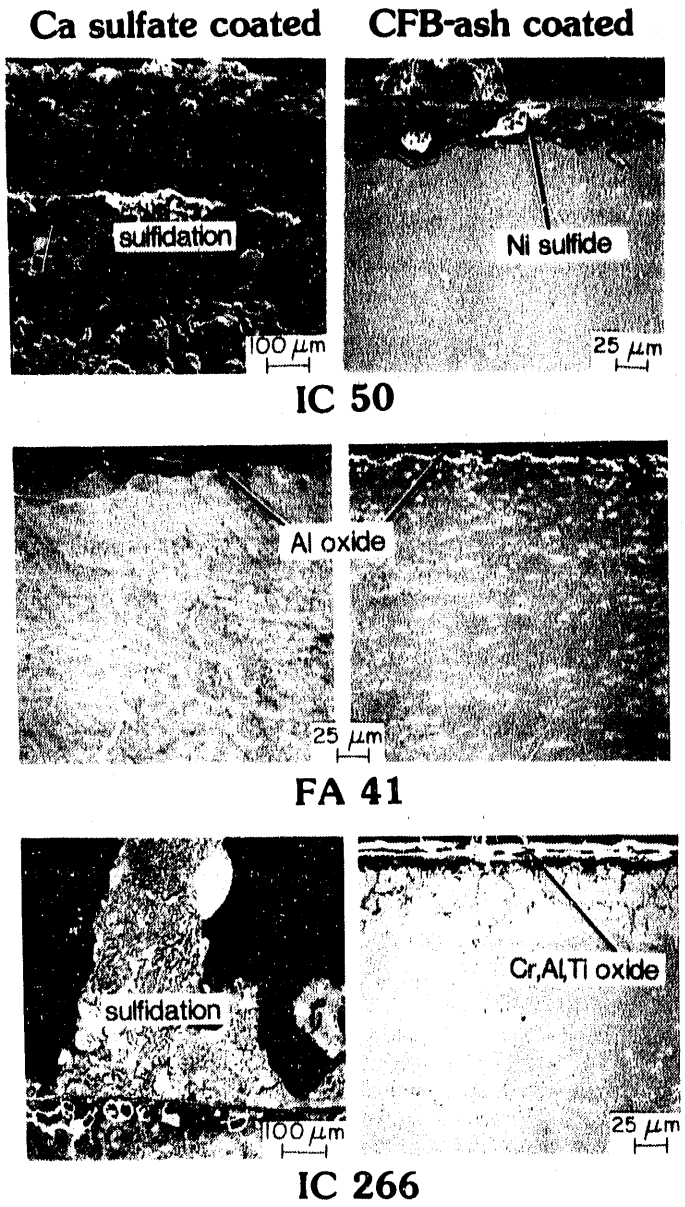

Fig. 54.
Microstructures of Coupon Specimens of Aluminide Alloys IC-50, FA-41, and IC-266 after 3000-h Exposure in Presence of $CaSO_4$ and CFB-Ash Deposits

The data for a few of the alloys are summarized below for comparison with the data developed in the laboratory test program.

Figure 55 is a plot of the scale thickness alone and scale thickness plus penetration depth as a function of in-bed exposure time for Type 304 stainless steel tested at temperatures between 810 and 871°C in several FBC systems. The data indicate that the scale thickness is negligibly small and increases to a constant value after 2000 h of exposure. The depth of penetration is approximately three times that of scale thickness and probably tends to increase with exposure time. One may infer from the data that the alloy has not undergone "breakaway" corrosion during exposure. Figure 56 ia similar plot of total corrosion as a function of exposure time for the steel tested at temperatures between 650 and

Table 8. Average Scale Thickness and Depth of Penetration, and Metal Recession Data for Several Alloys Exposed for 3000 h in Simulated FBC Environments (μm)

Material	With $CaSO_4$		With CFB Ash		Metal Recession	
	Average Scale Thickness	Average Depth of Penetration	Average Scale Thickness	Average Depth of Penetration	With $CaSO_4$	With CFB Ash
Internally Cooled Rings (metal temp. 871°C)						
304	20	23	24	14	65	134
800	Destroyed		27	30	-	128
RA 330	70	150	NE[a]	-	193	NE
310	70	230	17	C2	250	160
316	10	40	NE	-	98	NE
188	Internal attack		NR	-	-	NE
347	NE	-	32	40	NE	210
Coupons (metal temp. 899°C)						
253 MA	30	65	33	18	105	70
HK40	Destroyed		NE	-	-	NE
FW-4C	5	100	NE	-	203	NE
HR-3C	20	65	NE	-	125	NE
Mod. 800H	Destroyed		NE	-	-	NE
430	NE	-	120	48	NE	340
54E	30	33	33	30	50	84
53C	10	16	30	30	50	84
RV 8413	15	4	15	18	15	45
IC-50	Destroyed		50	30	-	80
FA-41	10	7	15	18	15	30
IC-266[b]	Destroyed		18	72	-	90

[a]NE = not exposed.
[b]Preoxidized sample.

700°C. Figure 57 shows a plot of corrosion rate for Type 304 stainless steel against in-bed exposure temperature obtained over a wide range of conditions and exposure times in several FBC test facilities. Corrosion rates were calculated under the assumption that parabolic kinetics (i.e., the amount of degradation is proportional to the square root of the duration of exposure) were operative for both scale thickness and penetration depth. In some instances, where scale thickness and penetration data are not reported, the metal loss information was used to calculate corrosion rates.

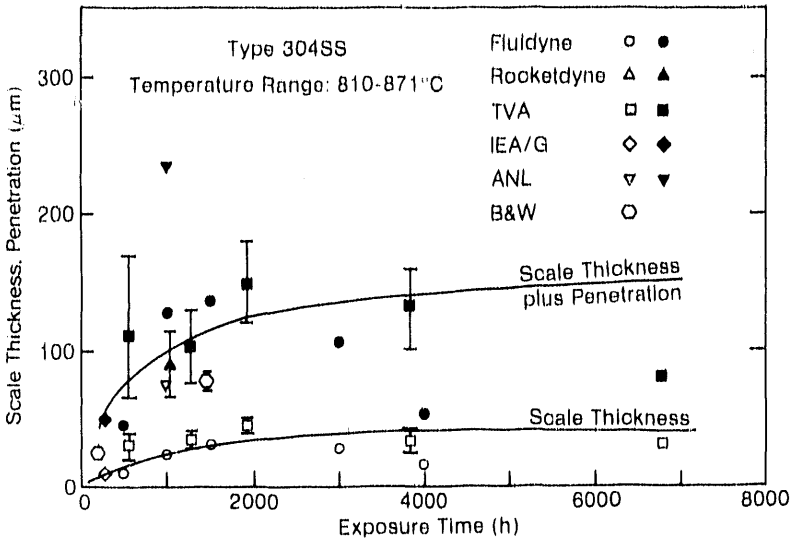

Fig. 55.
Scale Thickness and Penetration Depth for Type 304 Stainless Steel at Temperatures between 810 and 871°C

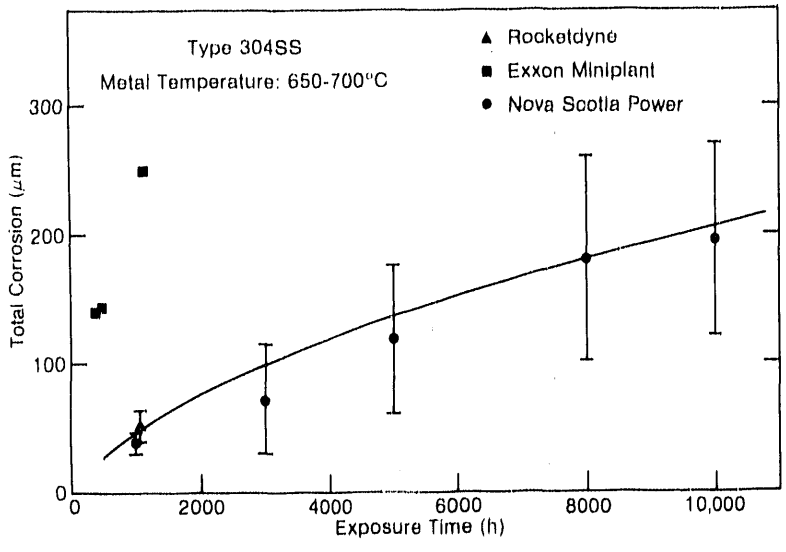

Fig. 56.
Total Corrosion of Type 304 Stainless Steel at Temperatures between 650 and 700°C

Figure 58 is a plot of the scale thickness alone and scale thickness plus penetration depth versus in-bed exposure time for Type 310 stainless steel at temperatures between 810 and 871°C in several FBC systems. The corrosion behavior of this steel is similar to that of Tpe 304 stainless steel; however, for a given exposure time, the depth of penetration for 310 steel is somewhat lower than for 304 steel. In addition, the 10,000-h data from the Nova Scotia test facility show acceptable corrosion behavior for this alloy. Figure 59 is a plot of corrosion rate for Type 310 stainless steel versus in-bed exposure temperature obtained over a wide range of conditions and exposure times in several FBC test facilities. A comparison of the laboratory and in-bed corrosion data shows that the former is higher by a factor of two; however, the laboratory data were obtained in an environment that was much more reducing (i.e., p_{O_2} and p_{S_2} in the vicinity of the CaO-CaS-$CaSO_4$ triple point) and can be considered an upper-bound rate for the material from the standpoint of corrosion.

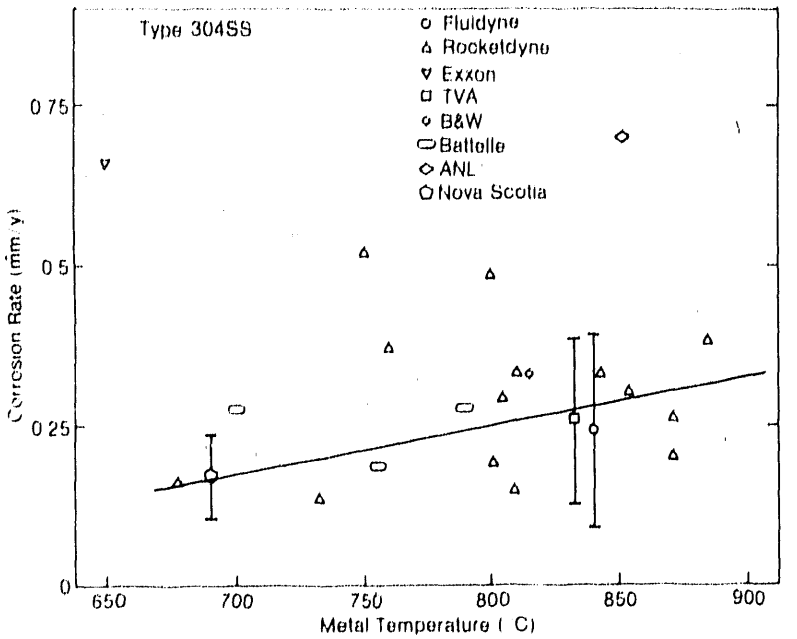

Fig. 57.
Variation of Corrosion Rate with Temperature for Type 304 Stainless Steel

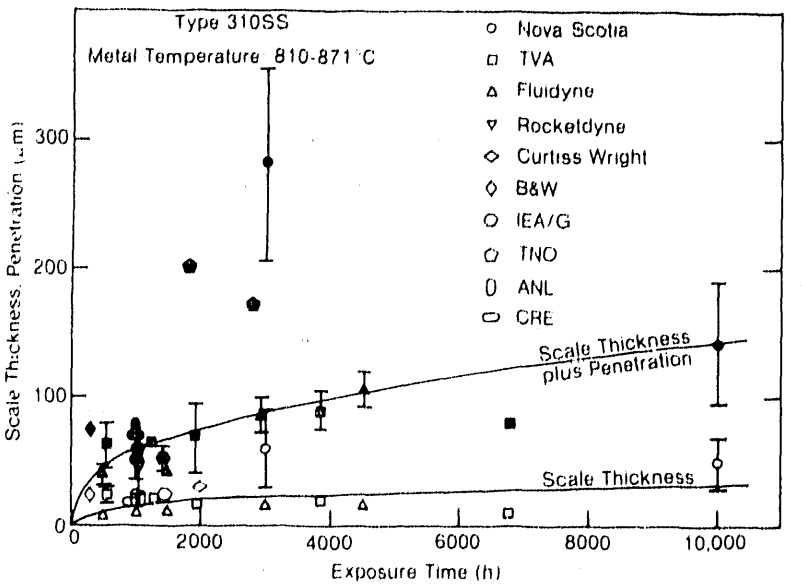

Fig. 58.
Scale Thickness and Penetration Depth Data from Several FBC Facilities for Type 310 Stainless Steel

Figure 60 is a plot of scale thickness and depth of penetration for Incoloy 800 versus exposure time in various FBC systems. It is evident from this figure that, although the scale thickness is fairly insensitive to exposure time beyond ≈2000 h, the penetration depth increases dramatically, especially in the 10,000-h-exposure results from the Nova Scotia facility. Figure 61 shows the corrosion rate, based on parabolic kinetics, as a function of alloy exposure temperature. Over the entire temperature range, the corrosion rate is approximately twice that observed for Type 310 stainless steel. Furthermore, the long-time performance of the alloy is not promising, because the life-limiting parameter, namely, the internal penetration depth, increases significantly with exposure time. In addition, the

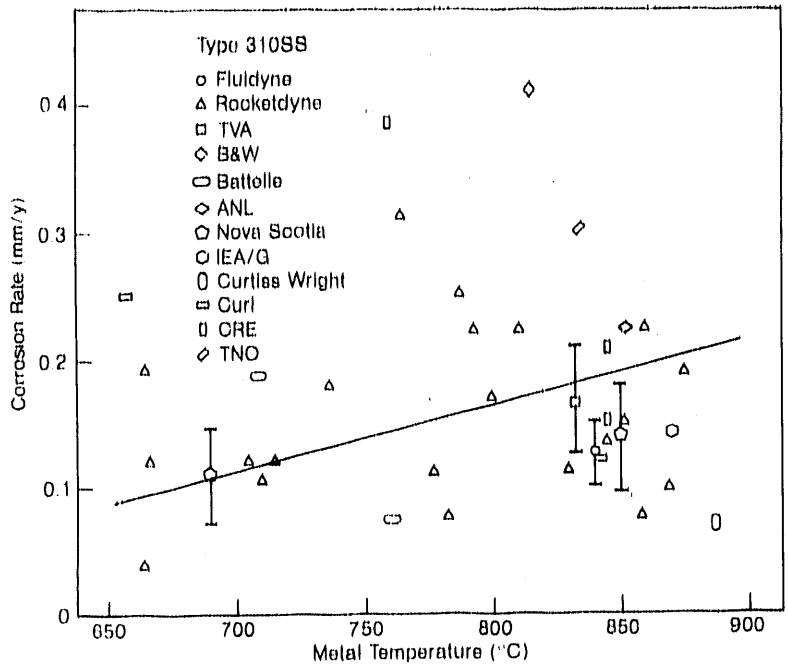

Fig. 59. Variation of Corrosion Rate with Temperature for Type 310 Stainless Steel, Observed at Several FBC Facilities

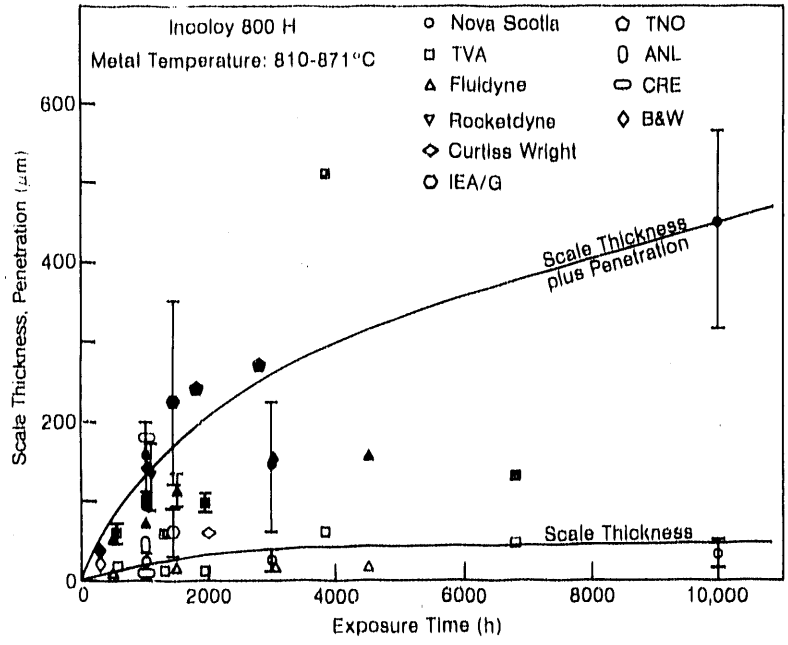

Fig. 60. Scale Thickness and Penetration Data from Several FBC Facilities for Incoloy 800

alloy is susceptible to catastrophic oxidation-sulfidation corrosion when exposed to low-p_{O_2} environments, as evidenced by the laboratory test results discussed in earlier sections of this report.

The corrosion test results presented in this report establish the role of several key variables in the corrosion of structural materials that are candidates for FBC application, and also aid in understanding the mechanism of corrosion in the dynamic environment of FBC systems. Materials degradation depends on local conditions that are prevalent near the area of attack, and these can fluctuate significantly over small intervals of distance and time.

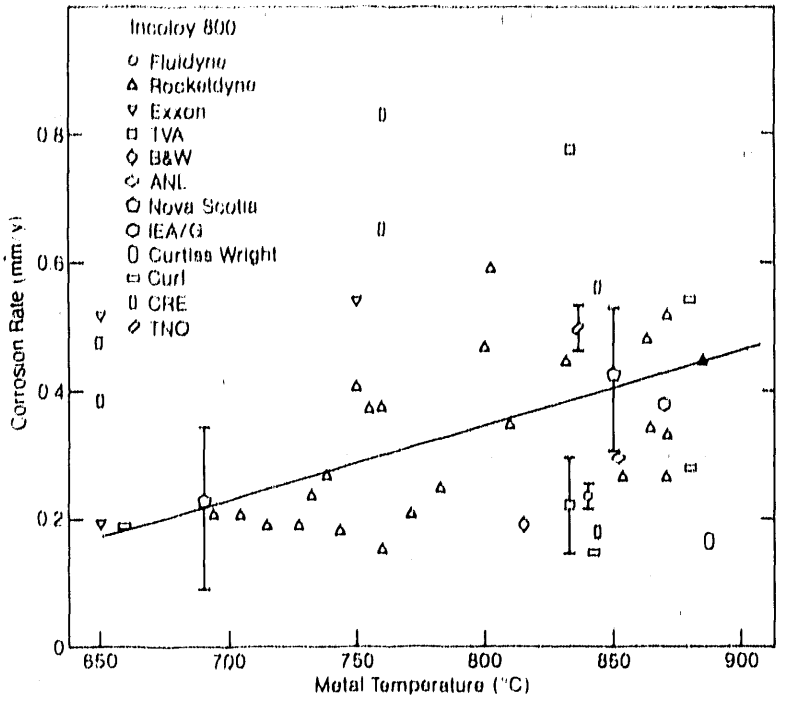

Fig. 61. Variation of Corrosion Rate with Temperature for Incoloy 800, Observed at Several FBC Facilities

If we could establish quantitative relationships among operating parameters and measurements of process conditions (as independent, controllable variables), and local bed conditions in the vicinity of in-bed component materials and the corrosion/erosion behavior of those components (as dependent variables), we would significantly speed the development of FBC technology.

SUMMARY

Laboratory tests have been conducted to examine the role of gas chemistry, sorbent, metal temperature, and gas cycling on the corrosion of heat exchanger and tube support materials in FBC systems. In addition, tests were conducted with spent-bed materials obtained from large FBC test facilities. Based on the test data, the following conclusions can be drawn:

1. The presence of a $CaSO_4$ deposit alone can lead to sulfidation of low-alloy steels, even at 593°C. The austenitic alloys developed (Ca,Cr) oxide and/or Cr_2O_3 scales at the lower temperatures but exhibited significant intergranular sulfidation at a metal temperature of 840°C.

2. The scale thickness and depth of intergranular penetration of $CaSO_4$-coated specimens tested in high-p_{O_2} environments are somewhat greater than those observed in argon exposures, but the rates ($<50\ \mu m\ y^{-1}$) are acceptable for materials such as Type 310 stainless steel in heat exchangers that operate at temperatures below 700°C.

3. Initially applied deposits of CaO were converted to $CaSO_4$ under the low-p_{O_2} exposure conditions of the present investigation. Such a reaction seems to increase the density (decrease the porosity) of deposits and

thereby reduce corrosion scale thickness, especially in high-chromium alloys. A low p_{O2} in the gas phase environment increases the corrosion of bare alloys as well as those coated with $CaSO_4$ and CaO, even at a metal temperature of 593°C.

4. The gas cycling experiment showed that sulfidation can be triggered even in Type 310 stainless steel with a cycle time of 100 h; no sulfidation was noted with a 10-h cycle time. Because the fraction of time spent under low-p_{O2} conditions was the same in both 100- and 10-h-cycle time tests, it can be concluded from the results that a sustained exposure (>10 h) to a low-p_{O2} atmosphere is required for initiation of sulfidation attack of the material.

5. Variations in relative time periods for high and low p_{O2} during an exposure cycle had almost no effect on the corrosion of alloys coated with either $CaSO_4$ or CaO, if the virgin specimens were exposed to a high-p_{O2} atmosphere at the start of the first cycle. Exposure of the specimens to a low-p_{O2} atmosphere at the start of the first cycle seemed to trigger a sulfidation reaction in CaO-coated Type 310 stainless steel.

6. A comparison of data obtained in the presence of $CaSO_4$ and CFB-ash deposits showed that austenitic stainless steels such as Types 304 and 316 showed acceptable corrosion behavior even after a 3000-h exposure in the presence of $CaSO_4$ deposit. However, the subsurface sulfidation noted in Type 316 stainless steel should caution against extrapolation of the data to longer exposure times. Type 310 stainless steel exhibited significant sulfidation attack in the presence of $CaSO_4$ deposits. In contrast, the austenitic steels exhibited a predominantly oxide mode of attack in the presence of CFB ash. Alloys such as Incoloy 800, Haynes 188, and RA 330 were susceptible to substantial/catastrophic attack in the presence of $CaSO_4$ deposits. In contrast, Incoloy 800 developed a thin oxide scale in the presence of CFB ash deposits.

7. Among the coupon specimens, alloys such as HK 40 and Mn-Nb-modified 800H exhibited substantial corrosive attack in the presence of $CaSO_4$ deposits. Alloys such as 253 MA, FW-4C, and 54E showed moderate corrosion, whereas alloys such as 53C and RV 8413 exhibited the least attack in the presence of $CaSO_4$ deposits. On the other hand, the presence of CFB ash had almost no deleterious effect on the corrosion behavior of all the tested alloys, except Alloy 430. Among the aluminides, only the iron-based aluminide (FA-41) exhibited superior resistance to sulfidation attack in the presence of either of the deposit materials.

8. In general, the corrosion data showed that scale thickness and internal penetration in the presence of CFB ash and an air atmosphere (assuming no combustion in the heat exchanger region) were much less than those obtained with $CaSO_4$ deposit and low-p_{O2} atmosphere (most severe conditions envisioned in bubbling beds). On the basis of these results, we conclude that corrosion degradation of metallic alloys and weldments will

be very minimal in CFB systems when compared with that in bubbling FBC systems.

9. Comparison of laboratory test data (developed in a low-p_{O_2} environment) with in-bed corrosion data showed that the corrosion rates determined in the laboratory are higher by a factor of ≈2 and that these rates can be treated as an upper-bound value if the alloys are not susceptible to breakaway corrosion.

ACKNOWLEDGMENTS

A major portion of this work was supported by the U.S. Department of Energy, Advanced Research and Technology Development, Fossil Energy (WBS Element ANL-3), under Contract W-31-109-Eng-38. The comparative testing of materials in the presence of bubbling-bed and CFB-ash deposits was supported by the U.S. Department of Energy, Office of Conservation and Renewable Energy, Energy Cascading Branch. D. L. Rink and R. W. Puccetti assisted with the experimental program and the microstructural analyses of exposed specimens.

REFERENCES

1. T. A. Godfrey and J. H. DeVan, *Corrosion of High-Temperature Materials in AFBC Environments*, Report ORNL/TM-7734/P2, Oak Ridge National Laboratory (1981).

2. A. J. Minchener, et al., *Materials Problems in Fluidized-Bed Combustion Systems*, Report EPRI CS-1853, Electric Power Research Institute (1981).

3. P. L. Daniel and J. Stringer, *Alloy Corrosion in an Atmospheric Fluidized Bed Coal Combustion Unit*, Mater. Performance, *20* (9):9 (1981).

4. J. Stringer, A. J. Minchener, D. M. Lloyd, and H. R. Hoy, *In-Bed Corrosion of Alloys in Atmospheric Fluidized Bed Combustors*, High Temp. Tech., *1*(1):27 (1982).

5. C. J. Spengler, *Evaluation of Heat Exchanger and Turbine Materials for Use in a Coal-Fired Fluidized-Bed Combustion Environment*, Final Report, WAD-10613-CE, Westinghouse R&D Center (1981).

6. S. Cohen, J. Mogul, and S. Wolosin, *Materials Experience in a Fluidized-Bed Coal Combustion System at Curtiss-Wright Corporation*, Preprint, Paper No. 161, CORROSION/80 National Assoc. Corrosion Eng., Chicago (1980).

7. H. R. Hoy and A. G. Roberts, *Investigations on the Leatherhead Pressurized Facility*, Proc. 6th Int. Conf. on Fluidized Combustion, Atlanta, 2, 241 (1980).

8. G. J. Lane, *Studies of In-Bed Corrosion in a Pressurized Fluidized-Bed Combustor*, Final Report, EPRI CS-1935, Electric Power Research Institute (1981).

9. K. Natesan, *Corrosion of Heat Exchanger Materials in Simulated Fluidized Bed Combustion Environments*, Corrosion, *38*(7):361 (1982).

10. P. J. Ficalora, *Hot Corrosion Reactions of $CaSO_4$ with Cr, Ni, Fe, and Several Alloys*, Report ORNL/TM-8735, Oak Ridge National Laboratory (1983).

11. A. Minchener, *Fluidized-Bed Combustion: Corrosion/Erosion Tests*, Program Book, DOE/EPRI/GRI/NBS 5th Annual Conf. on Materials for Coal Conversion and Utilization, Gaithersburg, MD, V-14 (1980).

12. A. A. Bolarski, V. Nagarajan, L. G. Wright, and H. E. Carlton, *Oxygen Partial Pressure Measurements Inside a 0.6 m Fluidized Bed Coal Combustor*, J. Inst. Energy, 59(430): 252 (1984).

13. A. J. Minchener, et al., *The Use of Solid State Electrochemical Probes for Characterization of Fluidized Bed Environments*, Proc. 8th Int. Conf. on Fluidized Bed Combustion, Houston, 2, 822 (1985).

14. E. B. Ljungstrom, *In-Bed Oxygen Measurements in a Commercial Size AFBC*, Proc. 8th Int. Conf. on Fluidized Bed Combustion, 2, 853 (July 1985).

15. R. Q. Vincent, *Mechanical Materials Performance of the TVA 20-MW AFBC Boiler*, Proc. 8th Int. Conf. on Fluidized Bed Combustion, 1, 218 (July 1985).

16. J. Campbell, *Phase II - Primary Heater Module, Final Report for the Period January 1984-March 1985*, RI/RD85-184, Vol. I, Rockwell International, Rocketdyne Division (April 1985).

17. M. A. Rocazella, I. G. Wright, and C. F. Holt, *The Corrosive Environment in the Fluidized-Bed Heat Exchanger for CCGT Service*, ASME Paper 83-GT-249, 28th Ann. Int. Gas Turbine Conf. (March 1983).

18. K. Natesan, *Effect of Sulfur Sorbent and Gas Cycling on Corrosion of FBC Materials at 866 K*, Proc. of FBC Materials Workshop, Nova Scotia, Canada, July 29-August 1, 1985, Electric Power Research Institute, Palo Alto, CA (1987).

19. K. Natesan, *Role of FBC Deposits in the Corrosion of Heat Exchanger Materials*, High Temp. Technol., 4, 193 (1986).

20. A. J. Minchener, P. T. Sutcliffe, I. S. Scott, R. S. Courtney, D. M. Lloyd, D. C. Read, T. Golesworthy, and J. E. Oakey, *Materials Evaluation for Fluidized-Bed Combustion Systems*, Report CS-3511, Electric Power Research Institute (1984).

21. F. C. Yang and D. P. Whittle, *High Temperature Corrosion of Iron in Sulfur Containing Atmospheres*, Proc. Symp. on Corrosion in Fossil Fuel Systems, I.G. Wright, ed., The Electrochemical Society, NJ, Vol. 83-5, 111 (1983).

22. K. Natesan, *Corrosion and Mechanical Behavior of Materials for Coal Gasification Applications*, Argonne National Laboratory Report ANL-80-5 (1980).

23. K. Natesan and W. F. Podolski, *Laboratory Tests in Support of Atmospheric Fluidized-ied Cogeneration Air Heater Experiment: Summary Report*, Argonne National Laboratory Report ANL-88-36 (July 1988).

24. K. Natesan and D. J. Baxter, *Oxygen-Sulfur Corrosion of Metals in Mixed-Gas Atmospheres*, Proc. 3rd Berkeley Conf. on Corrosion-Erosion Wear of Materials at Elevated Temperatures, NACE, Houston, p. 67 (1986).

25. K. Natesan, S. A. Miller, and W. F. Podolski, *An Assessment of the Performance of Heat Exchanger Materials in Fluidized Bed Combustors*, Argonne National Laboratory Report ANL-86-42 (February 1987).

26. K. Natesan, S. A. Miller, and W. F. Podolski, *Performance of Materials in Fluidized-bed Combustors*, J. Mater. Eng. *9*, 269 (1987).

END

DATE FILMED

12/11/90